THE EFFECTS OF DAYTIME MELATONIN ADMINISTRATION ON SLEEP, HIGHER COGNITIVE FUNCTION, AND CHANGES IN THE BRAIN

SAMANTHA EVE LEUNG

A THESIS SUBMITTED TO THE FACULTY OF GRADUATE STUDIES
IN PARTIAL FULFILLMENT OF THE REQUIREMENTS
FOR THE DEGREE OF
MASTER OF SCIENCE

GRADUATE PROGRAM IN BIOLOGY
YORK UNIVERSITY
TORONTO, ONTARIO

August 2014

ABSTRACT

This study investigated the effects of exogenous melatonin on people's sleep, ability to perform an emotional Stroop task, and underlying brain architecture. 10 healthy adults (age = 26.8 ± 6.25 years) underwent a baseline period followed by an experimental period whereby melatonin was administered at inappropriate times, with daily activity logs kept throughout. The emotional Stroop task was performed four times during each period, followed by an MRI scan. Following melatonin administration, sleep and wake times were significantly shifted and sleep quality ratings were significantly decreased compared to baseline values. Additionally, processing of emotional words but not faces was negatively affected by the melatonin treatment. Fractional anisotropy and mean diffusivity values were also significantly altered in the inferior frontal gyrus. It is inferred that the melatonin treatment induced circadian desynchronization, resulting in behavioural changes and structural alterations in brain regions involved in performance of the emotional Stroop task.

DEDICATION

To dad and mom, whose unconditional love and unending support have inspired me to become the person I am today. A lifetime of thank yous would never be enough, so I dedicate this thesis to you as a token of my gratitude.

ACKNOWLEDGMENTS

I would first like to thank Dr. Colin G.H. Steel and Dr. Joseph F.X. DeSouza, for without them this project would have never come to fruition. I would also like to thank Dr. Barry G. Loughton for his time and insight as my advisor. Last but not least, I would like to thank all my family, friends (a special thank you to Nicolas Chung), and lab mates (special thank yous to Michael Cardinal-Aucoin and Hedieh Tehrani) who have walked with me along this journey, for without your support I would not be where I am today.

TABLE OF CONTENTS

LIST OF FIGURES

LIST OF ABBREVIATIONS

AANAT – Arylalkylamine *N*-Acetyltransferase

ACC – Anterior Cingulate Cortex

AD – Alzheimer's Disease

ATP – Adenosine Triphosphate

BOLD – Blood Oxygen Level Dependent

cAMP – Cyclic Adenosine Monophosphate

CKII – Casein Kinase II

CLK – Clock Protein

CRY – Cryptochrome Protein (*Cry* – Cryptochrome Gene)

CYC – Cycle Protein

DBT – Double-Time Protein

DLMO – Dim-Light Melatonin Onset

DTI – Diffusion Tensor Imaging

EC – Early Chronotype

ELISA – Enzyme-Linked Immunosorbent Assay

FA – Fractional Anisotropy

fMRI – Functional Magnetic Resonance Imaging

GABA - Gamma-Aminobutyric Acid

HDL – High Density Lipoprotein

HEC – Hippocampal Entorhinal Cortex

HIOMT – Hydroxyindole-*O*-Methyltransferase

IFG – Inferior Frontal Gyrus

LC – Late Chronotype

LDL – Low Density Lipoprotein

LHT – Lateral Hypothalamic Tract

MCTQ – Munich Chronotype Questionnaire

MD – Mean Diffusivity

MRI – Magnetic Resonance Imaging

MT_1 and MT_2 – Melatonin Receptor Subtypes 1 and 2

NE – Norepinephrine

NPY – Neuropeptide Y

ON – Optic Nerve

PD – Parkinson's Disease

PER – Period Protein (*Per* – Period Gene)

PRC – Phase Response Curve

PVN – Paraventricular Nucleus

RHT – Retinohypothalamic Tract

ROI – Region of Interest

RT – Reaction Time

SC – Streamline Count

SCN – Suprachiasmatic Nucleus

SEM – Standard Error of the Mean

SGG – Shaggy kinase

TBSS – Tract-Based Spatial Statistics

TFCE – Threshold-Free Cluster Enhancement

TIM – Timeless Protein (*Tim* – Timeless Gene)

TTFL – Transcription-Translation Feedback Loop

1. Introduction

1.1 General Introduction

1.1.1 A Brief Historical Review of Chronobiology

The daily changes in environmental light conditions resulting from the rotation of the earth have had profound impacts on all aspects of life. One such impact has been on the evolution of rhythmic physiological processes in living organisms. The world in which we live consists of a solar day with alternating periods of light and dark, and as such, organisms have adapted by synchronizing their own activities with these light/dark cycles. This synchronization of activities is important as it allows for the anticipation of change before the need arises – for example, blood glucose levels rising prior to one's awakening – and as timing is required for anticipation, so too are clocks required for timing. Though much is now known about biological clocks and their sophisticated timing mechanisms, it is important to highlight the early experiments in plants and insects that aided in their discovery and the eventual discovery of the mammalian circadian system as a whole.

In 1729, Jean-Jacques d'Ortous de Mairan detailed the first encounter with internal biological clocks. de Mairan observed that the leaflets of the plant *Mimosa pudica* folded together and hung downwards during the night and unfolded and expanded during the day (de Mairan, 1729). He further noted that these behaviours did not change when *Mimosa pudica* was placed in continuous darkness – that is, the leaflets continued to fold and unfold rhythmically in synchrony with the external light/dark cycle, despite being unable to detect it directly (de Mairan, 1729). This simple yet remarkable experiment was the first demonstration of an internally generated 24 hour rhythmicity, contrary to previous presumption that they occurred as a direct response to environmental and external light cues. The work of de Mairan and others led

to the definition of three specific criteria that a rhythm must fulfill in order for it to be considered circadian in nature. First, circadian rhythms must persist in an aperiodic environment, as was exhibited by the behaviours of *Mimosa pudica* in the absence of light. Organisms placed in an aperiodic environment have rhythms that continue in the absence of environmental cues, free-running with a period length of approximately 24 hours. Second, circadian rhythms must have free-running period lengths that are close to, but not exactly, 24 hours. That is, in constant aperiodic environments the rhythm must persist such that the interval between consecutive peaks or troughs, also known as the period, is roughly 24 hours. Internal clocks have natural period lengths that are either slightly shorter or slightly longer than 24 hours (with the range being approximately 19 to 26 hours in length), and these varying period lengths are constant and characteristic of a particular clock. Lastly, the rhythm must have a period length that is temperature compensated. As biological clocks are relatively insensitive to temperature changes, the free running period length of the clock must also not change greatly with fluctuating temperatures.

A second key contribution to the study of biological clocks, or chronobiology, came with the conceptualization of the transcription-translation feedback loop (TTFL) in *Drosophila* by Hardin, Hall, and Rosbash (Hardin *et al*., 1990; Figure 1). In brief, the mechanisms of this first-described TTFL model were as follows: the CLOCK (CLK) and CYCLE (CYC) proteins within clock cells form a heterodimer and translocate into the nucleus, acting as a transcription activator by binding to the E-box element in the promoters of two of the most widely recognized clock genes, *period (Per)* and *timeless (Tim)*. As a result of the stimulation of these genes, transcription of *Per* and *Tim* mRNA and the eventual translation of the mRNA into PER and TIM proteins occurs. The PER and TIM proteins then come together to form PER/TIM heterodimers, the

formation of which inhibits the CLK/CYC heterodimers from further activating transcription. This binding of TIM to PER not only acts as a negative feedback on the TTFL, but also serves to protect PER from phosphorylation. During the day, TIM is degraded by cryptochrome (CRY), a protein that is involved in blue light photoreception in insects. Thus, in the presence of blue light during daytime CRY is activated, TIM is degraded, and PER is continuously susceptible to phosphorylation by double-time (DBT), a non-cyclical casein kinase. During the night, however, levels of TIM increase as there is no longer blue light input to CRY and therefore no more degradation of TIM. Concomitantly, protein phosphatase 2A works to undo the actions of DBT by cyclically dephosphorylating PER until the levels of PER are high enough to dimerize with TIM.

As our knowledge of the circadian system further developed, several deficiencies in this TTFL model were noted. Firstly, prokaryotic blue-green bacteria have molecular oscillators and are capable of performing circadian timekeeping, though they do not possess a nucleus nor any of the aforementioned mechanisms (Lakin-Thomas, 2000). Additionally, the proposed model consists of mechanisms that are not temperature compensated (Lakin-Thomas, 2000). Furthermore, the biochemistry of this TTFL model would occur quite rapidly, as transcription, translation and nuclear transport takes mere minutes; thus there must be an additional component to the model that slows the mechanism down to a circadian period length (Lakin-Thomas, 2000). Lastly, it seems that PER and TIM must be multifunctional, as their levels within clock cells are much higher than what is needed solely for transcription activation and inhibition purposes (Lakin-Thomas, 2000). Although now recognized as being overly simplistic and largely inadequate for explaining the molecular basis of the clock, the importance of this initial TTFL model cannot be overlooked as it demonstrated the first workings of the machinery within clock

cells.

The *Drosophila* TTFL is now known to consist of multiple interlocking feedback loops and involve several dozen genes and their protein products (Hardin, 2011). Posttranslational modifications to the key clock proteins are now also known to regulate the period length of the clock to about 24 hours by introducing temporal delays into the mechanism. For example, phosphorylation has been shown to affect the timing of the clock through its actions on PER and TIM. Direct phosphorylation of PER by DBT in the cytoplasm destabilizes PER until levels of TIM in the cytoplasm accumulate to sufficient levels, which introduces a temporal delay between transcription of *per* and *tim* and the dimerization of PER/TIM (Harms *et al*., 2004). Additionally, 3 kinases have been found in *Drosophila* that regulate the translocation of PER/TIM from the cytoplasm to the nucleus: DBT, SHAGGY (SGG), and Casein Kinase II (CKII). While DBT has been shown to play a role in the temporal gating of nuclear entry by phosphorylating PER (Bao *et al*., 2001), SGG and CKII have been shown to promote the nuclear accumulation of PER and TIM through the phosphorylation of TIM and PER, respectively (Martinek *et al*., 2001; Lin *et al*., 2002). As most features of the *Drosophila* clockwork are conserved in mammals, these advances have allowed for a better understanding of the mechanisms underlying not only the insect molecular clock, but the mammalian molecular clock as well.

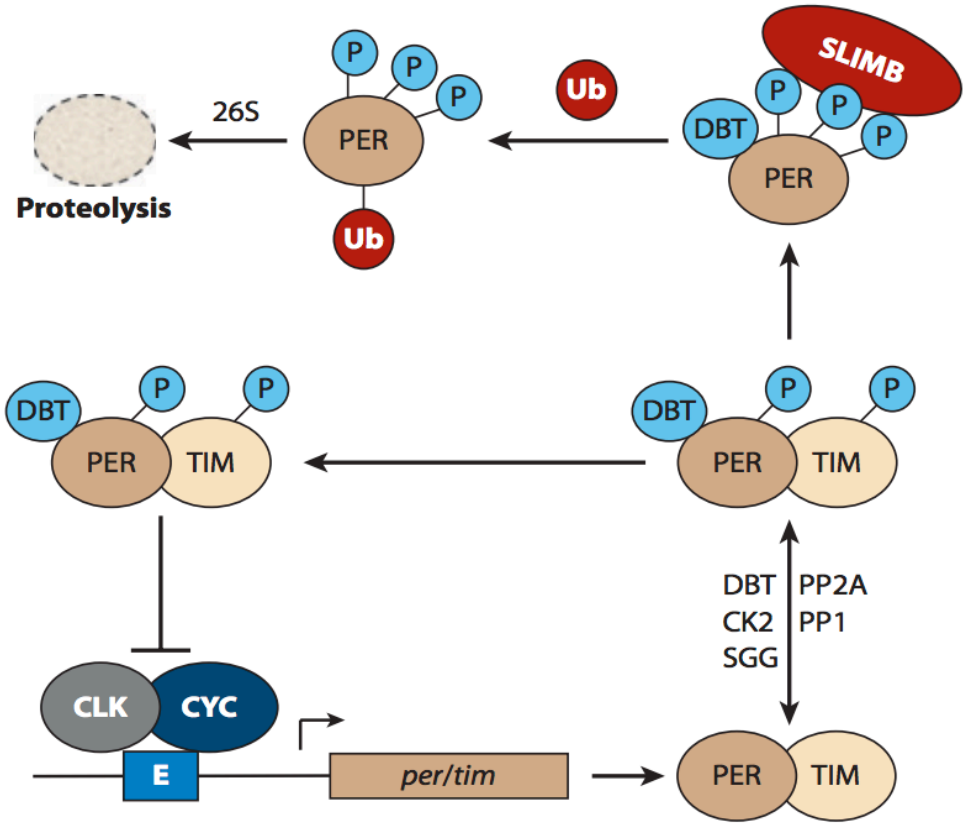

Figure 1. Model of the *Drosophila* TTFL. CLK and CYC act as activators while PER and TIM act as repressors. Image obtained from Allada and Chung, 2010.

1.1.2 Mechanisms of the Mammalian Molecular Clock

Much of our current knowledge in the field of chronobiology can be attributed to research on circadian rhythms in models varying from bacteria and plants to insects and birds. It was not until the relatively recent use of mammalian models that scientists were able to get a first glimpse of the workings behind the human circadian system. Though similar to that of lower animal models, the mammalian circadian system is much more complex and possesses a few significant differences that makes it unique and often times, difficult to study.

Mammals have an analogous core molecular mechanism to *Drosophila* that consists of two transcription factors: a mammalian homolog of CLOCK (CLK) and BMAL1. The CLK/BMAL1 heterodimers, similar to the CLK/CYC heterodimers in *Drosophila*, activate

transcription of the mammalian clock gene homologs of *period* (of which there are three genes; *Per1*, *Per2*, and *Per3*) and *cryptochrome* (of which there are two genes; *Cry1* and *Cry2*) by binding to the E-box element in the promoters of these genes (King *et al*., 1997; Gekakis *et al*., 1998). *Per* and *Cry* are subsequently transcribed and translated into their mRNA and protein counterparts, respectively, and the PER and CRY proteins then dimerize to form complexes that translocate into the nucleus. Inside the nucleus, these PER/CRY heterodimers work by inhibiting the CLK/BMAL1-induced transactivation of *Per* and *Cry* (Shearman *et al*., 2000; Lee *et al*., 2001; Sato *et al*., 2006). Unlike the *Drosophila* TTFL model, however, levels of PER do not fluctuate because of the phosphorylation/dephosphorylation process; rather, regulation in the mammalian model comes from the secondary and independent functions of PER and CRY. Ye *et al.* (2011) found that CRY binds to the CLK/BMAL1/E-box complex independently of PER and destabilizes it, resulting in the inhibition of transcription. They further found that PER interferes with the binding of CRY to CLK/BMAL1/E-box, thus allowing for continuous transcription activation as CRY is no longer able to destabilize the complex (Ye *et al*., 2011). Today, this modern model has become widely accepted and has allowed for a more comprehensive understanding of the mammalian circadian clock (Figure 2).

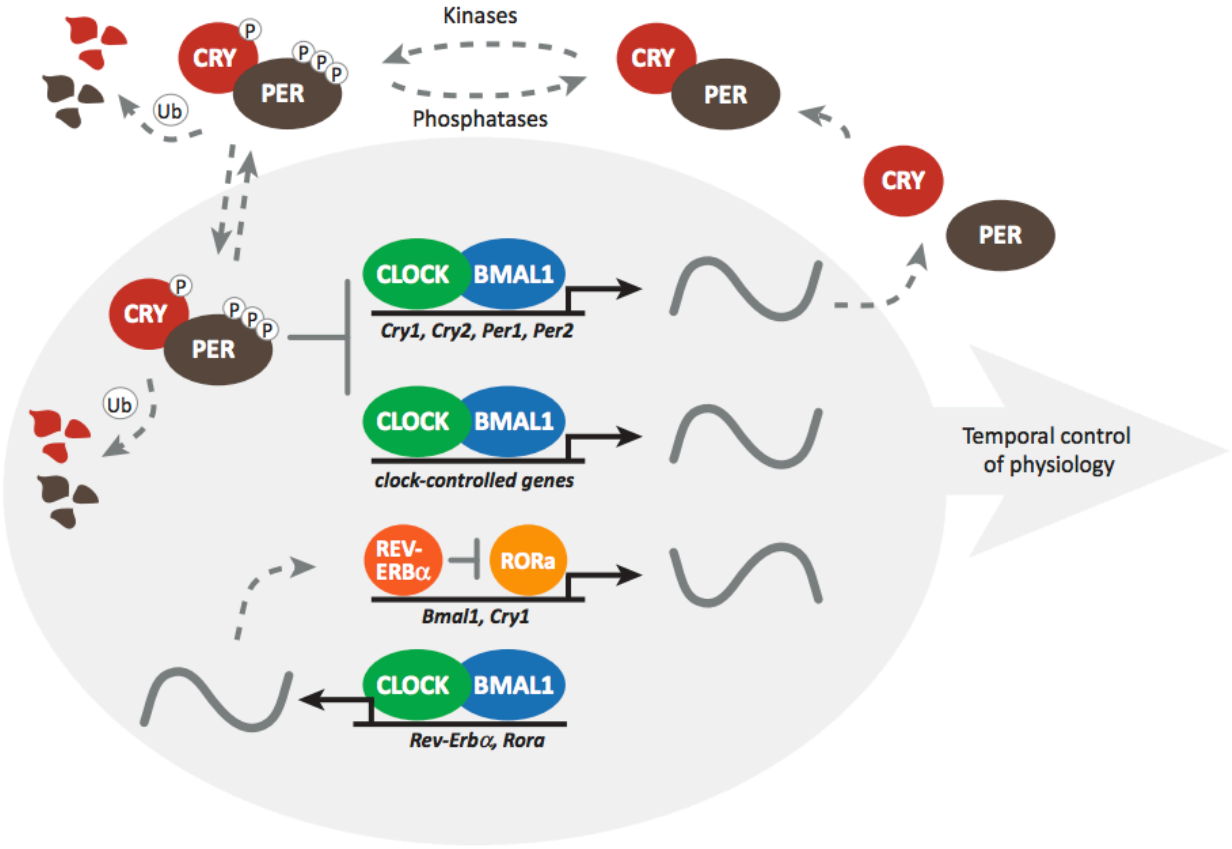

Figure 2. Model of the mammalian circadian clock. CLOCK and BMAL1 proteins act as activators while PER and CRY proteins act as repressors. Image obtained from Partch *et al*., 2014.

1.1.3 The Mammalian Circadian System

Endogenous circadian rhythms in mammals are generated and regulated by the "central clock" located in the suprachiasmatic nucleus (SCN) of the hypothalamus. The SCN was first discovered to play an important role in mammals by Robert Y. Moore in the early 1970s from studies using rats, mice, and hamsters. It was found that lesions of the SCN in these animals caused ablation of many important rhythms such as activity rhythms, sleeping rhythms, body temperature rhythms, and endocrine rhythms (Moore and Eichler, 1972; Moore and Lenn, 1972; Stephan and Zucker, 1972a and 1972b; Moore and Klein, 1974). The SCN was further found to control the period lengths of numerous free-running rhythms, though the clock cells within the

SCN are not directly photosensitive. It is now known that entrainment of these clock cells occurs through an alternate route – via neural pathways, primarily through the neural pathway from the eye. Two nerves connect the eyes to the brain: the optic nerve (ON), which acts as an indirect communication pathway connecting visual photoreception to the visual processing centers in the brain, and the retino-hypothalamic tract (RHT), which uses the neurotransmitter glutamate to provide direct nervous communication between the eyes and the SCN and is the primary route through which the SCN is entrained. The RHT is bidirectional, in that it not only provides afferent input from the eyes to the SCN, it also transmits efferent rhythmic output from the SCN back to the retina (Moore and Lenn, 1972; Johnson *et al*., 1988). Traditional clock genes are expressed in a variety of cell types in the mammalian retina, including photoreceptors and some retinal ganglion cells. These retinal ganglion cells are clock cells and are directly photosensitive as they contain an opsin-based pigment known as melanopsin (Hattar *et al*., 2002); these retinal ganglion cells have axons that travel down the RHT, directly innervating the SCN and providing light information to its component clock cells. Aside from the RHT, light information can also reach the SCN through the lateral hypothalamic tract (LHT), which innervates the SCN and relays information from the eyes by use of the neurotransmitter neuropeptide Y (NPY).

The circadian timing system in the head of mammals not only consists of the eyes and the SCN – a third structure known as the pineal gland aids in the overall organization of circadian rhythms. Though in birds the pineal gland is known to be an autonomous clock, the pineal gland in mammals is not; rather, it works as a "slave oscillator" that generates rhythmic output solely through its innervation by the SCN. Arguably one of the most important outputs of the pineal gland in mammals is that of melatonin – the SCN not only drives rhythmic melatonin synthesis in the pineal gland but also has receptors for melatonin itself, allowing for a feedback effect that

controls the phase of the rhythm (River-Bermudez *et al*., 2004; Bedrosian *et al*., 2013). Melatonin's main role in the circadian system is that of coordinating synchrony and phase in the divergent population of SCN clock cells, which all have slightly different free-running period lengths. Other synchronizing agents include the glutamatergic fibres originating from the retina, serotonergic fibres emanating from the raphe nuclei, NPY fibres coming from the intergeniculate leaflet, and other hormonal/metabolic signals. For a more in-depth discussion on melatonin, see section 1.3.

Of particular interest to chronobiologists is the fact that clock genes are not only expressed rhythmically in structures within the central nervous system (including but not limited to the cerebellum, hippocampus, arcuate nuclei, paraventricular hypothalamic nuclei, piriform and cerebral cortices, olfactory bulbs, amygdala, retina, and pineal gland), but also in several peripheral tissues such as the liver, pancreas, fat, gut, lung, and heart (Abe *et al*., 2002; Challet *et al*., 2003; Schibler *et al*., 2003; Amir *et al*., 2004; Gachon *et al*., 2004; Verwey and Amir, 2009; Mendoza *et al*., 2010). It is of importance to note that cells expressing clock genes are not necessarily clocks – the expression of clock genes must oscillate and undergo circadian cycling in the absence of external cues for it to be considered a genuine clock. Thus rhythmicity in the above-mentioned peripheral tissues originates from cellular clocks within the tissues themselves. Though the exact role of molecular oscillations for the function of peripheral organs is still unclear, it has been hypothesized that it either allows the organ to anticipate signals coming from the SCN, or it enables the organ to maintain robust rhythmicity by enhancing the signals (Pevet *et al*., 2006). Regardless of the reason, these central and peripheral oscillators work together to form an integral part of what is now known as the multi-oscillatory circadian network.

1.2 The Hormone Melatonin

1.2.1 The Signal of Night: Melatonin Synthesis and Control

Melatonin, also known as N-acetyl-5-methoxytryptamine, was first isolated in 1958 from bovine pineal gland (Lerner *et al*., 1960). The rise of pineal melatonin content during the night and the subsequent fall during the day was among the first physiological rhythms to be characterized as a true circadian rhythm (Ralph *et al*., 1971). This melatonin rhythm is now one of the most well-defined and well studied endogenous circadian rhythms to date. In mammals, the synthesis of pineal melatonin is driven by the SCN clock. Melatonin is synthesized from the amino acid tryptophan which is converted into 5-hydroxytryptophan by tryptophan-hydroxylase and then by decarboxylation into serotonin. From there, the metabolism of serotonin occurs in two steps. In the first step, arylalkylamine *N*-acetyltransferase (AANAT) catalyzes the conversion of serotonin to *N*-acetylserotonin, which is then *O*-methylated (the transfer of a methyl group from 5-adenosylmethionine to the 5-hydroxy group of *N*-acetyleserotonin) by hydroxyindole-*O*-methyltransferase (HIOMT) to form melatonin (Schomerus and Korf, 2005). Melatonin is not stored within the pineal but, following synthesis, is immediately released into the circulating blood stream where it has a relatively short half-life as it is rapidly 6-hydroxylated in the liver. Therefore, the rhythm of melatonin in the peripheral circulation reflects its rhythmic synthesis by the pineal. The enzyme AANAT mediates the rate-limiting step in melatonin synthesis and is responsible for generating the circadian rhythm of melatonin production. The presence of AANAT in pineal cells is regulated by the release of norepinephrine (NE) from the sympathetic nerve fibres originating from the SCN and innervating the pineal parenchyma, which release NE in a circadian manner during the night (Kalsbeek and Buijs, 2002; Moller and Baeres, 2002). The release of NE elevates intracellular cyclic AMP (cAMP) concentrations and

activates cAMP-dependent protein kinase A, allowing AANAT to be phosphorylated and thereby protecting it from degradation (Kalsbeek and Buijs, 2002). During the day, in the absence of NE stimulation, AANAT is immediately broken down by proteasomal proteolysis. Thus, melatonin levels are elevated during the night as AANAT is available for the metabolic conversion of serotonin to melatonin, but not during the day as AANAT is destroyed in the absence of noradrenergic stimulation.

The SCN directly drives the synthesis of melatonin through a multi-synaptic neural pathway which includes the pre-autonomic neurons of the paraventricular nucleus (PVN) of the hypothalamus, the sympathetic pre-ganglionic neurons of the spinal cord, and the noradrenergic sympathetic neurons of the superior cervical ganglion (Moore, 1996 a & b; Larsen *et al*., 1998; Teclemariam-Mesbah *et al.,* 1999). Early studies on the SCN's control of melatonin synthesis and release found gamma-aminobutyric acid (GABA) present in the neurons of the SCN (Okamura *et al*., 1989; Moore and Speh, 1993; Buijs *et al*., 1994). As light exposure causes activation of most SCN neurons, it was thought that GABA could be released from the SCN terminals as a response to light-induced activation of these neurons, in turn inhibiting the release of melatonin (Groos and Meijer, 1985). Kalsbeek *et al*. (2000) confirmed this hypothesis, finding that nocturnal light exposure causes the release of GABA in the vicinity of the PVN, inhibiting the PVN neurons that control the final part of the pineal-activating pathway. Moreover, it has been postulated that GABA may be released from the SCN terminals according to an endogenous circadian rhythm, and may even be partially responsible for the circadian rhythm of melatonin release. Though still up for debate, this hypothesis has been substantiated by studies that found that infusion of a GABA antagonist into the PVN of mice during the subjective day provoked the release of melatonin, with melatonin concentrations reaching nighttime levels at

the end of a 4 hour infusion (Kalsbeek *et al*., 2000; Perreau-Lenz *et al*., 2003). Further evidence for this hypothesis has come from studies by Perreau-Lenz *et al*. (2004, 2005), demonstrating that the SCN uses a combination of rhythmic daytime inhibitory signals (via release of GABA) and nighttime stimulatory signals (via release of glutamate) to control the daily rhythm of melatonin synthesis. Therefore, the presence of glutamate and the absence of GABA during the night activates the PVN neurons and stimulates the noradrenergic sympathetic neurons to release NE, in turn raising the levels of AANAT and allowing for the synthesis of melatonin from serotonin.

1.2.2 Role of Melatonin in the Circadian System

Melatonin serves as the "hormone of darkness" in the circadian system, relaying timing information and synchronizing the "central clock" in the SCN with the peripheral clocks scattered throughout the body (Hardeland *et al*., 2011; Pevet and Challet, 2011). As an output of the SCN clock, the nocturnal secretion of melatonin is able to distribute a circadian message to the entire body. The duration of melatonin secretion and the corresponding levels of melatonin in the circulating bloodstream reflect the length of the night and indicate a relative position within the 24 hour day. Therefore, the daily profile of melatonin secretion conveys internal information used not only for circadian timing, but also for seasonal temporal organization. Thus, changes in the duration of melatonin production throughout the year can be integrated by the brain to measure photoperiodic time. Though the role of melatonin in photoperiodic responses has been widely documented in animal models (for comprehensive reviews of photoperiodism in animals, see Bradshaw and Holzapfel, 2007 and Hazlerigg, 2012), there is little evidence of photoperiodic phenomena in humans and thus this role of melatonin will not be discussed within the framework of this thesis.

Three melatonin receptor subtypes have been identified, two of which are currently known to be found in mammals (MT_1 and MT_2 subtypes). Though both MT_1 and MT_2 subtypes are G protein-coupled receptors, they play different roles in the mammalian system. Activation of MT_1 receptors inhibits neuronal firing and induces arterial vasoconstriction, while activation of MT_2 receptors phase shifts circadian rhythms generated within the SCN and induces vasodilation (Dubocovich and Markowska, 2005). Both receptor subtypes have been localized within the central nervous system and in peripheral tissues of mammals. Though melatonin is ubiquitous in animals and potential target sites are numerous, binding sites have been reported to vary widely across mammalian species (Masson-Pevet *et al*., 1994; Morgan *et al*., 1994). Of the several dozen sites studied within the brains of animal models such as rats, Syrian hamsters, Siberian hamsters, white-footed mice, guinea pigs, rabbits, goats, sheep, vervet monkeys, baboons, rhesus monkeys, and humans, only the SCN and pars tuberalis of the pituitary showed consistency across all models. In humans, MT_1 receptor proteins have been found in Brodmann's area 10, putamen, caudate nucleus, nucleus accumbens, substantia nigra, amygdala, and hippocampus of the post-mortem human brain (Uz *et al*., 2005). The identification and localization of these receptors holds much importance as it allows for targeted regions of interest in which exogenous melatonin's effect on the human brain can be examined. Outside of the brain, animal and human melatonin binding sites have been characterized to include the spleen in guinea pigs, hamsters, mice, ducks, and pigeons, the ovaries and testes in chickens, the kidneys in ducks, and the spermatozoa in humans (Morgan *et al*., 1994). This widespread distribution of melatonin receptors both within and outside of the nervous system makes it the key agent to deliver circadian timing information throughout the body, and may play a role in the entrainment of peripheral oscillators in these tissues (Alonso-Vale *et al*., 2008; Brodsky and Zvezdina, 2010;

Chakravarty and Rizvi, 2011).

1.2.3 Melatonin as an Antioxidant

Melatonin plays a second crucial role in mammals: it helps to rid the body of free radicals, as it is one of the most powerful antioxidants found in humans (Vijayalaxmi *et al*., 1998). Due to melatonin's amphiphilic properties, it can cross physiological barriers that other antioxidants possessing only hydrophilic or lipophilic properties cannot. It is for this reason that melatonin is such a powerful antioxidant, as it is able to reduce oxidative damage in both the lipid and aqueous environments of cells (Reiter *et al*., 2004). Direct antioxidant properties of melatonin have been shown to occur through protection against DNA degradation and lipid peroxidation (Bonnefont-Rousselot and Collin, 2010). It is thought that protection against DNA degradation by melatonin may be due to the direct scavenging of free radicals along with the activation of DNA repair enzymes (Vijayalaxmi *et al*., 1998). Indeed, several studies have demonstrated the ability of melatonin to scavenge oxygen-derived free radicals, including hydroxyl free radicals (Poeggeler *et al*., 2002; Roberts *et al.*, 1998; Matuszak *et al*., 1997) and peroxyl free radicals (Livrea *et al*., 1997; Pieri *et al*., 1994). Furthermore, melatonin has been shown to exhibit an indirect antioxidant role by supporting superoxide dismutase and glutathione peroxidase activity (Korkmax and Reiter, 2008). Reiter *et al*. (2002) and Winiarska *et al*. (2006) found that melatonin activates γ–glutamylcysteine, stimulating glutathione production in cells and thereby increasing glutathione levels. In addition, it was found that melatonin promotes the activity of glutathione reductase, which converts oxidized glutathione back to its safer, reduced glutathione form (Reiter *et al*., 2002). Thus disturbances to the melatonin rhythm cause not only circadian disruption but also reduce antioxidant levels, which in turn, increases the risk of developing diseases.

1.2.4 Melatonin as a Chronobiotic

When it was first discovered that the SCN not only drives rhythmic output of melatonin but has receptors for melatonin itself, scientists were puzzled as to why this was the case. It has now been shown that circulating melatonin is able to feed back onto the SCN clock, affecting circadian regulation as demonstrated by the phase-shifting effects on the firing rate of SCN neurons (Gillette and McArthur, 1996). As such, research has now focused on the use of melatonin as a chronobiotic – a drug that shifts all circadian rhythms in a desired direction (advance or delay) and acts as a Zeitgeber (German word for "time giver", referring to cues or signals that clocks synchronize to) to maintain a stable phase once the desired shift has been obtained.

It has long been known that daily administration of melatonin acts on activity rhythms in rodents – studies using subcutaneous injections, infusions, or melatonin administered via drinking water all demonstrated the ability to entrain free-running rhythms in rats (Redman *et al*., 1983; Pitrosky *et al.,* 1999; Slotten *et al*., 1999). According to the non-parametric model of entrainment, this synchronization process occurs through progressive daily phase shifts. In respect to melatonin, researchers studying its entrainment limits have concluded that daily phase shifts as a result of exogenous melatonin range from a minimum of half an hour to a maximum of an hour and a half (Slotten *et al*., 2002). When administered to humans in accordance with the melatonin phase response curve (PRC) first documented by Lewy *et al*. (1998), which illustrates the relationship between the time exogenous melatonin is taken and the effects it has on the rhythm, it can produce phase advances that reset the circadian clock to an earlier time, or phase delays that reset the circadian clock to a later time. The most current melatonin PRC demonstrates that while exogenous melatonin administered around the time of endogenous

melatonin secretion causes little phase resetting, exogenous melatonin administered at least two hours prior to endogenous melatonin secretion causes phase advances and exogenous melatonin administered at least two hours after endogenous melatonin secretion causes phase delays (Breslow *et al*., 2013)

Melatonin appears to have a dual effect on the molecular machinery of clock cells, as it has been observed that *Cry1* mRNA expression peaks during the night when blood plasma melatonin levels are high and *Per1* mRNA expression peaks early in the day when melatonin levels in the bloodstream are low (Pevet *et al*., 2006). It therefore appears that *Per1* expression is linked to the decline in melatonin levels, while *Cry1* expression is gated by its release. However, Poirel *et al*. (2003) observed that administration of exogenous melatonin did not alter transcriptional regulation of the clock genes *Per1*, *Per2*, *Clock*, *Bmal1*, *Cry1* and *Cry2* in rats. It was thus concluded that these genes are not the initial target that mediates melatonin-induced phase advances or delays, and that the chronobiotic effect must lie elsewhere and rely on other regulatory mechanisms. In support of this conclusion, Agez *et al*. (2007) found that acute injected melatonin induced an immediate phase advance of the expression rhythm of REV-ERBα, a nuclear receptor that acts as a transcriptional repressor. This finding suggests that this transcription factor, and not the clock genes themselves, may be the primary molecular target involved in the chronobiotic effect of melatonin (Agez *et al*., 2007).

The chronobiotic properties of melatonin may help to explain the wide range of its reported effects – for example, improved cardiovascular, digestive and immune functions – and demonstrates that it may be suitably used as a pharmacological drug to manipulate circadian rhythms. Indeed, melatonin has been shown to help shift workers entrain to their schedule, thus improving their sleep duration and quality (Zee and Goldstein, 2010). Furthermore, documented

responses to administration of exogenous melatonin have validated its efficacy in both advancing and delaying the circadian clock and its resulting rhythms, providing evidence for the use of melatonin to help shift workers entrain to their work schedule (Folkard *et al*., 1993; Burgess *et al*., 2002; Burgess *et al*., 2008; Burgess *et al*., 2010; Zee and Goldstein, 2010). The most convincing data to be obtained thus far, however, have come from studies on blind individuals, who often experience sleep disturbances because their activity rhythms can fall out of phase with social cues for sleeping and wakefulness. Exogenous melatonin administered daily has been shown to entrain the sleep/wake cycle of these individuals to a 24 hour period, resulting not only in a stable sleep/wake rhythm but in improvements to their quality of life as well (Skene and Arendt, 2006 and 2007).

1.3 Our 24/7 World: Circadian Disruption and its Consequences

1.3.1 Temporal Disruption and Desynchronization

In today's 24/7 world, shift work has become increasingly commonplace to meet society's ever-increasing demands. Although shift work has long been associated with minor health problems such as gastrointestinal disorders, abnormal metabolic responses, and sleep disorders, the more serious risks to long-term shift workers are only recently coming to light (Arendt, 2010). Of the major diseases that have been found to afflict shift workers, the two most well documented associations are between shift work and cardiovascular disease, and female shift workers and breast cancer (Arendt, 2010). Shift workers have been reported to have an increased risk for developing cardiovascular disease and its associated health problems (Peter *et al*., 1999), including obesity, high triglyceride levels, and low high-density lipoprotein (HDL) cholesterol concentrations among other metabolic abnormalities (Al-Naimi *et al.*, 2004; Karlsson

et al., 2001, 2003). It has also been shown that women who work on a rotating night shift schedule have a 36% greater chance of developing breast cancer than women who have never worked rotating shifts, with the risk rising further as the duration of participation in shift work increases (Schernhammer *et al.*, 2001). The epidemiological evidence correlating work-related temporal disruptions and breast cancer have been so convincing that in 2008, Denmark officially recognized shift work as an occupational hazard and as a result, became the first country to pay government compensation to women who developed breast cancer while working long-term night-shifts (Chustecka, 2009).

These health problems are manifestations of a breakdown of the circadian timing system, and as this vital system is important for proper physiological function disruption is expected to produce serious effects. Thus shift workers working out of phase with their internal biological clock undergo what is known as internal desynchronization – a state in which the body's internal clocks are out of synchrony with each other and with the external environment (Arendt, 2010). As much of the lives of shift workers are spent out of phase with local time due to their constantly changing shift schedules, their circadian clocks often cannot completely readjust their circadian rhythms, resulting in a state of permanent internal desychronization. In a similar manner, those who suffer from jet lag experience the unpleasant effects of undergoing circadian disruption. Flying across different time zones produces a misalignment of the body's multiple internal clocks with each other and between them and the external environment. Over time, the clocks will resynchronize with each other and the outside world and the jet lag symptoms will subside. Under normal circumstances, experiencing jet lag does not pose a serious health risk; it does, however, become an issue of concern when dealing with those working as pilots, co-pilots, and flight attendants. With the growing awareness of these potential issues, the aviation industry

has made efforts to combat the effects of internal desynchronization by attempting to minimize the impact of jet lag on flight crews that cross many time zones.

One of the main problems afflicting workers who participate in rotating/night shifts is the exposure to light at night, the occurrence of which disrupts normal circadian physiology and behavioural rhythms. As mentioned in section 1.1.2, light is detected by photoreceptive ganglion cells in the eye, projecting down the RHT and entraining the clock cells within the SCN. These SCN clock cells control melatonin synthesis in the pineal gland, and therefore exposure to extended periods of light at night can drastically alter melatonin levels (Reiter *et al*., 2011). Disruption of this melatonin rhythm, a crucial part of the mammalian circadian timing system, can evoke a multitude of downstream events including altering the rhythmicity of release of several hormones (e.g., prolactin, glucocorticoids, and serotonin) (Stevens *et al*., 2009; Reiter *et al*., 2011; Gaston *et al*., 2013), eventually leading to the development of the health problems mentioned above. Thus understanding the link between temporal disruption and desynchronization and finding ways to minimize disruption of the circadian system is a crucial step in reducing the adverse effects of shift work and jet lag.

1.3.2 Light at Night and Human Health

Almost all manifestations of health problems associated with circadian disruption stems from the extended exposure to light at night. It has been found that it takes only 39 minutes of human exposure to a low-level incandescent light bulb during nighttime to suppress melatonin levels by 50% (Schulmeister *et al*., 2004). At the cellular level, constant light-induced interruption of nightly melatonin secretion has been shown to affect basic processes associated with the acquisition and utilization of energy, functionally altering the regulation of body mass, the efficiency of gut metabolism, and the synthesis of adenosine triphosphate (ATP) in the heart

(Navara and Nelson, 2007). Exposure to light at night has also been demonstrated to affect insulin resistance, carbohydrate and lipid metabolism, hypertension, coronary heart disease, and myocardial infarction (Haus and Smolensky, 2006). Of all these health problems, none have been more extensively studied than those of coronary heart disease and cancer.

As of 2012, diseases of the heart are the second leading cause of death in Canada (Statistics Canada, 2012), with only cancer outranking it in the number of deaths per year. As such, much research has been directed towards revealing the underpinnings of the association between shift work and heart disease. Knutsson *et al*. first reported in 1986 that shift workers have a 40% increased risk of developing heart disease compared to non-shift workers. Several hypotheses have since been put forth in an attempt to explain this purported link, including the stress of shift work disturbing normal metabolic and hormonal functions (Harma, 2006), and the high percentage of shift workers that engage in health-adverse behaviours such as smoking, drinking, and having a poor diet (Zhao and Turner, 2008). Most notable, however, has been the discovery that depressed melatonin levels due to exposure to light at night have negative effects on the heart. Bulloguh *et al*. (2006) found that melatonin reduces the activity of the sympathetic nervous system and in turn, significantly reduces norepinephrine turnover in the heart. Melatonin is thus beneficial as norepinephrine and epinephrine have both been shown to accelerate the uptake of low-density lipoprotein (LDL) cholesterol. Shift workers may therefore be at an increased risk of developing cardiovascular disease as their melatonin levels are consistently low, resulting in over-activity of the sympathetic nervous system, increased levels of norepinephrine, epinephrine and LDL cholesterol, and decreased levels of HDL cholesterol over time.

A growing number of studies have also suggested that internal desynchronization may

play a key role in the occurrence of endocrine malignancies. The association between disrupted circadian rhythms and the increased rates of cancer has been reported to be due to two main processes: the direct actions of depressed melatonin levels and the secondary endocrine modulations resulting from light exposure and/or sleep disruption. Davis *et al*. (2012) found disturbances in the endogenous sex hormone concentrations of women working night shifts compared to those working day shifts, with night shift working women having elevated levels of follicle stimulating hormone and luteinizing hormone during both night work and daytime sleep compared to day shift working women during nighttime sleep. Indeed, alterations of endogenous sex hormone levels have been well established as being a risk factor for developing breast cancer, the most common type of cancer to afflict women shift workers. On the other hand, the melatonin hypothesis suggests that reduced pineal melatonin secretion may increase the risk of breast cancer by interacting with high levels of estrogen, a known promoter of breast tissue proliferation (Anisimov *et al*., 2004). Melatonin is thought to have a protective effect as it has been shown to prevent the proliferation of tumor cells by shifting the cell balance from proliferation to differentiation, and has also been shown to promote the apoptosis of cancer cells (Navara and Nelson, 2007). In addition, melatonin has been reported to provide protection against cancer development by inhibiting the cell growth of breast cancer cells expressing estrogren receptors (Sanchez-Barcelo *et al*., 2012). Though the exact role of melatonin in relation to these health problems is still unclear, there continues to be an increasing number of studies that support the link between the melatonin hypothesis and shift work.

1.4 The Circadian System and Cognitive Processes

1.4.1 Circadian Rhythm of Learning and Memory

The ability to consciously exert control over one's cognitive performance is dependent upon the combined action of three processes: the circadian process, the homeostatic process, and sleep inertia (Golombek *et al*., 2013). As various cognitive functions throughout the day are regulated by the circadian system, cognitive ability may be impaired if the circadian system is disrupted. One such example is the decrease in cognitive performance due to internal desynchronization. Several studies using both animal and human models have demonstrated an influence of circadian timekeeping on learning and memory (Tapp and Holloway, 1981; Cho *et al*., 2000; Cho, 2001; Ralph *et al.*, 2002). In particular, it has been shown that chronic phase shifts of the light/dark cycle affect memory in rats and mice (Devan *et al*., 2001; Loh *et al*., 2010). Moreover, induced circadian disruption in adult female hamsters was demonstrated to suppress hippocampal neurogenesis, leading to drastic and persistent impairments in learning and memory (Gibson *et al*., 2010). Similarly, deficits in learning and memory in humans have been observed in chronically jet-lagged flight attendants (Cho *et al*., 2000; Cho, 2001). Other studies on people whose circadian rhythms have been disrupted as a consequence of night or shift work have also shown changes in cognitive efficiency. For example, it was documented that shift workers had cognitive impairments that included slowed/delayed reaction times (RT), increased error rates, reduced vigilance, memory impairments (including problems with verbal memory), poor motivation, increased performance variability, reduced subjective alertness, and lower subjective well-being scores (Dijk *et al*., 1992; Horowitz *et al.*, 2001; Santhi *et al*., 2007 and 2008).

Although circadian desynchronization has been documented on multiple occasions to transiently impair several cognitive performance, the exact way in which this occurs is currently not well understood. Kiessling *et al*. (2010) hypothesized that perturbations of cognitive function

may be due to the misalignment of the transcriptional feedback loops driving the molecular clock, as circadian disruption (and jet lag in particular) is characterized by the non-uniform phase resetting of genes that operate in both the positive and negative feedback branches of the clock. In 2005, Rouch *et al*. found that among former shift workers who had stopped shift work for over 4 years, cognitive performance seemed to improve, suggesting a possible reversal of the detrimental effects of shift work. If Kiessling and colleagues' hypothesis is true, Rouch *et al*.'s findings may indeed be a result of the gradual realignment of the feedback loops in the molecular clock, a scenario that is not too farfetched as the body's clocks undergo a similar resynchronization process when recovering from jet lag. In reality, though, shift work is necessary to sustain the world in which we live; thus, developing effective treatments for circadian disorders may be an important strategy for improving the social aspects related to internal desynchronization and cognitive deficiencies, including increasing public safety, health, well-being, and productivity.

1.4.2 Neural Correlates of Attention and Inhibition

The ability to focus attention and plan goals and behaviours accordingly is pertinent to the survival of mankind in this multifaceted world. Just as important, however, is the ability to suppress inappropriate and misguided actions when faced with ambiguous stimuli. Often times, situations arise in which complex decision-making strategies and coordination of actions are required – for example, when faced with competing demands and more than one response option (Behrens *et al*., 2007; Cisek *et al*., 2009). A commonly used experimental task that embodies such a situation is the Stroop task, first developed by J. Ridley Stroop in 1935. In the Stroop task, participants are asked to name the colour of the ink that a colour word is written in (Stroop, 1935). Use of these variables allows for two possible conditions – one in which the ink colour

and the written word match, and one in which the ink colour and the written word do not match. What is known as the Stroop effect occurs when the name of a colour is printed in a colour not denoted by the word (i.e. when the word "blue" is written in red ink), creating a conflict situation between what is automatically read and what response must be given (Stroop, 1935). Participants must therefore inhibit the prepared response of reporting the written word and instead direct attention to the less habitual response of reporting the ink colour, with the result being an increased amount of errors and longer RTs as compared to situations in which no conflict is present (i.e. when the word "blue" is written in blue ink).

An altered version of the Stroop task, known as the emotional Stroop task, uses affective face/word combinations rather than the original Stroop colour/word combinations to create interference situations in which a prepotent response must be inhibited to give a correct answer. Such incongruent conditions, whereby the facial emotion does not match the superimposed affective word (i.e. a happy face with the word "sad" written over top), have also been shown to elicit the well-documented Stroop effect. It has previously been demonstrated in both the Stroop and emotional Stroop tasks that processing of word reading occurs faster than the processing of colour naming or identifying facial expressions (Stroop, 1935; Ovaysikia *et al.*, 2011). Thus in conflict situations inhibition processes resulting from top-down control must be exerted to inhibit the automatic nature of reading out the word – a difficult process that has consistently been shown to be more prone to errors (Ovaysikia *et al.*, 2011).

Previous research on higher cognitive functions has shown the prefrontal cortex to be implicated in response suppression and selection (Miller, 2000; Miller and Cohen, 2001). More specifically, the inferior frontal gyrus (IFG), an area that has been reported to play a key role in language production and response inhibition, was found to exhibit strong lateral activation

during incongruent blocks in both the expression ("report the facial emotion") and word ("report the written word") instruction conditions of the emotional Stroop task (Ovaysikia *et al*., 2011). Additionally, unpublished data from a study performed by DeSouza *et al.* (2003) demonstrated strong bilateral activation of the basal ganglia, specifically the putamen, in participants performing an anti-saccade task. In line with findings from the emotional Stroop task, inhibitory (anti-saccade) blocks of this task resulted in greater activation of the basal ganglia than the reactionary (pro-saccade) blocks (DeSouza *et al*., 2003). Other regions of the brain, namely the amygdala and associated limbic structures, have been shown to be activated in response to affective facial expressions and emotionally salient words (Egner *et al.*, 2008). One particular limbic structure of interest to the current work is the hippocampus. Beyond its role in processing affective faces and words, the hippocampus has been reported to be involved in the consolidation of information from short- to long-term memory (Squire, 1992; Sutherland *et al.*, 2001; Eichenbaum *et al*., 2007), and has also been well documented to be involved in spatial navigation (Morris *et al.*, 1982; Sutherland *et al.*, 1982; Jarrard, 1993; Maguire *et al.*, 1998; Maguire *et al.*, 2000; Clark *et al.*, 2004; Shrager *et al*., 2007). These above-mentioned brain regions are of importance not only because they have been implicated in the inhibition network as well as in the processing of emotion, but also because they have been characterized to have a high concentration of both MT_1 and MT_2 receptor subtypes in animals and humans alike (Morgan *et al.*, 1994; Uz *et al.*, 2005). These brain areas therefore act as ideal regions of interest (ROI) for functional magnetic resonance imaging (fMRI) and diffusion tensor imaging (DTI) analyses, as they combine the study of circadian dysfunction with cognitive performance on the emotional Stroop task.

1.5 Diffusion Tensor Imaging as a Tool for Neural Structural Analysis

1.5.1 DTI Metrics: Fractional Anisotropy, Mean Diffusivity and Fibre Count

Diffusion tensor imaging (DTI) is a non-invasive magnetic resonance imaging technique that maps the *in vivo* diffusion process of water molecules in biological tissue. First used in the mid-1980s, DTI has now gained acceptance in the field as it allows for a better understanding of the brain's structural connectivity through the reconstruction of its major fibre bundles and the production of neural tract images. DTI measurements provide indication of the brain's structure as water diffusion depends on tissue architecture – that is, water diffuses more freely if there is more space between obstacles such as neurons, glial cells, and blood vessels, while less space between these obstacles as a result of cells or blood vessels increasing in size or number results in more restricted diffusion (Le Bihan *et al.*, 2001; Hagmann *et al.*, 2006; Jones *et al*., 2012). During image acquisition, a diffusion gradient is applied that produces a random distribution of proton spin phases and results in an attenuated signal amplitude. The amount of signal reduction depends on the strength of the gradient (known as the *b*-value), as well as the direction that the gradient is applied. In order to model diffusion in three-dimensional space, a tensor ellipsoid with three perpendicular axes (known as eigenvectors) and three distinct diffusion coefficients (known as eigenvalues) must be constructed by applying a minimum of 6 gradient directions, although current practice generally dictates the use of 30 or 64 directions. With the ellipsoid fitted, DTI measurements can then be obtained from each voxel (also known as a volumetric or 3-dimensional pixel) that reflect the average amount of restriction experienced by water molecules moving along the axis of the applied gradient (Jones *et al*., 2012; Soares *et al*., 2013).

DTI analysis consists of four main measurements: fractional anisotropy, mean diffusivity, axial diffusivity, and radial diffusivity. Fractional anisotropy (FA) is a normalized scalar measure

used to characterize the degree of anisotropic diffusion (Soares *et al*., 2013). It is important to note that no directionality can be inferred from FA values alone. Directional information can only be deduced by examining colour-coded FA maps that have specific colours assigned to specific orientations – for example, red representing left-to-right orientation, green representing posterior-to-anterior orientation, and blue representing inferior-to-superior orientation (Soares *et al*., 2013). FA is calculated by dividing the square root of the sum of squares of the diffusivity differences by the sum of squares of the diffusivities and multiplying the division score by $1/\sqrt{2}$ for normalization (Soares *et al*., 2013). When the diffusion coefficients of the second and third axes are small relative to the principle axis, the number in the numerator is almost equal to the number in the denominator and the resulting FA value is close to 1. An FA value of 1 represents purely anisotropic diffusion, or diffusion occurring only along the principle axis. Conversely, when the diffusion coefficient of the second and third axes are large relative to the principle axis, the number in the numerator is much smaller than the number in the denominator, resulting in an FA value that is close to 0. An FA value of 0 represents purely isotropic diffusion, or diffusion occurring along all possible axes. Hence in the brain, FA values are generally lowest in areas containing cerebral spinal fluid as there is little present to restrict diffusion, and highest in areas of dense white matter as tightly packed neurons greatly minimize the possible diffusion directions. Mean diffusivity (MD), also known as the apparent diffusion coefficient, is a scalar measure used to describe the rate of diffusion, regardless of direction (Soares *et al*., 2013). MD values are calculated as the mean of the three eigenvalues (represented as λ_1, λ_2, and λ_3), and are represented in units of m^2/s (Soares *et al*., 2013). Axial diffusivity represents the major eigenvalue of the ellipsoid diffusion tensor, and is the diffusion coefficient that signifies diffusivity along the principle axis (Soares *et al*., 2013). Lastly, radial diffusivity is the average

of the two remaining eigenvalues, and is the average of the diffusion coefficients that represents diffusivity along the two minor axes (Soares *et al*., 2013).

These DTI measurements are not all that can be inferred from the raw data – a technique known as probabilistic tractography can also be used to model fibre orientations in the brain, thus providing more information on white matter microstructure. Probabilistic tractography recreates fibres thought to represent the axons of neurons by starting at a region called the seed region and checking to see whether adjacent voxels have a principal eigenvector in line with the previous voxel (Hagmann *et al*., 2006; Jones *et al*., 2012). If so, the process is repeated, with the outcome being that a neural tract emanating from the seed region and terminating at a secondary location in the brain is inferred. Beyond visually displaying these tracts, tractography also produces a connectivity index along a white matter pathway called a streamline count (SC) that reflects fibre orientation and represents the possible number of valid tracks from a particular point, or between two points in the brain. These SC values can vary widely from brain region to brain region, as well as from person to person. It is important to note that changes in the above-mentioned DTI measurements have clearly been demonstrated to be correlated with changes in brain architecture and white matter microstructure (for a review of white matter modeling, see Nilsson *et al*., 2013).

As DTI is a relatively new technique, the literature remains largely focused on its use in pathology. Only one peer-reviewed article could be found on DTI that pertained to circadian rhythms, and as such the next section will discuss this article in more detail.

1.5.2 DTI and Chronotypes

Chronotypes refer to endogenous dispositions in humans that are categorized according to

the circadian phase of the biological clock and therefore reflect preferences in circadian rhythms (Kerkhof and Van Dongen, 1996; Katzenberg *et al*., 1998). Though the term chronotype encompasses a wide range of cognitive (e.g., efficiency and alertness) and physiological functions (e.g., hormone levels and body temperature), its use commonly refers to sleep and wake habits alone. Thus, those who wake up early, are most alert in the first part of the day, and have difficulty staying up late are referred to as morning people, larks, or early chronotypes (EC); those who sleep late into the day, are most alert in the late evening hours, and go to bed late are referred to as evening people, owls, or late chronotypes (LC). It has been shown that LCs have a large discrepancy between individual sleep preferences and normal day to day schedules, such as in a 9-to-5 working world (Roenneberg *et al*., 2003). As such, deficits in sleep often accumulate over the week, leading to reports of poor sleep quality, tiredness, and psychological disturbances (Giannotti *et al*., 2002). In addition, LCs have been found to consume more legal stimulants (such as nicotine and alcohol) than ECs (Giannotti *et al*., 2002). It has been postulated that LCs exhibit a chronic form of functional jet lag, as their endogenous sleep/wake rhythms do not fit conventional societal schedules (Wittmann *et al*., 2006). As a result of this long-term desychronization between LCs' endogenous rhythms and the external environment, physiological impairments arise and stress is induced due to increased cortisol levels (Cho, 2001). Evidence of structural changes in the brain have been found in people exposed to high levels of cortisol for five years, and cognitive deficits as a result of temporal lobe atrophy have also been demonstrated in those suffering from chronic jet lag (Cho, 2001). Thus, Rosenberg *et al*. (2014) aimed to deduce whether chronic differences in sleep preferences due to chronotype-specificities are associated with structural differences in the brain, and whether chronotype-specificity and health-impairing behaviour are associated with specific neural mechanisms.

Using a 30 direction DTI scan, Rosenberg and colleagues (2014) collected data from 16 healthy male ECs and 23 healthy male LCs between the ages of 18 and 35. They hypothesized that LCs would differ significantly in their lifestyle habits from ECs and that LCs would exhibit significantly different DTI metrics than ECs in the anterior cingulate cortex (ACC), corpus callosum, frontal lobe, and temporal lobes. Consistent with previous literature and with their hypothesis, it was indeed found that LCs consumed significantly more nicotine and alcohol than ECs. They reported no significant correlation between alcohol and nicotine consumption and significant DTI metrics. It was also found that LCs demonstrated significantly lower FA values in the white matter underlying the left ACC, the left frontal lobe, and the left cingulate, and significantly higher MD values in the left cerebrum and left frontal lobe compared to ECs. The differences between LCs and ECs in ACC and temporal lobe white matter were of particular interest, as LCs have been reported to be at a higher risk of developing bipolar disorder and depression (characterized by white matter ACC abnormalities) (Wood *et al.*, 2009; Levandovski *et al*., 2011) and chronic jet lag has been found to result in atrophy of the temporal lobe (Cho, 2001). As such, these significant differences in DTI metrics may be used as an indicator for the development of disease and chronic functional jet lag during aging. Although still preliminary in nature, this study holds much importance as it is the first published report linking endogenous circadian rhythms with structural differences in the brain across ECs and LCs. As the brain is the central component of the mammalian circadian timing network, future research in the field of circadian rhythms should aim to incorporate neuroscience techniques in order to gain a better understanding of the mammalian circadian system as a whole.

1.6 Objectives, Research Questions and Hypotheses

Though much is now known about the use of melatonin to entrain the circadian clock and its resulting effects on rhythmical phenomena such as sleep and the daily rise and fall of core body temperatures (Arendt 2006), little is known about the effects melatonin treatments may have on one's cognitive abilities. Cognitive impairments as a result of shift work or jet lag have only been measured using rudimentary reactionary tasks (Darwent *et al*., 2010; Zhou *et al*., 2011); no studies have used tasks requiring higher cognitive function, nor have any studies looked at the resulting effects on the brain. Furthermore, no studies to date have used melatonin in an attempt to induce desynchronization in a person's once synchronous circadian system. This study thus aims to answer the following research questions:

1) Can exogenous melatonin administered at inappropriate times mimic the internal desynchronization often experience by people participating in shift work or undergoing jet lag, as inferred by behavioural and cognitive changes?
2) Does exogenous melatonin administered at inappropriate times result in deficits in higher cognitive function, as measured by performance in an attention-demanding emotional Stroop task?
3) Does exogenous melatonin administered at inappropriate times alter white matter microstructure in the brain, specifically in areas associated with higher cognitive function?

It is hypothesized that: 1) sleep and wake cycles will be altered, interpreted to indicate that melatonin is an effective agent in shifting participants' internal clocks out of phase with the external environment and with each other; 2) administration of exogenous melatonin will result in significantly increased RTs and errors for both instruction sets on the emotional Stroop task;

and 3) administration of exogenous melatonin will result in significantly altered DTI metrics, particularly in the areas of the IFG and the hippocampus.

2. Materials and Methods

2.1 Participants

Ten healthy, right-handed participants (4 males and 6 females, mean age ± SD = 26.8 ± 6.25 years) were included in this within-subject, single-blind-designed study. All participants were screened prior to the start to ensure that they had no history of neurological disorder and were free of prescription medication, with the exception being the use of hormonal birth control. All participants were fluent in English and had normal or corrected-to-normal visual acuity. All procedures and protocols were approved by the York University Human Participants Review Subcommittee and Ethics Review board (certificate #2012 – 209). All participants gave their informed consent prior to participating in the study and were debriefed accordingly.

2.2 Behavioural Procedures

2.2.1 Behavioural Logs and Questionnaires

All participants were asked to keep a log of their daily behaviours for the duration of the study, which consisted of a minimum of two weeks prior to the start of baseline testing, during the two weeks of baseline testing, and during the eight days of experimental manipulation (see Appendix A for a timeline of data collection). These behaviours included their time of waking, sleeping, and meals taken, as well as a brief list of activities they participated in throughout the day. These behavioural logs were reviewed on an ongoing basis to ensure that all subjects exhibited a consistent pattern of behaviours (i.e. that their sleeping, waking, and eating schedules did not deviate drastically from day to day). From these logs, participants' sleep and wake times were charted and their dim-light melatonin onset (DLMO) time was estimated by subtracting 2.5

hours from their average baseline sleep time. This calculation was based on Martin and Eastman's (2002) work, which demonstrated that healthy adults' reported sleep times occur 2 to 3 hours after DLMO. Furthermore, participants were asked to fill out the online Munich Chronotype Questionnaire (MCTQ) and to e-mail the resulting PDF file to the researcher when completed. These PDF files, which contain the participants' chronotypes, were taken into consideration when analyzing their melatonin profiles (see Appendix B for an example). The MCTQ can be found at:

https://www.bioinfo.mpg.de/mctq/core_work_life/core/introduction.jsp.

2.2.2 Emotional Stroop Task

In order to assess participants' cognitive abilities, an altered version of Ovaysikia *et al*.'s (2011) emotional Stroop task was used. The emotional Stroop task was chosen as it employs the use of two distinctly different components (i.e. a picture of a face and a word) compared to the colour/word Stroop task, which only employs the use of word stimuli. Having both faces and words thus allowed for better interpretation of the data, as faces and words are processed through different pathways in the brain. The emotional Stroop task was coded and presented using Presentation 12.1 (Neurobehavioural Systems, Inc., CA, USA). All pictures were taken using a Sony DSLRA330L camera. Affective words were superimposed at a 45° angle over the face images using Eye Batch 2.1 (Atalasoft Inc., Easthampton, MA, USA) and all images were processed to equalize the isoluminance levels. Participants sat at a table with their head placed in a head-chin rest during data collection, and the lights in the experimental room were extinguished during the data collection period. There were a total of 216 different combinations of faces and words (happy, neutral, and sad), with 12 different individual identities. Images were presented on a high contrast black background at a visual angle of 12.50° horizontally and 18.66°

vertically. Fixation crosses were presented at a visual angle of 2.4° at the center of the screen. Prior to administering the task, participants were instructed and underwent a practice session consisting of one run with the instruction to "attend and respond to the word" and a second run with the instruction to "attend and respond to the face". The task employed a block-design paradigm as follows: (1) an instruction screen appears for ten seconds, reminding participants of the instruction previously given as well as indicating the response buttons for the corresponding emotions (1 for happy, 2 for neutral, 3 for sad; see Figure 3); (2) 12 pictures are presented in succession for two seconds each, during which time participants must process the image on the screen and give a response – these 12 pictures make up one block; (3) a fixation cross appears for eight seconds, after which the next block of 12 pictures begins; (4) at the end of 15 blocks (five congruent blocks and ten incongruent blocks), a final fixation cross appears for 16 seconds, indicating the end of a run. The order of blocks was consistent between all runs and participants, with the pattern of one congruent block followed by two incongruent blocks being repeated five times per run. Each run lasted for a total of 498 seconds, with the starting instruction set (face or word) counterbalanced between participants. Participants performed 4 runs of each instruction set for each of the baseline and experimental periods, after which the latency of responses (reaction time, or RT) and the accuracy of the responses were analyzed using MATLAB version 7.10 (Natick, MA, USA). RTs and errors were averaged within each of the incongruent and congruent conditions separately for the face and word instruction sets. Statistical tests were performed using repeated measures ANOVAs on IBM SPSS Statistics version 20 (Armonk, NY, USA). This paradigm differed from that of Ovaysikia *et al*. (2011) in several ways: first, a block-design with 12 pictures per block was used as opposed to a pseudo-event related design with 6 pictures per block; second, response images were not used in the current study; third, each

picture was presented for a total of two seconds compared to the 250ms presentation previously used; and fourth, the fixation crosses appeared for eight seconds instead of one second. All other components of the paradigm remained the same.

Figure 3. Example images from the emotional Stroop paradigm. 3 congruent and 3 incongruent pictures are shown. 12 congruent or incongruent pictures were displayed for 2 seconds each in their respective blocks. Participants were instructed to either attend to and report the facial emotion, or attend to and report the written word. Image obtained from Ovaysikia *et al*., 2011.

2.3 Desychronization Protocol

In an attempt to recreate the internal desynchronization that is often experienced by people participating in shift work or who suffer from jet lag, eight administrations of 1.5mg sublingual melatonin pills were used to shift participants' internal clocks out of phase with the external environment and with each other. Sublingual pills were used in order to deliver the melatonin into the blood stream as a Zeitgeber pulse. The pills were prepared by cutting 3mg Webber Naturals Melatonin tablets (Coquitlam, BC, Canada) in half, grinding them into a fine powder and transferring them into a size 4 gelatin capsule (Pompano Beach, FL, USA). To take the pill, participants were instructed to place the pill under their tongue and to keep it there until

fully dissolved (approximately five minutes). Each participant was given eight of these pills along with a desynchronization protocol consisting of specific times during the day at which they were to take the pills (see Appendix C for an example). The desynchronization protocol was specific to participants' daily behaviours as well as to their chronotypes, and consisted of two days of taking the pill in the early afternoon and two days of taking the pill in the late morning, repeated twice over eight days. This protocol was designed based on a well-established melatonin phase-response curve (Lewy *et al*., 1998) to ensure that participants were fully subjected to internal desynchronization, as the melatonin pills were given when melatonin levels are generally low.

2.4 Biological Samples and Assays (ELISAs)

2.4.1 Saliva Samples

Prior to the start of saliva sample collection, participants were provided with a set of pre-numbered, 1.5ml graduated microtubes (Diamed Lab Supplies Inc., Mississauga, ON, Canada; product number DIATEC610-3168). The numbers on these collection containers matched a specifically designed collection protocol that catered to both participants' chronotype and their daily behaviours. This protocol allowed for more sparse collection during daytime hours (when melatonin levels are generally very low) (Pandi-Perumal *et al*., 2006) and more frequent sampling starting at a computed DLMO time and through the evening (when melatonin levels begin to rise and stay elevated, respectively). Participants were instructed to refrain from eating, drinking and brushing their teeth at least 15 minutes prior to starting the collection, as well as to rinse their mouths thoroughly with cold water before providing the saliva sample. Participants were also instructed to provide a minimum of 1ml of saliva per collection, using the markings on

the side of the collection container as reference points (see instructions in Appendix D). During the baseline period, participants were asked to provide saliva samples over three days (see Appendix E for an example). These saliva samples were refrigerated between 2 – 8°C during the week the sampling took place, then placed in a -80°C freezer for storage until assayed. Similarly, participants were asked to provide saliva samples over eight days during the experimental period. These samples were also refrigerated between 2 – 8°C during the week the sampling took place, then placed in a -80°C freezer for storage until assayed.

2.4.2 Enzyme-Linked Immunosorbent Assay

To establish the melatonin profiles of each participant, preliminary enzyme-linked immunosorbent assays (ELISAs) were performed to determine the concentration of melatonin in two subjects' baseline saliva samples. However due to unforeseen circumstances regarding issues with funding (see Appendix G and H), ELISAs could not be completed for the remainder of the collected samples. The ELISA kits used were developed by IBL International and distributed by AFFINITY Diagnostics Corporation (Toronto, ON, Canada). The ELISA follows a capture antibody technique, whereby competition occurs between a biotinylated and a non-biotinylated antigen for a fixed number of antibody binding sites on the highly specific polyclonal Kennaway G280 anti-melatonin antibody. The amount of bound biotinylated antigen, which is inversely proportional to the concentration of melatonin in the sample, is determined by use of an enzyme marker (streptavidin conjugated to horseradish peroxidase) and a chromogenic substrate (tetramethylbenzidine) that results in a colour change from blue to yellow once an acidic stop solution is added. The optical density of the solution can then be read with a spectrophotometer at 450nm and quantification of the unknowns can be determined by comparing the enzymatic activity of the unknowns against a standard curve. The analytical

sensitivity (limit of detection) of the ELISA kits for melatonin in saliva was 0.3pg/mL. For this study, each saliva sample was run in duplicate in order to minimize experimental error. The optical densities of the samples were read using a Thermo Scientific Multiskan Spectrum spectrophotometer (Thermo Fisher Scientific Inc., Waltham, MA, USA). All procedures were conducted as per IBL International's Non-Extraction Melatonin Saliva ELISA Instructions for Use manual and no changes were made to this protocol. The resulting data were plotted in MATLAB version 7.10 (Natick, MA, USA) and a cosinor analysis was carried out (Lerchl and Partsch, 1994), whereby the sum of squares equation was used to fit a sinusoidal curve to the data points by squaring and summing the distances between each point to find the smallest sum of squares value.

2.5 Scanning Procedures

Participants were each scanned using magnetic resonance imaging (MRI) on two occasions: once after the baseline period and once immediately after the experimental period. The baseline scans occurred within one week of participants providing their saliva samples for the baseline period; the experimental scans occurred on the last of the eight days that participants provided their saliva samples for the experimental period. All scanning sessions occurred within within one to two weeks of administering the last emotional Stroop test. Each scanning session was 20 minutes in length and involved three components: an anatomical scan (6 minutes), a resting-state scan (8 minutes) and a DTI scan (4.5 minutes). All imaging was performed using a 3-Tesla Siemens Tim Trio whole body MRI scanner equipped with a 32-channel head coil, located in the Sherman Health Sciences Building of the Center for Vision Research at York University. Participants lay supine in the scanner with earplugs and cushions around their heads

so as to reduce both acoustic noise and head motion. Participants were instructed to close their eyes and let their mind wander for the resting state scan, while for the anatomical and DTI scans participants had the option to keep their eyes open or closed.

T1-weighted anatomical images were acquired with the following parameters: spin echo, matrix = 256 x 256 pixels, voxel size = $1mm^3$, TR = 1900ms, TE = 2.52ms, flip angle = 9°. T2*-weighted images were acquired with the following parameters: GRAPPA echo planar imaging with an acceleration factor of 2x, slices = 32, matrix = 56 x 70 pixels, FOV = 210mm x 168mm, voxel size = 3mm x 3mm x 4mm, TR = 2000ms, TE = 30ms, flip angle = 90°. Diffusion-weighted images were acquired with the following parameters: slices = 60, base resolution = 122 x 122 pixels, reconstructed matrix = 976 x 976 pixels, FOV = 240mm, voxel size = 1.97mm x 1.97mm x 2mm, TR = 8300ms, TE = 100ms, flip angle = 90°, slice thickness = 2mm, inter-slice interval = 138ms, gradient directions = 30, b value = $1000s/mm^2$.

2.6 Data Analysis

2.6.1 DTI Pre-processing

From the scans, DTI data were chosen to be analyzed as this technique is highly sensitive to changes in the brain (Jones *et al*., 2012). All DTI data analyses were performed using FSL version 4.1.9 (Analysis Group, FMRIB Software Library, Oxford, UK). Prior to preprocessing, all raw DTI and T1 series images were converted from DICOM to 4D NIfTI nii files using the dcm2nii program (developer Chris Rorden, South Carolina, USA) to ensure compatibility with the FSL software. Once converted, the Eddy Current Correction option in the FDT Diffusion Toolbox version 2.0 was used to perform motion correction, correcting for any movement and distortions that may have occurred during the scanning session. The BET Brain Extraction

Toolbox version 2.1 was then used to generate skull-stripped images for each subject. The fractional intensity threshold was lowered from the default of 0.5 to 0.3 in order to prevent parts of the cortex being removed with the skull during the process of brain extraction. Once complete, the diffusion tensor model was fitted to the data using the DTIFIT Reconstruct Diffusion Tensors option in the FDT Diffusion Toolbox. This step fit a diffusion tensor model at each voxel, generating eigenvector, eigenvalue, fractional anisotropy (FA) and mean diffusivity (MD) maps. Following DTIFIT, a Bayesian Estimation of Diffusion Parameters Obtained Using Sampling Techniques (BEDPOST) analysis was conducted using the BEDPOSTX Estimation of Diffusion Parameters option in the FDT Diffusion Toolbox. This analysis yielded files necessary to carry out probabilistic tractography once registration was complete. Registration allows tractography results to be stored in spaces other than diffusion space, and was carried out using the Linear Image Registration Tool within the FDT Diffusion Toolbox. The files resulting from registration are transformation matrices between diffusion, structural and standard space, with the transformation matrices between diffusion and structural space being derived using 6 degrees of freedom and the transformation matrices between structural and standard space being derived using 12 degrees of freedom.

2.6.2 Tract-Based Spatial Statistics and Voxelwise Statistics

Tract-based spatial statistics (TBSS) were run using FSL version 4.1.9 (Analysis Group, FMRIB Software Library, Oxford, UK). TBSS is commonly conducted through use of FA images in voxelwise statistical analyses. In this study, TBSS was run in order to localize changes in the brain related to performing and learning an attentional task while undergoing internal desynchronization. First, all subjects' FA images were eroded slightly and the end slices zeroed to remove likely outliers from the diffusion tensor fitting. Non-linear registration (one

registration per subject) was then run in order to align all subjects' FA images using a $1mm^3$ FMRIB58_FA standard space image as the target. Following registration, each subject's FA image was non-linearly transformed to the target and affine-aligned to bring them into the 1x1x1mm MNI152 standard space, which resulted in the transformation of each subject's original FA images into standard-space versions. These standard-space FA images were then merged into a single 4D image file and the mean of all FA images created, with this mean then being skeletonised. The mean FA skeleton image was then thresholded at a value of 0.2, which produced a binary skeleton mask that defines the set of voxels used in subsequent analyses. Lastly, all subjects' aligned FA data were projected onto the mean FA skeleton, which resulted in a single 4D image file containing the projected skeletonised FA data.

Voxelwise statistics were run using the projected skeletonized 4D image file to determine which FA skeleton voxels were significantly different between the two groups of subjects. The randomize tool was used to run the statistics, with the design matrix set up as a *t*-test for a simple two-group comparison (baseline vs. experimental condition). In addition to the randomize tool, the threshold-free cluster enhancement (TFCE) option was used for robust cluster-based thresholding. This statistical test resulted in two TFCE *p*-value contrast image files that are fully corrected for multiple comparisons across space (contrast 1: baseline > experimental; contrast 2: experimental > baseline), with a threshold of 0.95 giving rise to significant clusters of FA voxels in each of the contrasts. From these contrast image files, whole brain and ROI specific FA values from the IFG were extracted for raw data comparison between the baseline and experimental two conditions.

The entirety of this procedure was repeated to determine significant differences in MD voxels in each of the contrasts. Similar to TBSS with the FA data, the original nonlinear

registration was applied to the MD data and all subjects' warped MD data were merged into a single 4D image file. This 4D image file was then projected onto the original mean FA skeleton, as the original FA data were used to find the projection vectors for the MD data. This resulted in a 4D projected MD data file on which the voxelwise statistics were run (in the same manner as described above). From these contrast image files, whole brain and ROI specific MD values from the IFG were extracted for raw data comparison between the two conditions.

2.6.3 Tractography

Probabilistic tractography was carried out using the PROBTRACKX Probabilistic Tracking option in the FDT Diffusion Toolbox of FSL. Prior to running tractography, two single masks of the left and right hippocampi, the seed ROIs, were made in FSLView version 3.1.8, defining the voxels from which streamline quantification (tractography) would emanate. This was done by locating the desired structure on the Juelich Histological Atlas and creating a binary mask on the T1 image of the Montreal National Institute's MNI152 1mm standard brain. Once complete, the mask image was loaded into FDT and the previously calculated standard to diffusion transformation matrix was defined, as the seed image was created in standard and not diffusion space. A single waypoint mask of the inferior frontal gyrus (IFG) with both the left and right hemispheres defined was used as an inclusion mask – that is, tracts that did not pass through this mask were discarded from the calculation of the connectivity distribution. The IFG was chosen as an ROI for this study as fMRI results previously published by Ovaysikia *et al*. (2012) demonstrated strong bilateral activation of this area when participants performed the emotional Stroop task. The number of samples (or the number of individual pathways that are drawn through the probability distributions on the principle fibre direction) was set to 5000, and the curvature threshold (or the limit of how sharply pathways can turn as an exclusion criteria for

implausible pathways) was set to 0.2 (corresponding to a minimum angle of approximately 80°). The Loopcheck option was also selected, which allowed the program to terminate pathways that traveled to a point where they have already been. The step length was set to 0.5mm and the maximum number of steps was set to 2000, which together, corresponds to a distance of 1m (after which samples are terminated). This tractography procedure resulted in an image of the connectivity distribution summed from all the voxels in the seed ROI and passing through the defined waypoint masks.

3. Results

3.1 Behavioural Results

3.1.1 Validation of Emotional Stroop Paradigm

The current emotional Stroop task was first used by Ovaysikia *et al*. (2011), who demonstrated that participants had a significantly higher mean RT and a significantly greater amount of errors when instructed to respond to the facial emotion compared to the written word. In an attempt to validate this paradigm for our purposes, the four baseline runs of each instruction set were averaged for all 10 participants of the current experiment to determine whether the same trends would be found. A paired samples Student's *t*-test was performed on the RTs of the face and word instruction sets, as well as on the number of errors in the face and word instruction sets (Table 1 in Appendix F). Indeed, it was found that participants had a significantly higher mean RT ($t_{(9)} = 10.492$, $p < 0.001$) and a significantly greater amount of errors ($t_{(9)} = 4.675$, $p < 0.001$) when instructed to respond to the facial emotion compared to the written word (Figure 4).

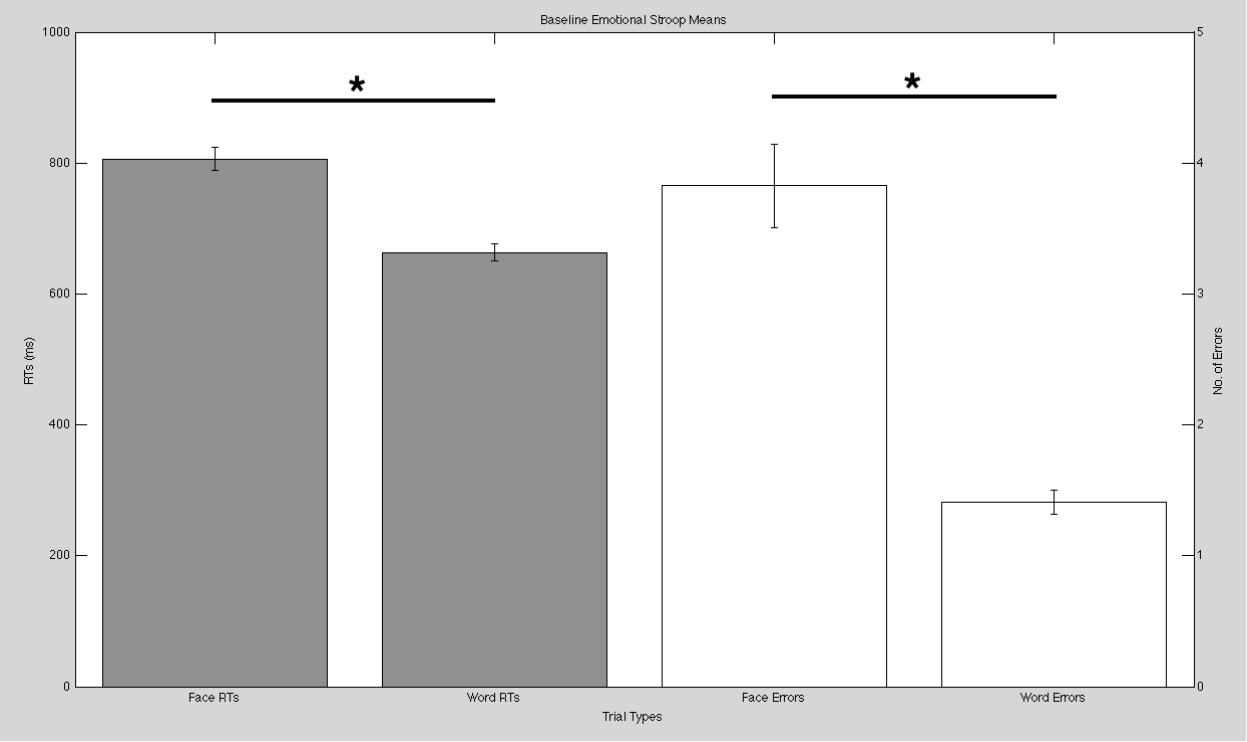

Figure 4. Overall mean reaction times (RTs; grey bars) and errors (white bars) from ten subjects performing the emotional Stroop task during the baseline period. Congruent and incongruent trials have been collapsed within each instruction set to validate the emotional Stroop test by showing that the current data corroborate those published by Ovaysikia *et al.* (2011). The error bars signify the standard error of the mean (SEM). There was a statistically significant difference between the face and word instruction sets for both the RTs ($p < 0.001$) and errors ($p < 0.001$).

Further breaking down each instruction set into its component congruent and incongruent trials revealed an expected Stroop effect, whereby the incongruent trials resulted in longer RTs and more errors, regardless of instruction. Results from a paired samples Student's *t*-test performed on the RTs of the congruent and incongruent trials for the face instruction (Table 2 in Appendix F) demonstrated a significantly higher mean RT for the incongruent trials ($t_{(9)} = 4.783$, $p < 0.001$; Figure 5) compared to the congruent trials. Similarly, results from a paired samples Student's *t*-test performed on the RTs of the congruent and incongruent trials for the word instruction (Table 2 in Appendix F) demonstrated a significantly higher mean RT for the incongruent trials ($t_{(9)} = 2.357$, $p < 0.05$; Figure 5) compared to the congruent trials. Moreover, results from a paired samples Student's *t*-test performed on the total number of errors of the

congruent and incongruent trials for the face instruction (Table 2 in Appendix F) demonstrated a significantly greater amount of errors for the incongruent trials ($t_{(9)} = 5.325$, $p < 0.001$; Figure 5) compared to the congruent trials. Lastly, results from a paired samples Student's *t*-test performed on the total number of errors of the congruent and incongruent trials for the word instruction (Table 2 in Appendix F) also demonstrated a significantly greater amount of errors for the incongruent trials ($t_{(9)} = 5.075$, $p < 0.001$; Figure 5) compared to the congruent trials. Overall, the incongruent trials of the face instruction set resulted in the longest RTs and the greatest amount of errors, followed by the congruent trials of the face instruction set, the incongruent trials of the word instruction set, and the congruent trials of the word instruction set, which produced the shortest RTs and the least amount of errors.

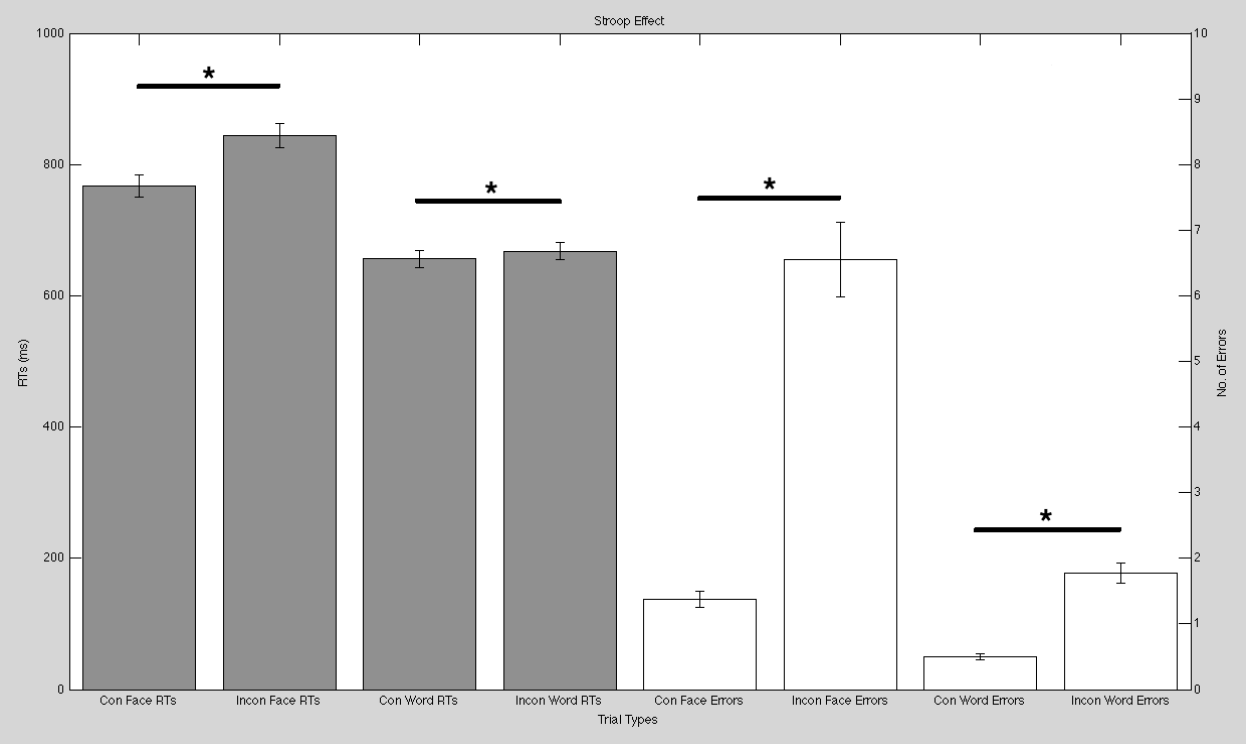

Figure 5. Overall mean reaction times (RTs; grey bars) and errors (white bars) from ten subjects performing the emotional Stroop task during the baseline period. The error bars signify the standard error of the mean (SEM). A Stroop effect is demonstrated, with significantly longer RTs for the incongruent trials in both the face ($p < 0.001$) and word ($p < 0.05$) instruction sets, as well as significantly more errors for the incongruent trials in both the face ($p < 0.001$) and word ($p < 0.001$) instruction sets.

3.1.2 Behavioural Measures: Sleep Times

To assess the effect of the melatonin treatment on sleep, participants' logs of their daily sleep times during both baseline and experimental periods were analyzed. Participants' sleep times were normalized to time of dim-light melatonin onset (DLMO = time 0), and a paired samples Student's *t*-test was performed (Table 3 in Appendix F). There was a significant difference between baseline and experimental sleep times for all participants' pooled sleep data ($t_{(9)} = 2.945$, $p < 0.05$), with a leftward-shifted mean and a lower amplitude of distribution during the experimental period (Figure 6).

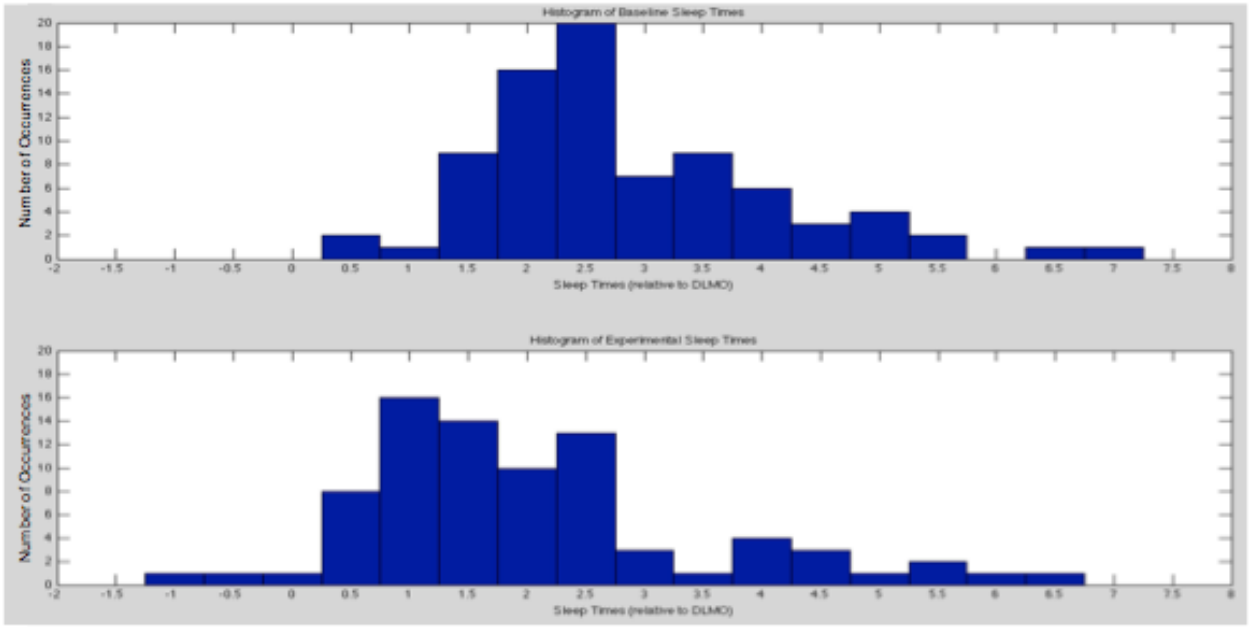

Figure 6. Histogram of ten subjects' baseline (top panel) and experimental (bottom panel) sleep times. Numbers on the x-axis represent times relative to dim-light melatonin onset (DLMO = time 0); numbers on the y-axis represent frequency (i.e. the number of occurrences). All ten subjects took part in the **melatonin** treatment. There was a statistically significant difference between the baseline and experimental sleep times ($p < 0.05$).

Further breaking down the data into the individual baseline and experimental days demonstrated a strong effect of the melatonin treatment on participants' sleep times. Administering the melatonin treatment in the afternoon on days 1, 2, 5, and 6 of the experimental

period resulted in an overall shift towards earlier than average sleep times, while administering the melatonin treatment in the morning on days 3, 4, 7, and 8 of the experimental period resulted in an overall shift towards later than average sleep times (Figure 7). Paired samples Student's *t*-tests indicated significant differences between day 1 of melatonin treatment and all days preceding it ($p < 0.05$ for all comparisons) as well as between day 1 and day 4 of melatonin treatment ($p < 0.005$), indicating that the melatonin treatment worked as expected. Of interest to note is that day 1 of the experimental period demonstrated the largest effect of melatonin on sleep, as all participants' sleep times shifted to an earlier than average time (Figure 7). No significant difference in variability between baseline and experimental sleep times was found ($p > 0.1$), though a trend of increasing variability was demonstrated over the course of the eight day experimental period (insets in Figure 7 and Figure 8).

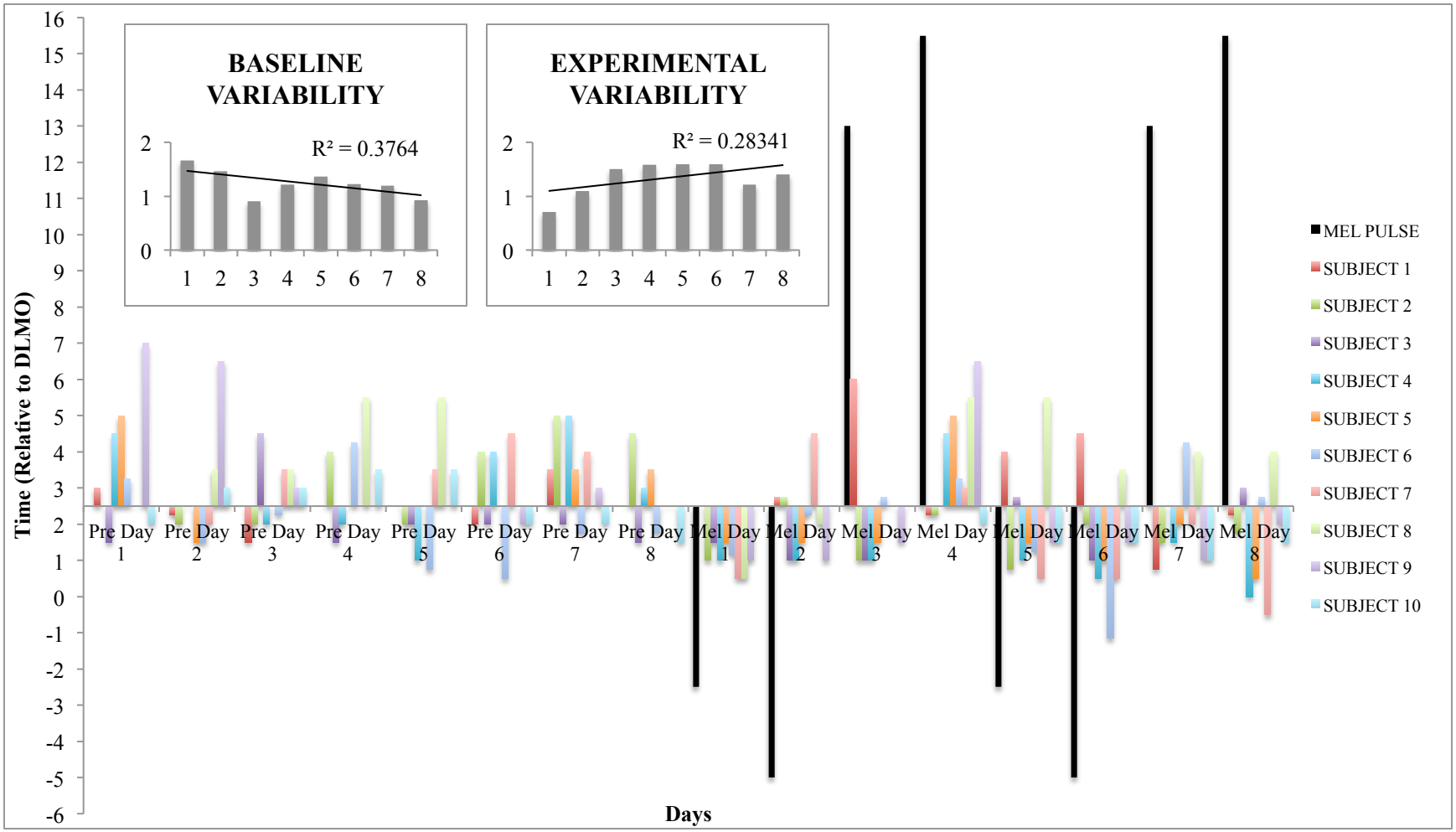

Figure 7. Individual baseline and experimental sleep data from all ten subjects. The first 8 groupings on the x-axis represent the 8 baseline days, while the last 8 groupings represent the 8 experimental days. Numbers on the y-axis represent sleep times relative to dim-light melatonin onset (DLMO = 0). The x-axis crosses at time 2.5 on the y-axis, which is the average sleep time. Bars below the x-axis represent sleep times occurring before average; bars above the x-axis represent sleep times occurring after average. Coloured bars represent each individual subjects' sleep times on that specific day; black bars represent exogenous melatonin administered to participants during the eight days of the experimental period. Graphical insets show a trend of decreasing variability in sleep times during the baseline period and a trend of increasing variability in sleep times during the experimental period, though no statistically significant difference was found ($p > 0.1$).

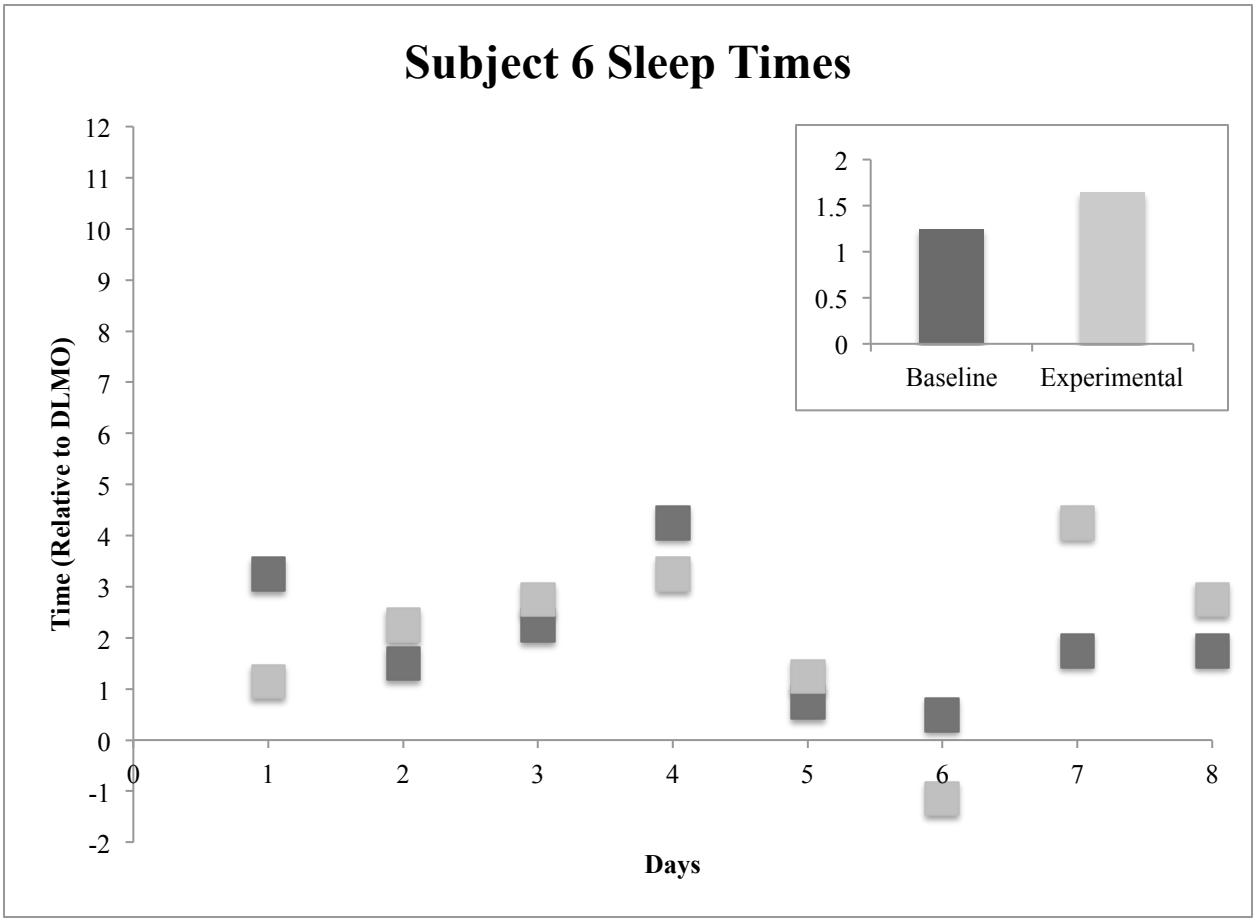

Figure 8. Example of Subject 6's sleep data. Numbers on the x-axis represent the 8 baseline and 8 experimental days; numbers on the y-axis represent times relative to dim-light melatonin onset (DLMO = time 0). Dark grey squares represent baseline sleep times; light grey squares represent experimental sleep times. Graphical inset shows an increase in variability between baseline and experimental sleep times.

3.1.3 Behavioural Measures: Wake Times

To assess the effect of the melatonin treatment on waking, participants' logs of their daily wake times during both baseline and experimental periods were analyzed. Similar to the analysis of sleep times, participants' wake times were normalized to time of dim-light melatonin onset (DLMO = time 0), and a paired samples Student's *t*-test was performed (Table 4 in Appendix F). There was no significant difference between baseline and experimental wake times as demonstrated by the resulting two-tailed *p* value ($t_{(9)} = 1.788$, $p > 0.05$). However, as an estimate of directionality was previously hypothesized, a one-tailed *p* value was chosen in favour of the

two-tailed p value to indicate significance. As such, the results demonstrate a significant difference between baseline and experimental wake times ($t_{(9)} = 1.788$, $p < 0.05$), with a slightly leftward-shifted mean and a slightly lower amplitude of distribution during the experimental period (Figure 9).

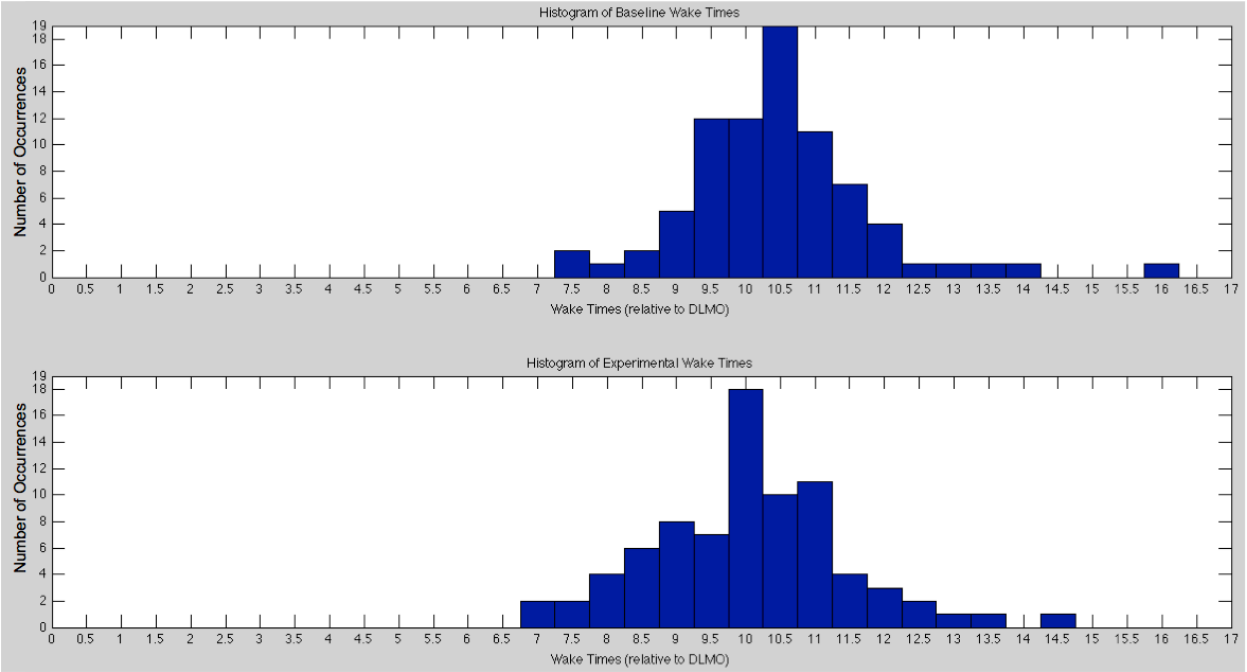

Figure 9. Histogram of ten subjects' baseline (top panel) and experimental (bottom panel) wake times. Numbers on the x-axis represent times relative to dim-light melatonin onset (DLMO = time 0); numbers on the y-axis represent frequency (i.e. the number of occurrences). All ten subjects took part in the **melatonin** treatment. There was a statistically significant difference between the baseline and experimental wake times ($p < 0.05$, one-tailed t-test).

Further breaking down the data into the individual baseline and experimental days also demonstrated an effect of the melatonin treatment on participants' wake times. Administering the melatonin treatment in the afternoon on days 1, 2, 5, and 6 of the experimental period resulted in an overall shift towards earlier than average wake times, while administering the melatonin treatment in the morning on days 3, 4, 7, and 8 of the experimental period resulted in an overall shift towards later than average wake times (Figure 10). Of interest to note is that days 1 and 8 of the experimental period shifted all but one participants' wake times in the same direction (Figure

10). No significant difference in variability between baseline and experimental sleep times was found ($p > 0.5$), though a slight trend of increasing variability was demonstrated over the course of the eight day experimental period (insets in Figure 10 and Figure 11).

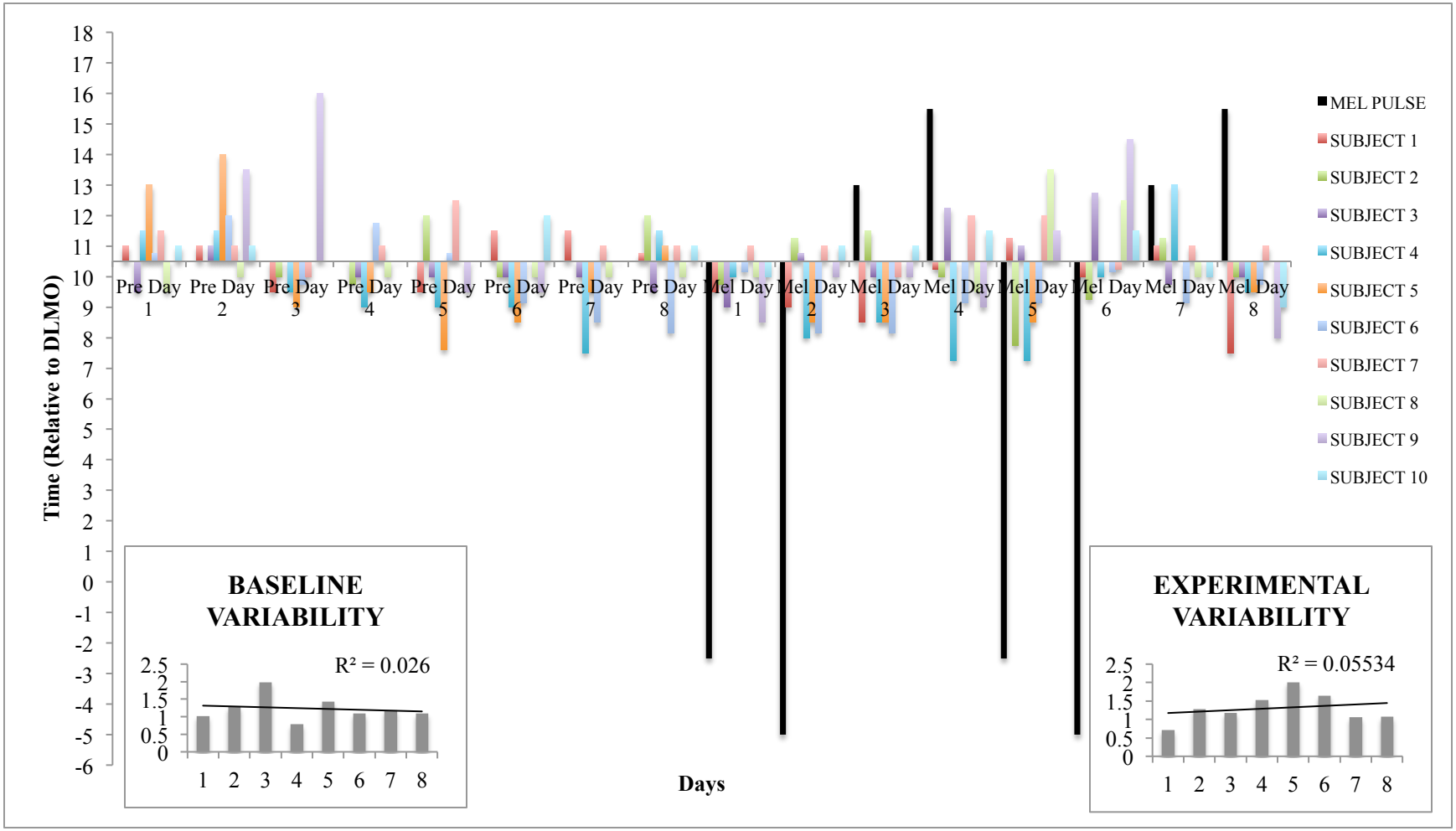

Figure 10. Individual baseline and experimental wake data from all ten subjects. The first 8 groupings on the x-axis represent the 8 baseline days, while the last 8 groupings represent the 8 experimental days. Numbers on the y-axis represent wake times relative to dim-light melatonin onset (DLMO = 0). The x-axis crosses at time 10.5 on the y-axis, which is the average wake time. Bars above the x-axis represent wake times occurring before average; bars above the x-axis represent wake times occurring after average. Coloured bars represent each individual subjects' wake times on that specific day; black bars represent exogenous melatonin administered to participants during the eight days of the experimental period. Graphical insets show almost no change in variability in wake times during the baseline period and a slight trend of increasing variability in wake times during the experimental period, though no statistically significant difference was found ($p > 0.5$).

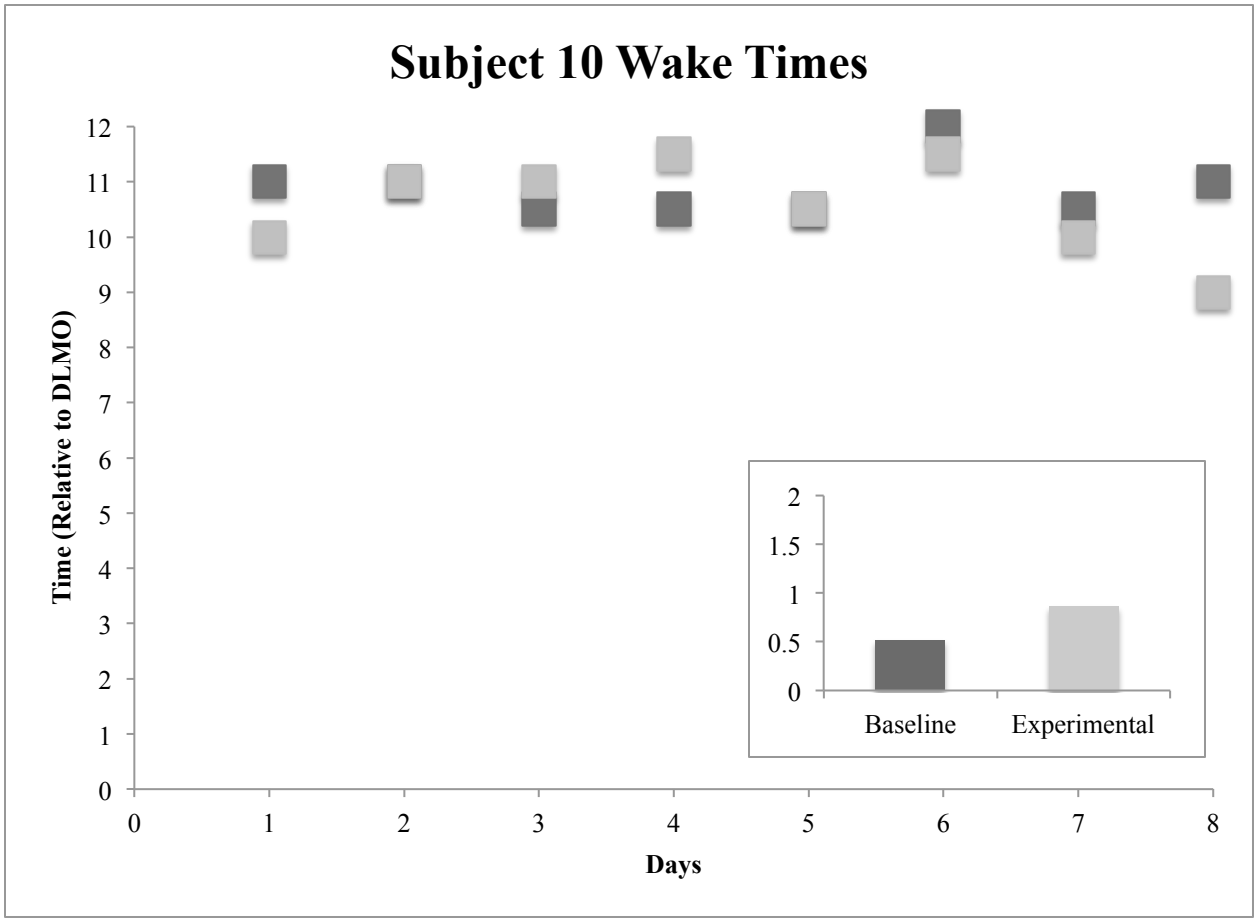

Figure 11. Example of Subject 10's wake data. Numbers on the x-axis represent the 8 baseline and 8 experimental days; numbers on the y-axis represent times relative to dim-light melatonin onset (DLMO = time 0). Dark grey squares represent baseline wake times; light grey squares represent experimental wake times. Graphical inset shows an increase in variability between baseline and experimental wake times. Note that the baseline and experimental data points for days 2 and 5 overlap.

3.1.4 Behavioural Measures: Sleep Quality Ratings

To assess the effect of the melatonin treatment on sleep quality, participants' logs of their daily sleep quality ratings during both baseline and experimental periods were analyzed. Two participants did not report their sleep quality ratings and were thus left out of the analysis. The third participant's sleep quality ratings were determined to be outliers as they did not fit the consistent trend exhibited by the remaining participants, and the data were thus excluded from the analysis. The exclusion of these three participants resulted in a sample size of seven for each

of the baseline and experimental periods; thus a linear mixed models test was used for the analysis (Table 5 in Appendix F). A significant difference between baseline and experimental sleep quality ratings was found ($t_{(6)} = 3.007$, $p < 0.005$; Figure 12). On average, participants reported a poorer quality of sleep during the experimental period than the baseline period, with more ratings of 2 (poor sleep), 3 (average sleep) and 4 (good sleep) than 5 (excellent sleep).

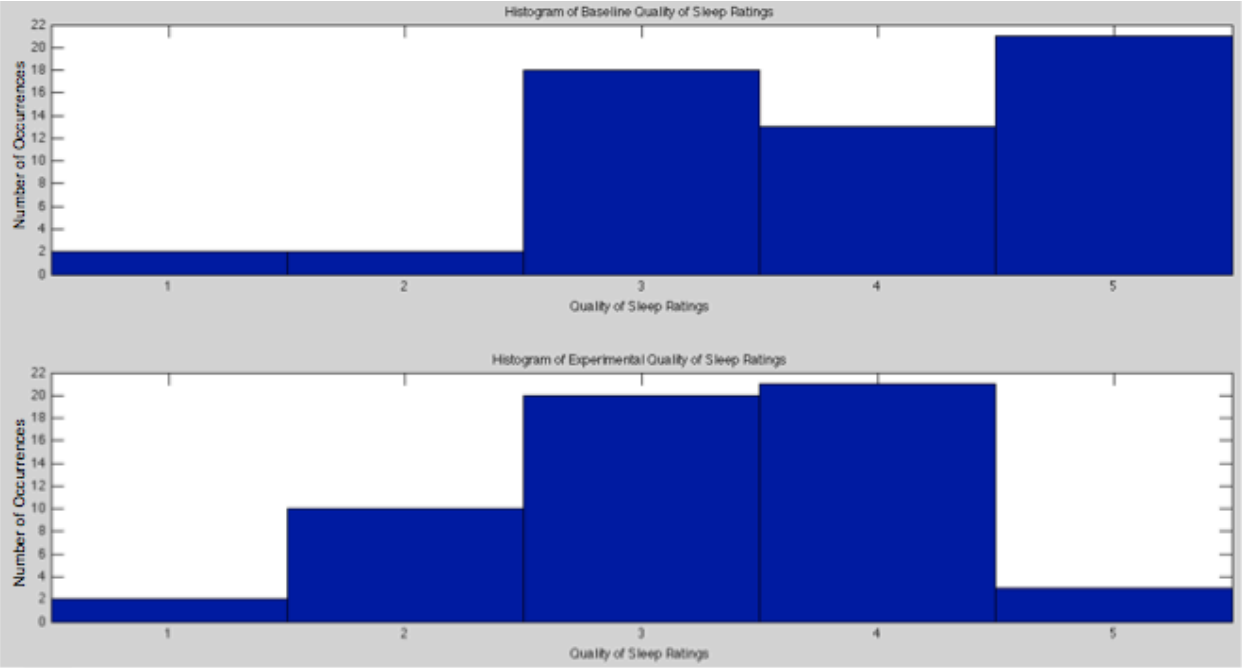

Figure 12. Histogram of seven subjects' baseline (top panel) and experimental (bottom panel) quality of sleep ratings. Two of the remaining three subjects did not report their sleep quality ratings throughout the experiment and one subject's ratings were determined to be outliers, thus these participants were excluded from the analysis. Numbers on the x-axis represent subjects' self-reported quality of sleep (1 = very poor; 2 = poor, 3 = average; 4 = good; 5 = excellent); numbers on the y-axis represent frequency (i.e. the number of occurrences). All seven subjects took part in the **melatonin** treatment. There was a statistically significant difference between the baseline and experimental quality of sleep ratings ($p < 0.005$).

3.1.5 Emotional Stroop Task

During the eight-day experimental period, participants were tested on the emotional Stroop task four times. Participants' performance on this task was used as a measure of cognitive ability while undergoing the melatonin treatment. Paired samples Student's *t*-tests revealed a

Stroop effect in three of the four conditions (Table 6 in Appendix F), with the incongruent trials resulting in significantly higher mean RTs in the face instruction ($t_{(9)} = 4.973$, $p < 0.001$) and significantly more errors in both the face ($t_{(9)} = 5.075$, $p < 0.001$) and word ($t_{(9)} = 8.187$, $p < 0.001$) instructions (Figure 13). There was no significant difference in RTs between the congruent and incongruent trials for the word instruction ($t_{(9)} = 0.880$, $p > 0.1$; Figure 13).

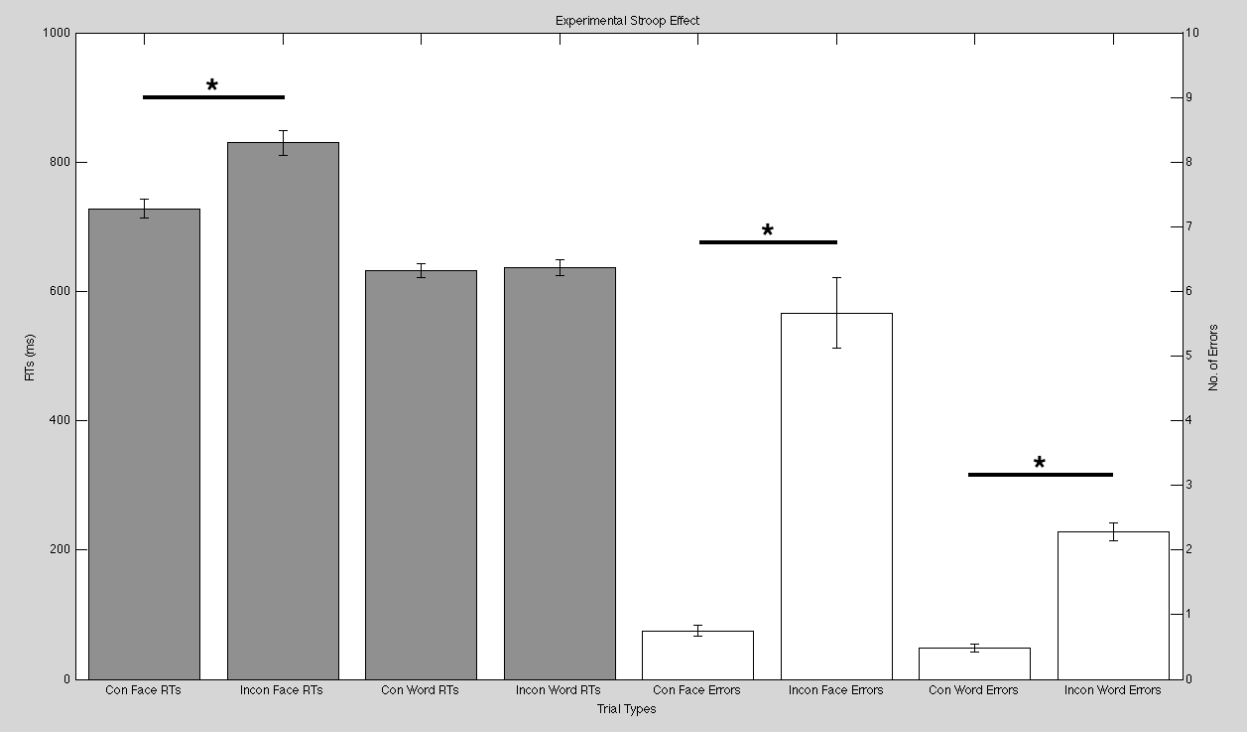

Figure 13. Overall mean reaction times (RTs; grey bars) and errors (white bars) from ten subjects performing the emotional Stroop task during the experimental period. The error bars signify the standard error of the mean (SEM). A Stroop effect is seen in three of the four conditions, with significantly longer RTs for the incongruent trials in the face ($p < 0.001$) but not the word ($p > 0.1$) instruction set, and significantly more errors for the incongruent trials in both the face ($p < 0.001$) and word ($p < 0.001$) instruction sets.

In order to delineate further trends in the data, congruent and incongruent baseline and experimental trials for each instruction set were compared by use of paired samples Student's *t*-tests (Table 7 in Appendix F). These analyses revealed that participants responded significantly faster in the experimental period for the congruent trials of the face instruction ($t_{(9)} = 2.424$, $p < 0.05$) as well as for the incongruent trials of the word instruction ($t_{(9)} = 3.132$, $p < 0.01$), but not

for the incongruent trials of the face instruction ($t_{(9)} = 2.046$, $p > 0.05$) nor for the congruent trials of the word instruction ($t_{(9)} = 2.192$, $p > 0.05$; Figure 14). It was also found that participants made significantly fewer errors in the experimental period for the congruent trials ($t_{(9)} = 2.216$, $p < 0.05$) but not for the incongruent trials ($t_{(9)} = 1.135$, $p > 0.1$) of the face instruction (Figure 14). Conversely, participants made significantly more errors in the experimental period for the incongruent trials of the word instruction ($t_{(9)} = 2.173$, $p < 0.05$), but did not make significantly more or fewer errors for the congruent trials of the same instruction ($t_{(9)} = 0.142$, $p > 0.1$; Figure 14).

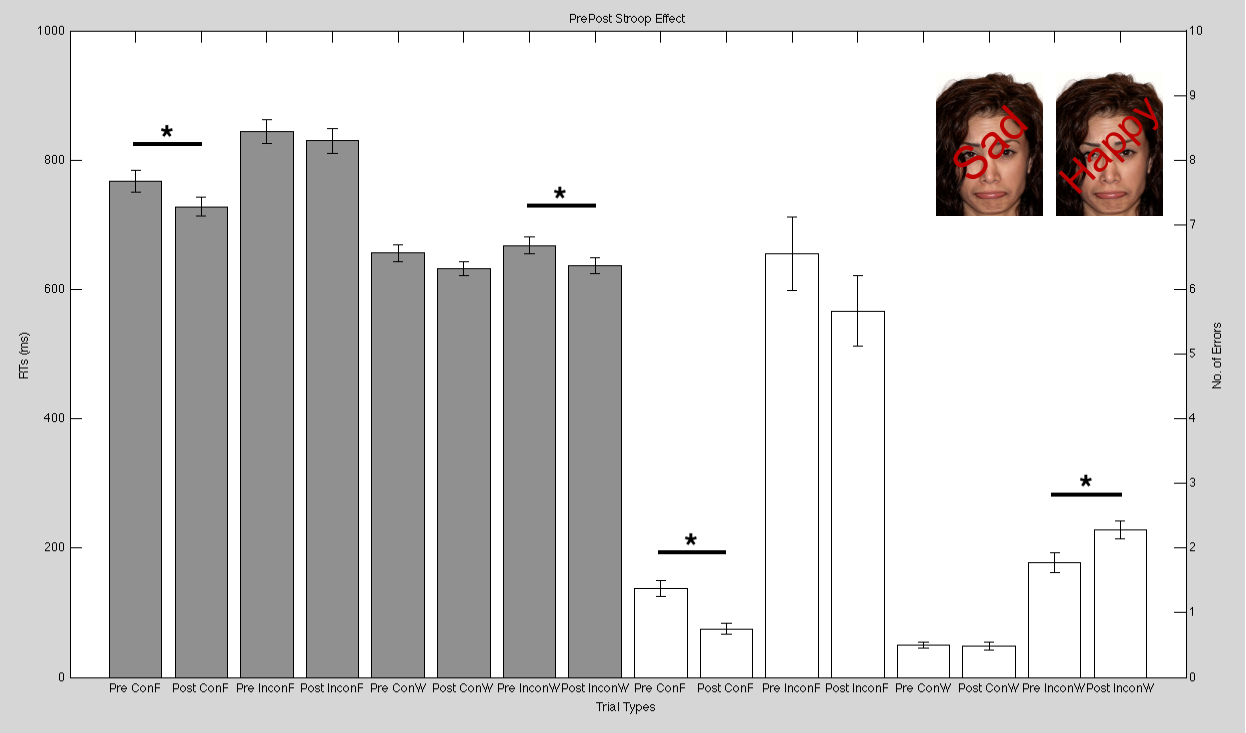

Figure 14. Overall mean reaction times (RTs; grey bars) and errors (white bars) from ten subjects performing the emotional Stroop task. All ten subjects took part in the **melatonin** treatment, and their baseline and experimental period performances are shown for each instruction set (face and word). The instruction sets are further broken down into their component congruent and incongruent trials. The error bars signify the standard error of the mean (SEM). There was a statistically significant difference between the baseline and experimental periods for RTs in the congruent trials of the face instruction set ($p < 0.05$), as well as for RTs in the incongruent trials of the word instruction set ($p < 0.01$). There was no statistically significant difference between the baseline and experimental periods for RTs in the incongruent trials of the face instruction set ($p > 0.05$), nor for RTs in the congruent trials of the word instruction set ($p > 0.05$). A similar trend is seen for the errors, with the congruent trials of the face instruction set and the incongruent trials of the word instruction set reaching statistical significance between the baseline and experimental periods ($p < 0.05$ for both), but the errors in the incongruent trials of the face instruction set and the congruent trials of the word instruction set not reaching significance ($p > 0.1$ for both).

To determine whether there were interactions between the baseline and experimental periods, the congruent and incongruent trials, and the face and word instructions, a 3-way repeated measures ANOVA was performed for both the RTs and errors. Three within-subject factors with two levels each were used: period (baseline, experimental), congruency (congruent, incongruent), and instruction (face, word). Results from the first repeated measures ANOVA demonstrated a significant main effect of period on RTs ($F_{(1,9)} = 7.406$, $p < 0.05$), a significant

main effect of congruency on RTs ($F_{(1,9)}$ = 31.835, p < 0.001), and a significant main effect of instruction on RTs ($F_{(1,9)}$ = 121.543, p < 0.001) – that is, the baseline and experimental periods, the congruent and incongruent conditions, and the face and word instructions all had significant effects on RTs. There was also a significant interaction found between the factors of congruency and instruction on RTs ($F_{(1,9)}$ = 20.509, p < 0.01), as well as between the factors of period, congruency, and instruction on RTs ($F_{(1,9)}$ = 5.063, p < 0.05; see Table 8 in Appendix F). The interactions between the factors of period and congruency and the factors of period and instruction on RTs did not reach significance ($F_{(1,9)}$ =1.206, p > 0.1 and $F_{(1,9)}$ = 0.005, p > 0.5, respectively). Results from the second repeated measures ANOVA demonstrated a significant main effect of congruency on errors ($F_{(1,9)}$ =38.881, p < 0.001) and a significant main effect of instruction on errors ($F_{(1,9)}$ =22.613, p < 0.001; Table 9 in Appendix F) – that is, the congruent and incongruent conditions and the face and word instructions all had significant effects on the error rates. The main effect of period on errors did not reach significance ($F_{(1,9)}$ =0.999, p > 0.1). There was also a significant interaction found between the factors of congruency and instruction on errors ($F_{(1,9)}$ =19.253, p < 0.005; Table 9 in Appendix F). The interactions between the factors of period and congruency, the factors of period and instruction, and the factors of period, congruency and instruction on errors did not reach significance ($F_{(1,9)}$ = 0.150, p > 0.5, $F_{(1,9)}$ = 3.929, p > 0.05, and $F_{(1,9)}$ = 1.255, p > 0.1, respectively; Table 9 in Appendix F).

3.2 Diffusion Tensor Imaging

3.2.1 Tract-Based Spatial Statistics and Voxelwise Statistics

To determine changes in white matter microstructure in the brain as a function of the melatonin treatment, TBSS and voxelwise statistics were performed on all participants' baseline

and experimental period DTI data. These analyses yielded voxels of significance at a 95% confidence interval in the left and right IFG for both FA and MD maps. FA values within the whole brain (Figures 15 and 16; $t_{(9)} = 9.528$, $p < 0.001$) as well as within the left IFG (Figures 17, 18 and 19; $t_{(9)} = 5.223$, $p < 0.001$) and right IFG (Figures 20, 21 and 22; $t_{(9)} = 2.993$, $p < 0.01$) decreased significantly in the experimental scan compared to the baseline scan (Table 10 in Appendix F).

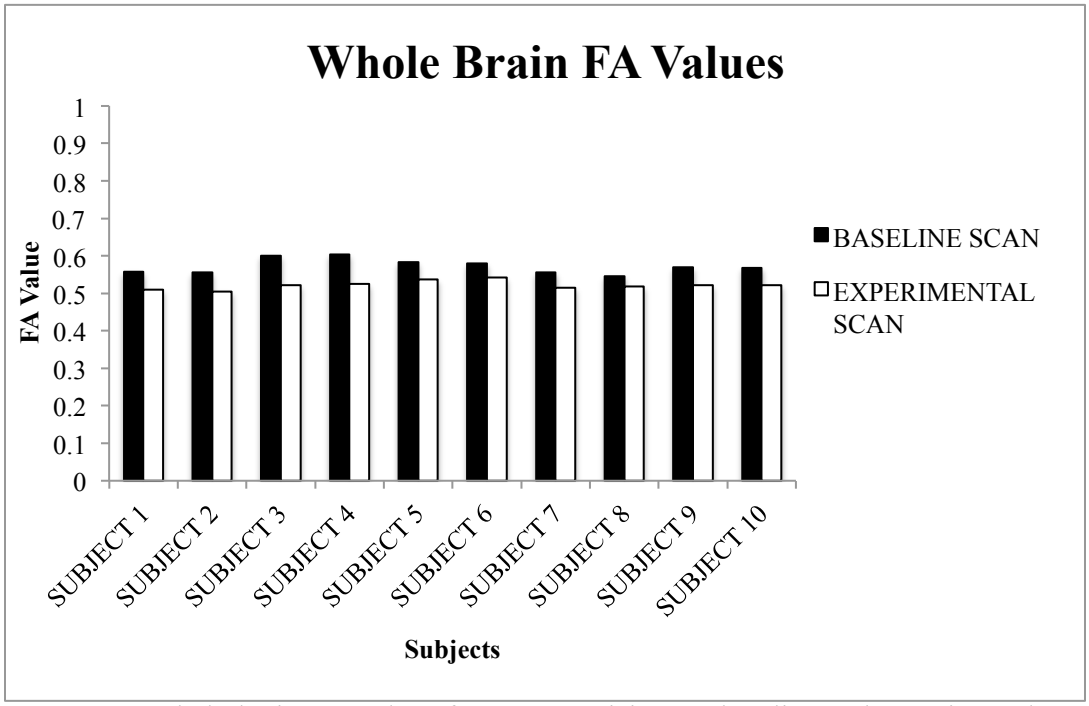

Figure 15. Whole brain FA values from ten participants' baseline and experimental scans. FA values range from 0 to 1. The black bars represent FA values from participants' baseline scan; white bars represent FA values from participants' experimental scan. Decreases in FA values from the baseline to experimental scans can be seen.

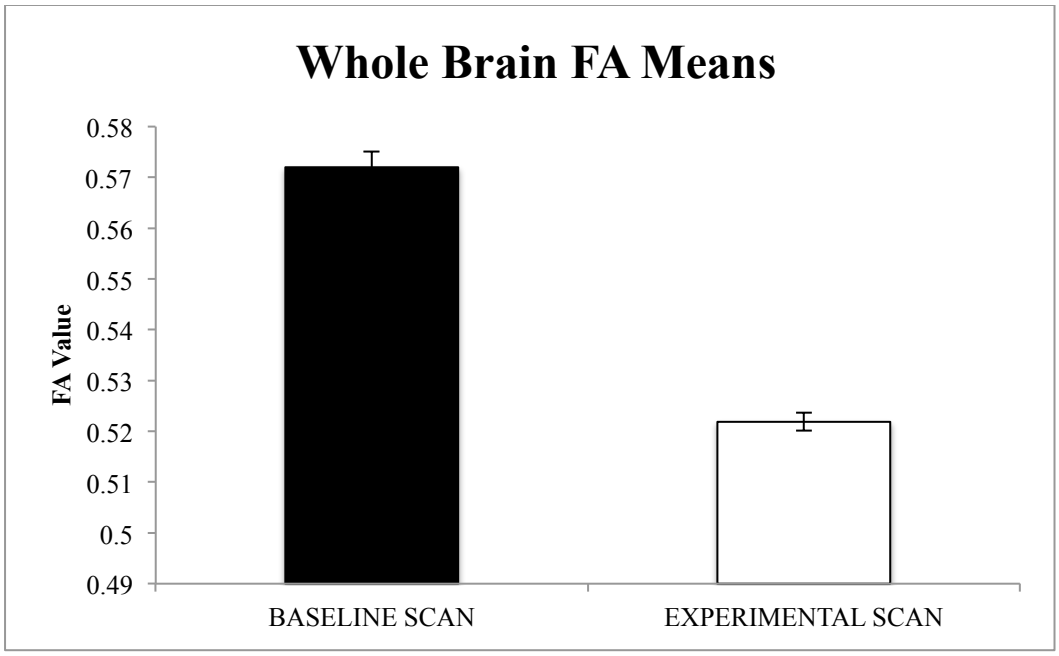

Figure 16. Whole brain FA means from ten participants' baseline and experimental scans. Participant data have been averaged within each scanning period to demonstrate the significant decrease in FA values during the experimental scan ($p < 0.001$). The error bars signify the standard error of the mean (SEM).

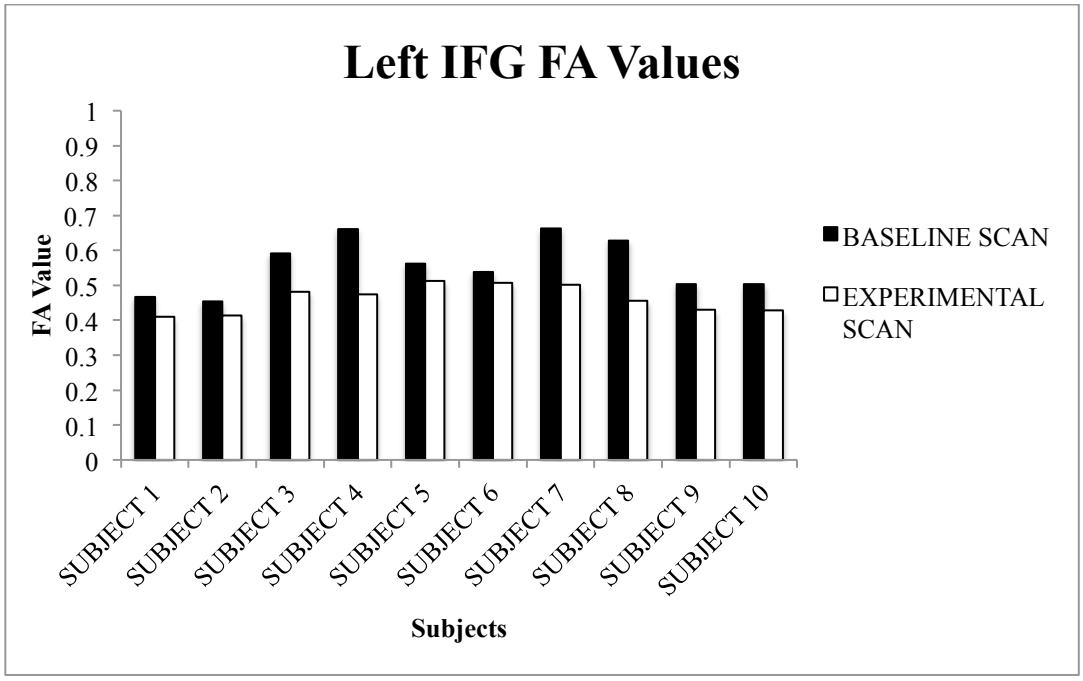

Figure 17. FA values from the left IFG from ten participants' baseline and experimental scans. FA values range from 0 to 1. The black bars represent FA values within the left IFG from participants' baseline scan; white bars represent FA values within the left IFG from participants' experimental scan. Decreases in FA values from the baseline to experimental scans can be seen.

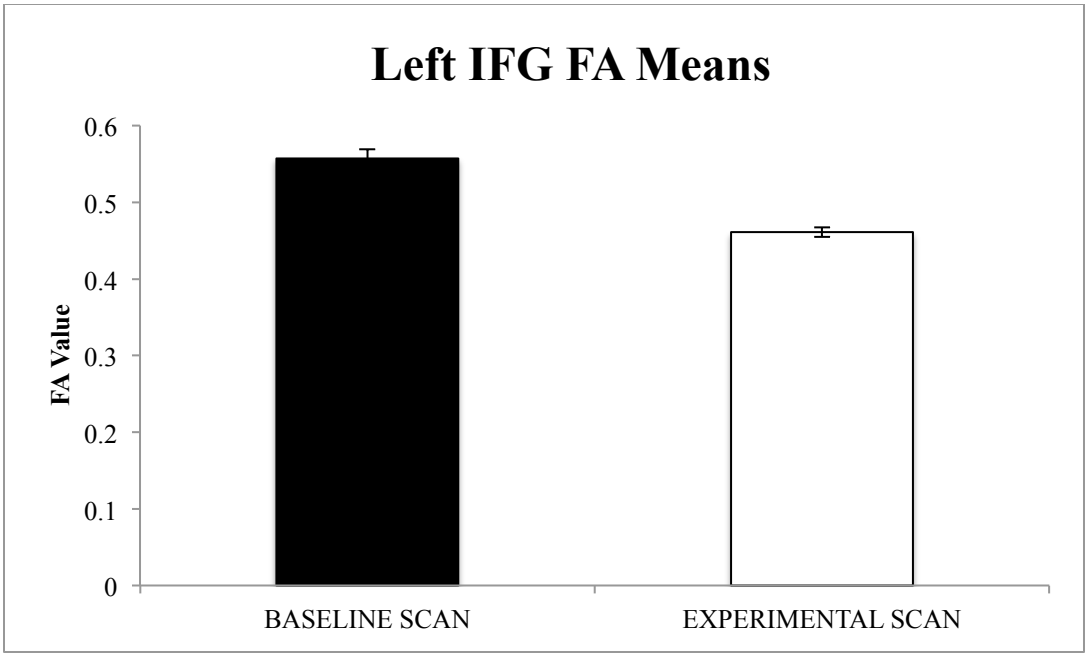

Figure 18. FA means from the left IFG from ten participants' baseline and experimental scans. Participant data have been averaged within each scanning period to demonstrate the significant decrease in FA values within the left IFG during the experimental scan ($p < 0.001$). The error bars signify the standard error of the mean (SEM).

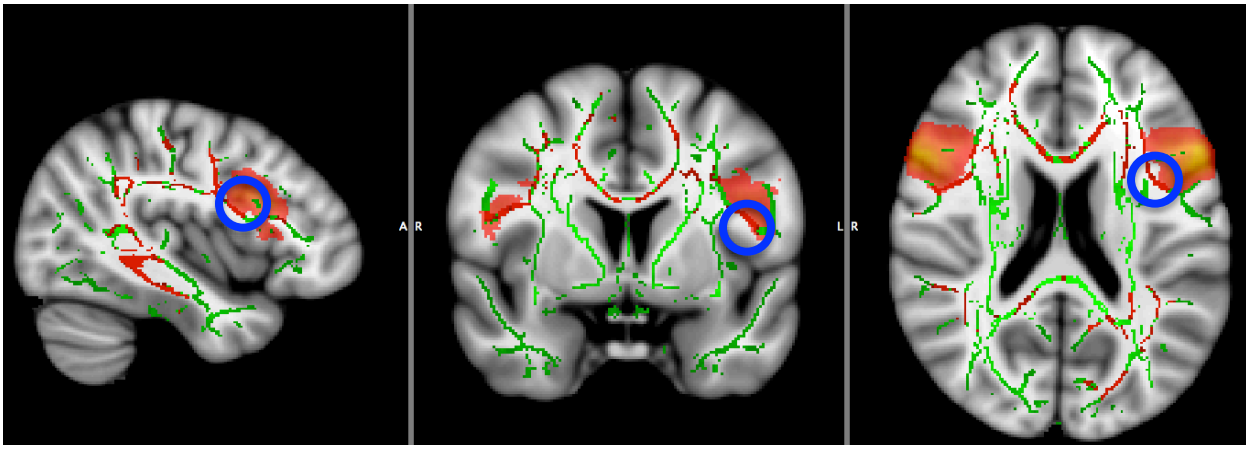

Figure 19. Tract-based spatial statistics (TBSS) images from ten subjects' fractional anisotropy (FA) data for the experimental > baseline contrast. All three brain images are presented in radiological convention. Voxelwise statistics were run on the 4D skeletonised FA image created during TBSS pre-processing. The green tracts represent the mean skeletonized FA data, while the red tracts represent voxels that resulted in significantly different FA values at a confidence interval of 95%. The left and right IFG are highlighted, and the blue circles represent significant voxels within the left IFG that were used for analysis. MNI coordinates used: x = -41, y = 3, z = 20.

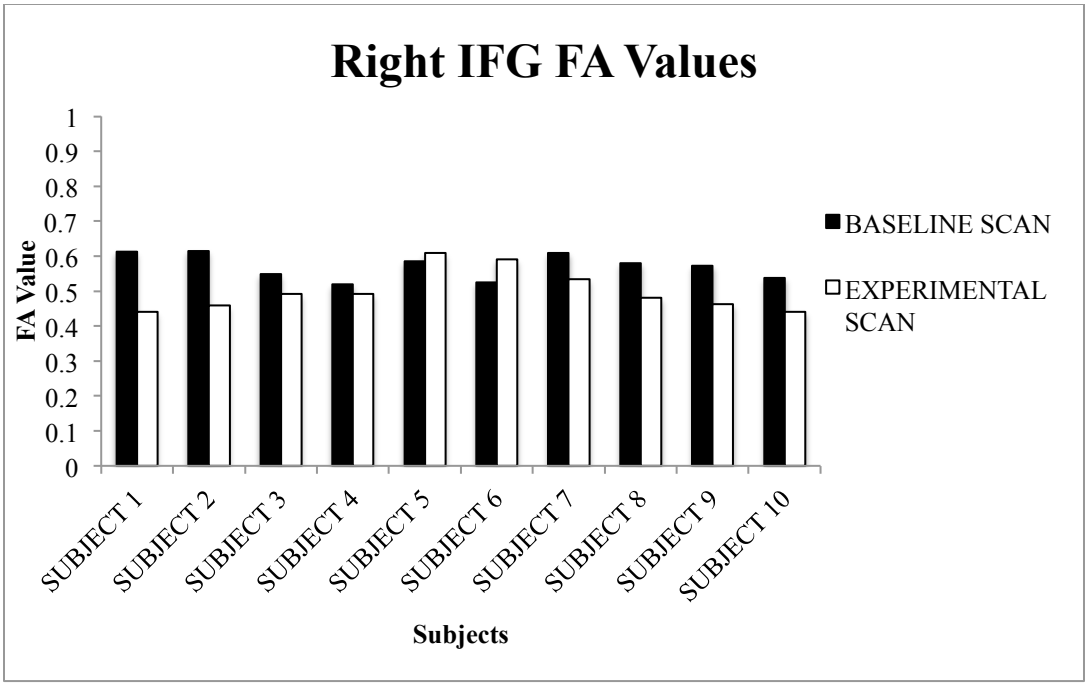

Figure 20. FA values from the right IFG from ten participants' baseline and experimental scans. FA values range from 0 to 1. The black bars represent FA values within the right IFG from participants' baseline scan; white bars represent FA values within the right IFG from participants' experimental scan. Decreases in FA values from the baseline to experimental scans can be seen.

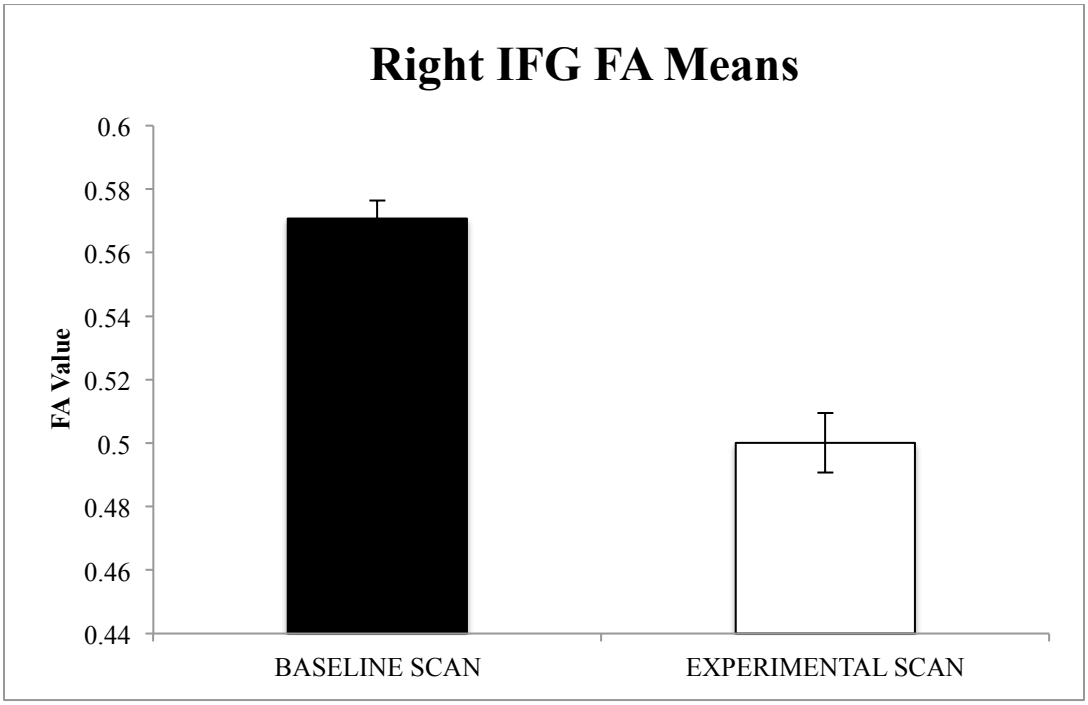

Figure 21. FA means from the right IFG from ten participants' baseline and experimental scans. Participant data have been averaged within each scanning period to demonstrate the significant decrease in FA values within the right IFG during the experimental scan ($p < 0.01$). The error bars signify the standard error of the mean (SEM).

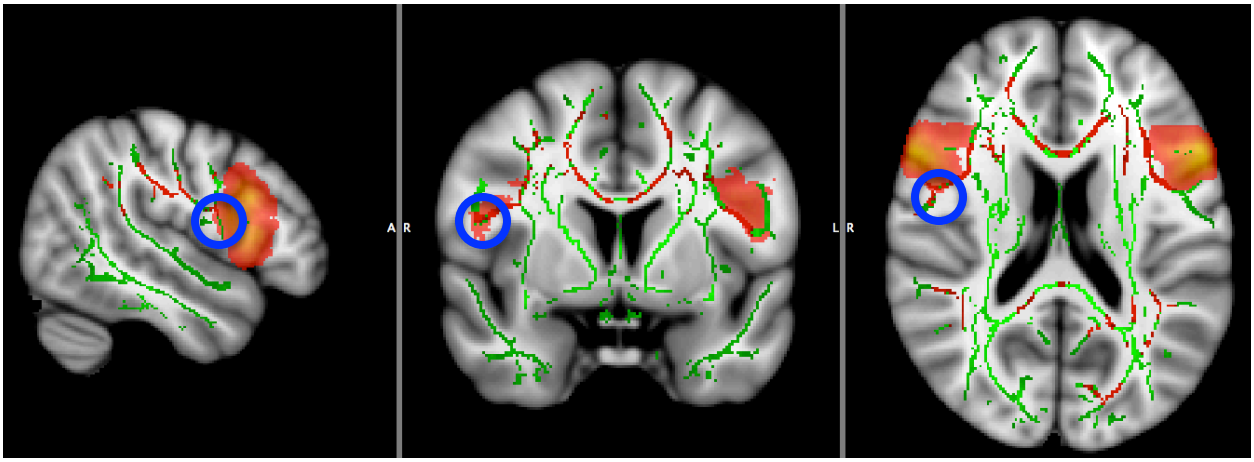

Figure 22. Tract-based spatial statistics (TBSS) images from ten subjects' fractional anisotropy (FA) data for the experimental > baseline contrast. All three brain slices are presented in radiological convention. Voxelwise statistics were run on the 4D skeletonised FA image created during TBSS pre-processing. The green tracts represent the mean skeletonized FA data, while the red tracts represent voxels that resulted in significantly different FA values at a confidence interval of 95%. The left and right IFG are highlighted, and the blue circles represent significant voxels within the right IFG that were used for analysis. MNI coordinates used: x = 50, y = 1, z = 20.

Conversely, MD values within the whole brain (Figures 23 and 24; $t_{(9)} = 8.082$, $p < 0.001$) as well as within the left (Figures 25, 26 and 27; $t_{(9)} = 2.254$, $p < 0.05$) and right IFG (Figures 28, 29 and 30; $t_{(9)} = 3.665$, $p < 0.005$) increased significantly in the experimental scan compared to the baseline scan (Table 11 in Appendix F). As with the FA values, the right IFG demonstrated a greater increase in MD values than the left IFG, though the change in MD values in both hemispheres did reach significance. TBSS and voxelwise statistics did not yield any voxels of significance at a 95% confidence interval in the left or right hippocampus.

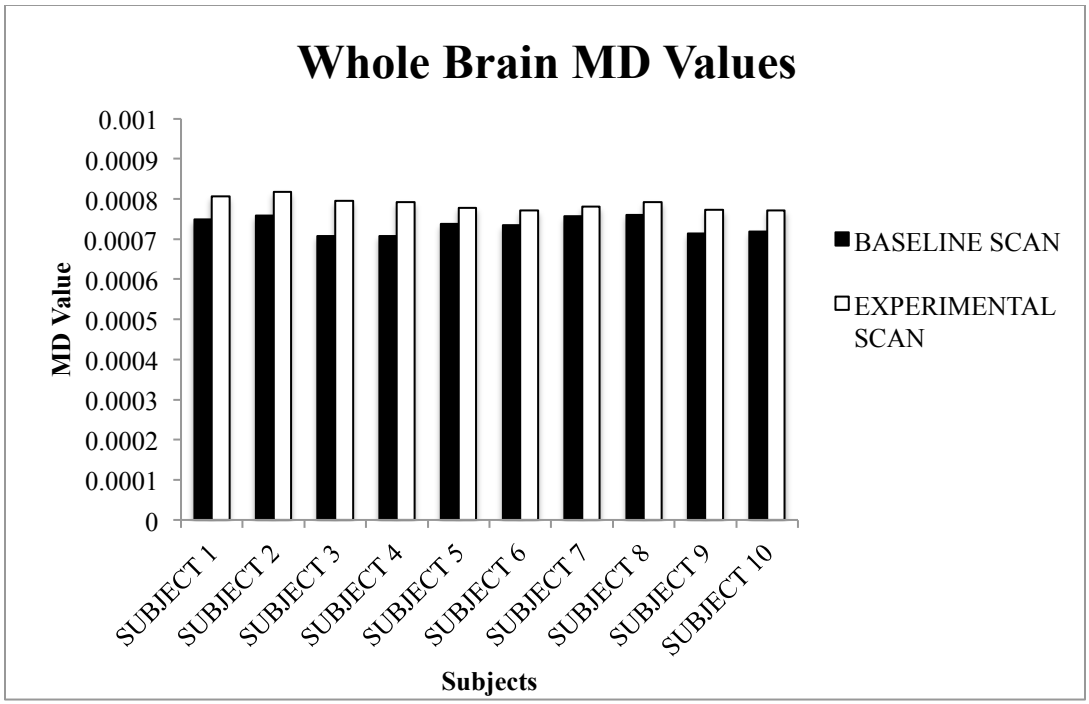

Figure 23. Whole brain MD values from ten participants' baseline and experimental scans. MD values have physical unites of m^2/s. The black bars represent MD values from participants' baseline scan; white bars represent MD values from participants' experimental scan. Increases in MD values from the baseline to experimental scans can be seen.

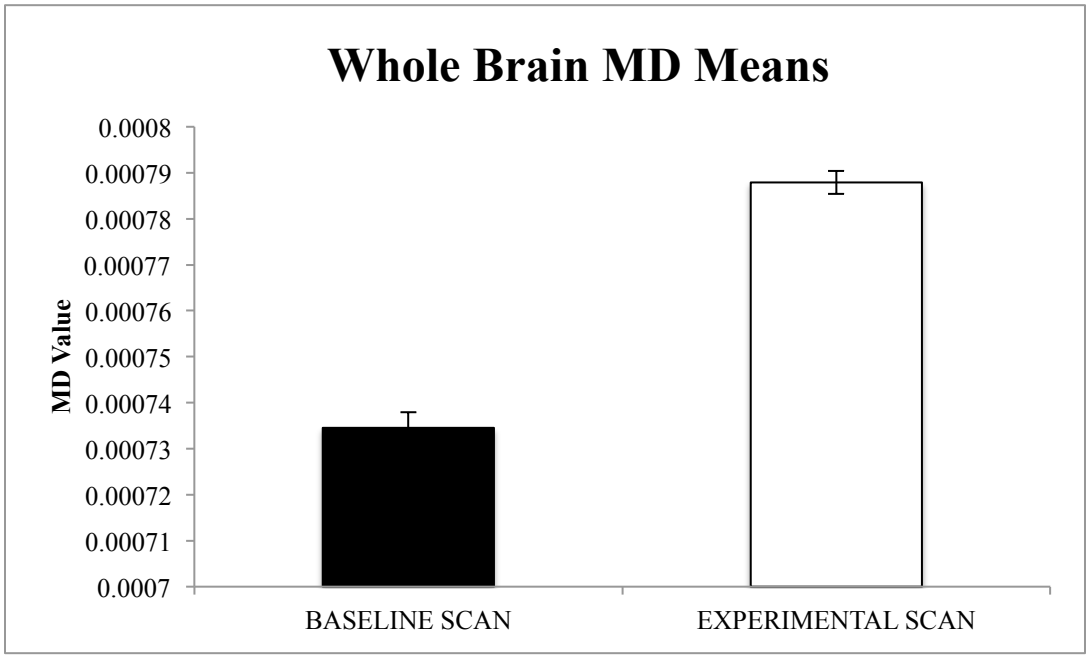

Figure 24. Whole brain MD means from ten participants' baseline and experimental scans. Participant data have been averaged within each scanning period to demonstrate the significant increase in MD values during the experimental scan ($p < 0.001$). The error bars signify the standard error of the mean (SEM).

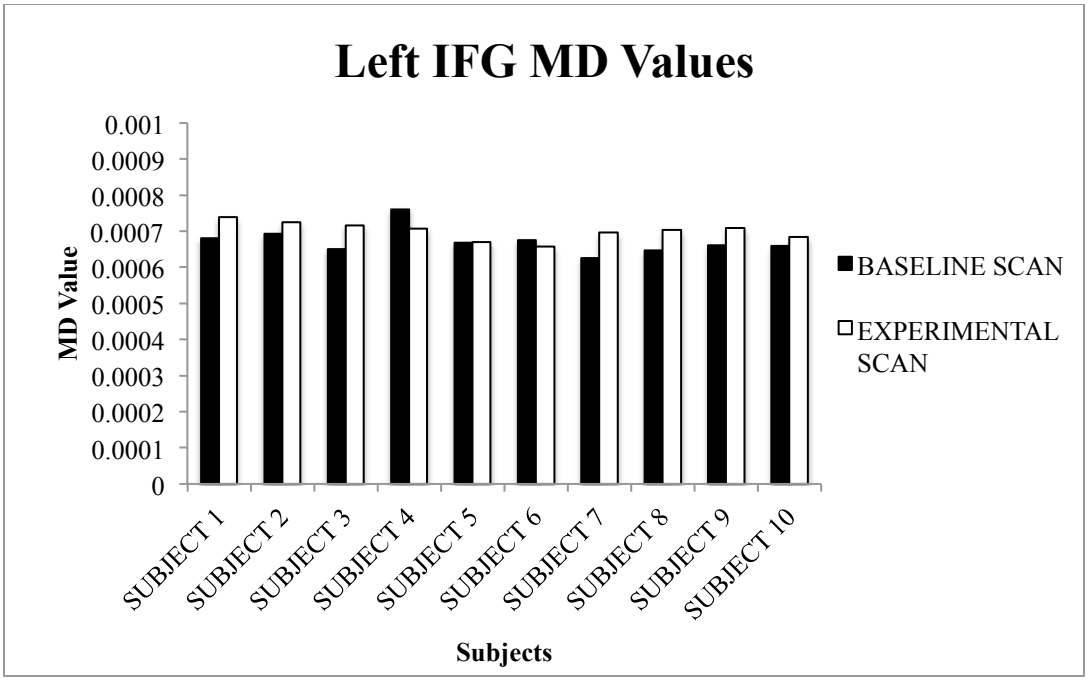

Figure 25. MD values from the left IFG from ten participants' baseline and experimental scans. MD values have physical units of m^2/s. The black bars represent MD values within the left IFG from participants' baseline scan; white bars represent MD values within the left IFG from participants' experimental scan. Increases in MD values from the baseline to experimental scans can be seen.

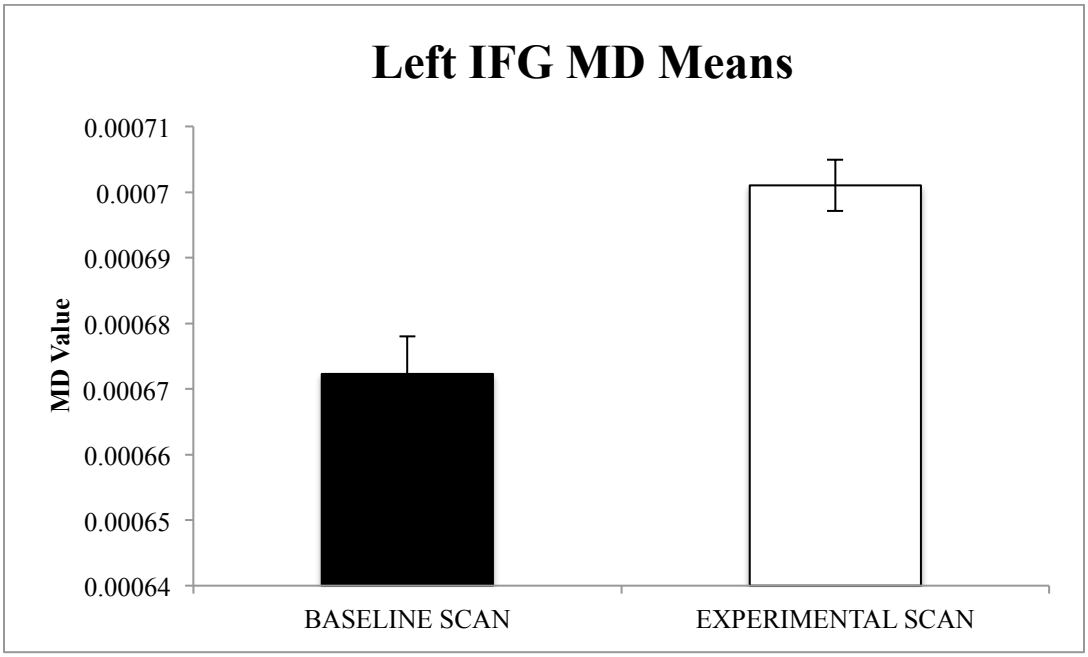

Figure 26. MD means from the left IFG from ten participants' baseline and experimental scans. Participant data have been averaged within each scanning period to demonstrate the significant increase in MD values within the left IFG during the experimental scan ($p < 0.05$). The error bars signify the standard error of the mean (SEM).

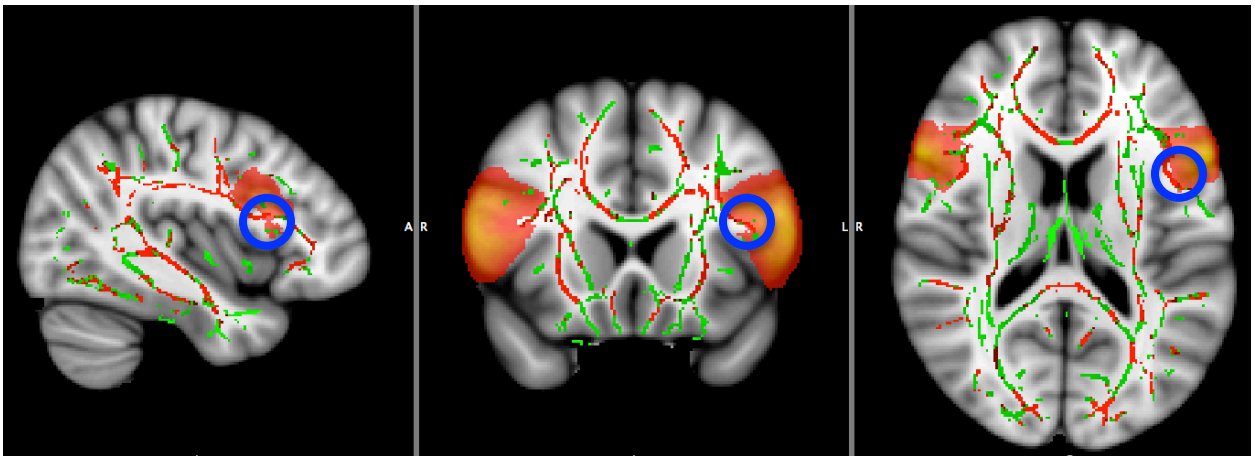

Figure 27. Tract-based spatial statistics (TBSS) images from ten subjects' mean diffusivity (MD) data for the baseline > experimental contrast. All three brain images are presented in radiological convention. Voxelwise statistics were run on the 4D skeletonised FA image created during TBSS pre-processing. The green tracts represent the mean skeletonized FA data, while the red tracts represent voxels that resulted in significantly different MD values at a confidence interval of 95%. The left and right IFG are highlighted, and the blue circles represent significant voxels within the left IFG that were used for analysis. MNI coordinates used: x = -40, y = 19, z = 16.

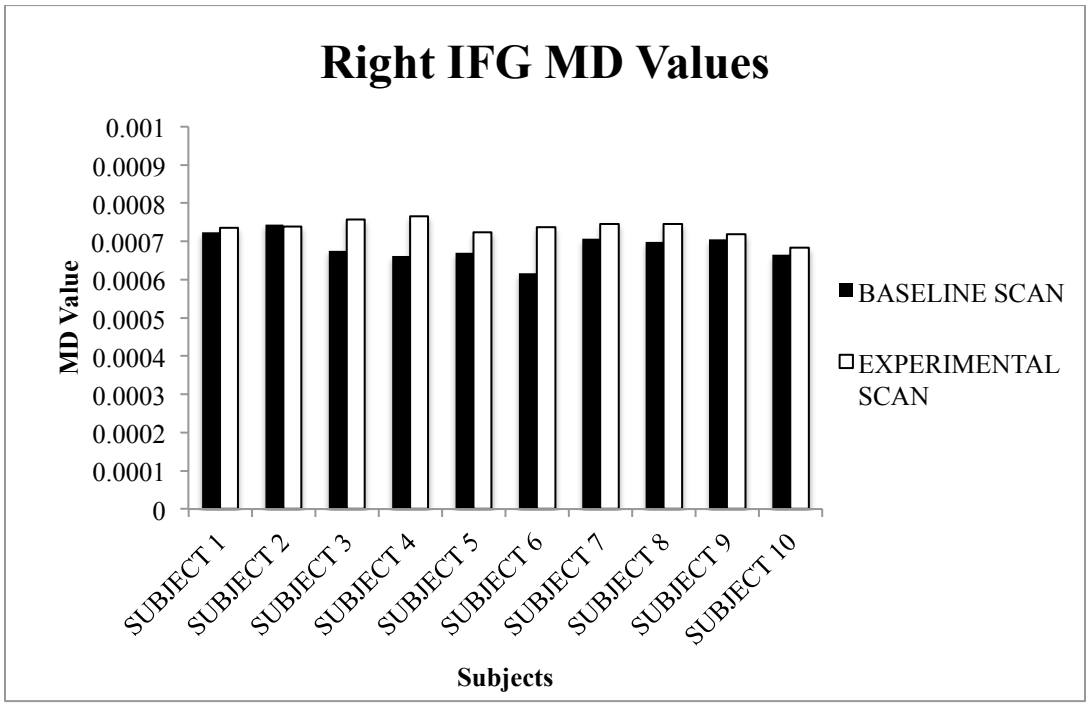

Figure 28. MD values from the right IFG from ten participants' baseline and experimental scans. MD values have physical units of m^2/s. The black bars represent MD values within the right IFG from participants' baseline scan; white bars represent MD values within the right IFG from participants' experimental scan. Increases in MD values from the baseline to experimental scans can be seen.

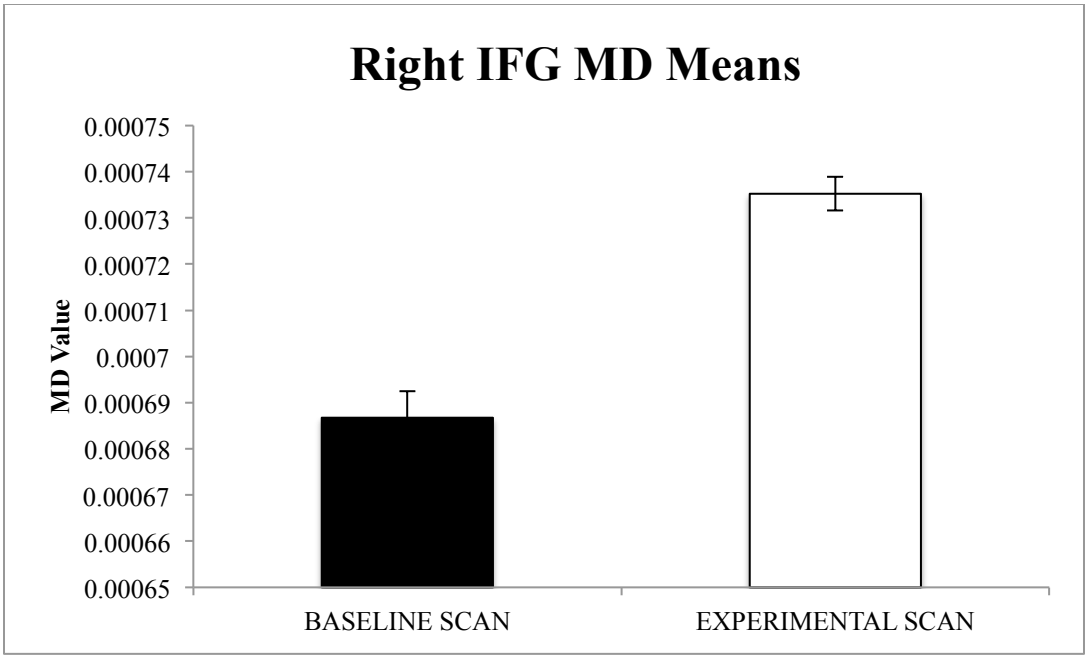

Figure 29. MD means from the right IFG from ten participants' baseline and experimental scans. Participant data have been averaged within each scanning period to demonstrate the significant increase in MD values within the right IFG during the experimental scan ($p < 0.005$). The error bars signify the standard error of the mean (SEM).

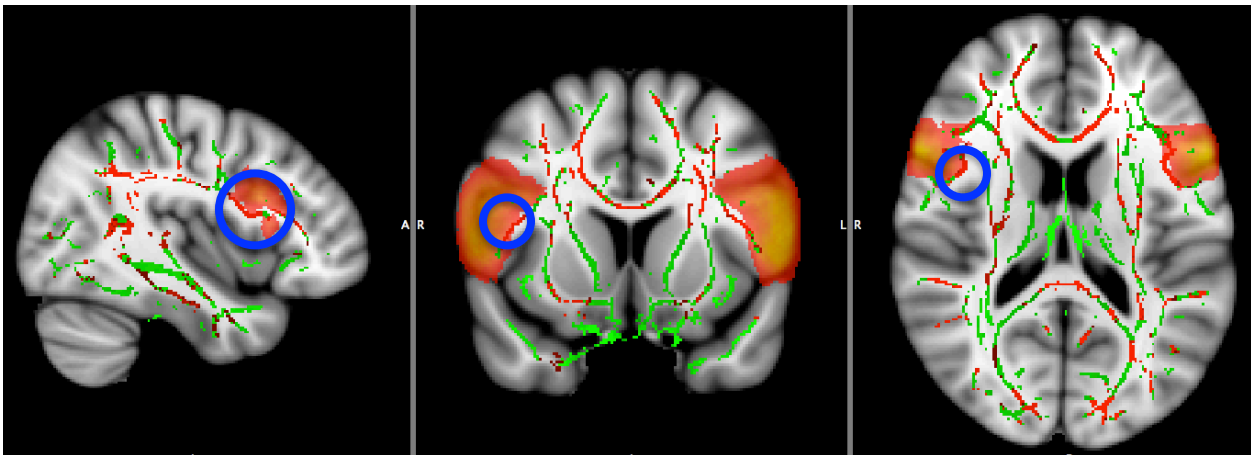

Figure 30. Tract-based spatial statistics (TBSS) images from ten subjects' mean diffusivity (MD) data for the baseline > experimental contrast. All three brain slices are presented in radiological convention. Voxelwise statistics were run on the 4D skeletonised FA image created during TBSS pre-processing. The green tracts represent the mean skeletonized FA data, while the red tracts represent voxels that resulted in significantly different MD values at a confidence interval of 95%. The left and right IFG are highlighted, and the blue circles represent significant voxels within the right IFG that were used for analysis. MNI coordinates used: x = 41, y = 12, z = 20.

3.2.2 Tractography

To assess changes in white matter pathways underlying areas of higher cognitive function, probabilistic tractography was carried out using the left and right hippocampal entorhinal cortex (HEC) as seed regions and the left and right IFG as target regions. Paired samples *t*-tests were performed on the baseline and experimental SC values from each hemisphere independently (Table 12 in Appendix F), and no significant differences between baseline and experimental scans were found in either the left (Figures 31 and 32; $t_{(9)} = 0.733$, $p > 0.1$) or right (Figures 31 and 33; $t_{(9)} = 0.330$, $p > 0.1$) hemisphere. Furthermore, no consistent trends in SC values were found within or between participants (Figure 34).

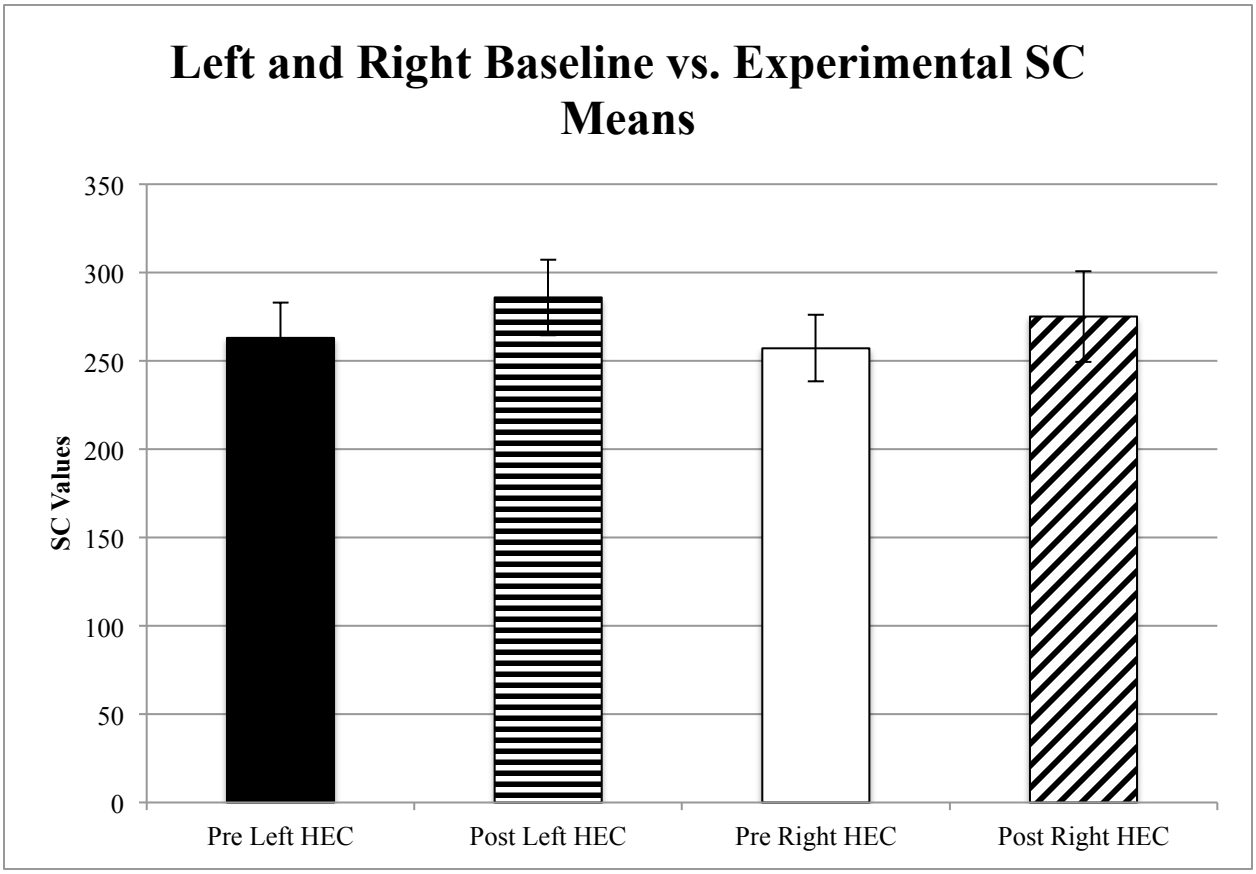

Figure 31. SC means from ten participants' baseline and experimental scans. Participant data have been averaged within each scanning period and seed region hemisphere to demonstrate that no significant changes in SC values were found ($p > 0.1$). The black bars represent SC values from the baseline scan with streamlines originating from the left HEC and terminating at the left and right IFG; the horizontal striped bars represent SC values from the experimental scan with streamlines originating from the left HEC and terminating at the left and right IFG; the white bars represent SC values from the baseline scan with streamlines originating from the right HEC and terminating at the left and right IFG; the diagonal striped bars represent SC values from the experimental scan with streamlines originating from the right HEC and terminating at the left and right IFG. The error bars signify the standard error of the mean (SEM).

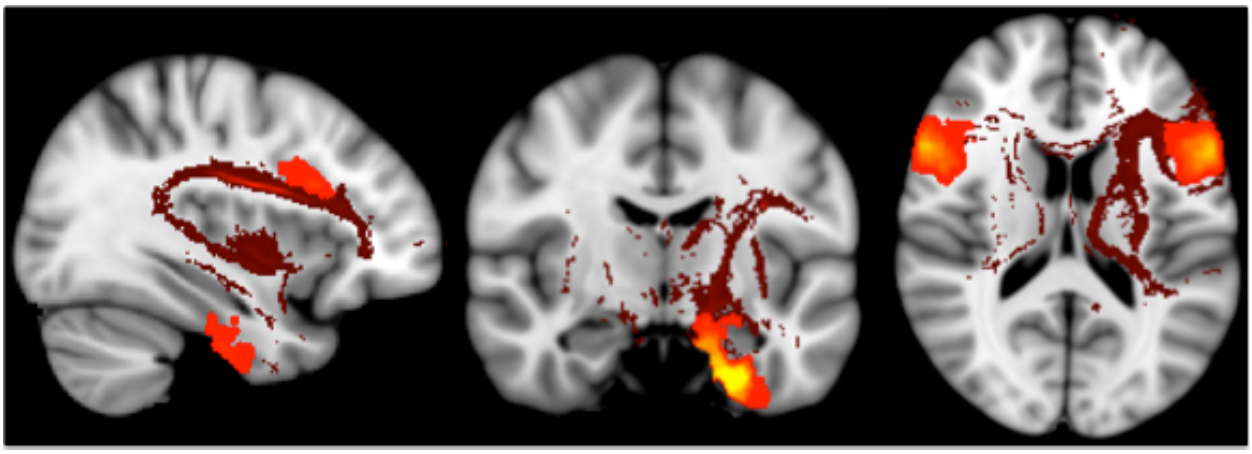

Figure 32. Probabilistic streamlines (brown) are shown from one subject, originating from the left HEC (red and yellow areas at the bottom of the sagittal and coronal slices) and terminating at the left and right IFG (red and orange areas at the top of the sagittal and transverse slices). All three brain slices are presented in radiological convention.

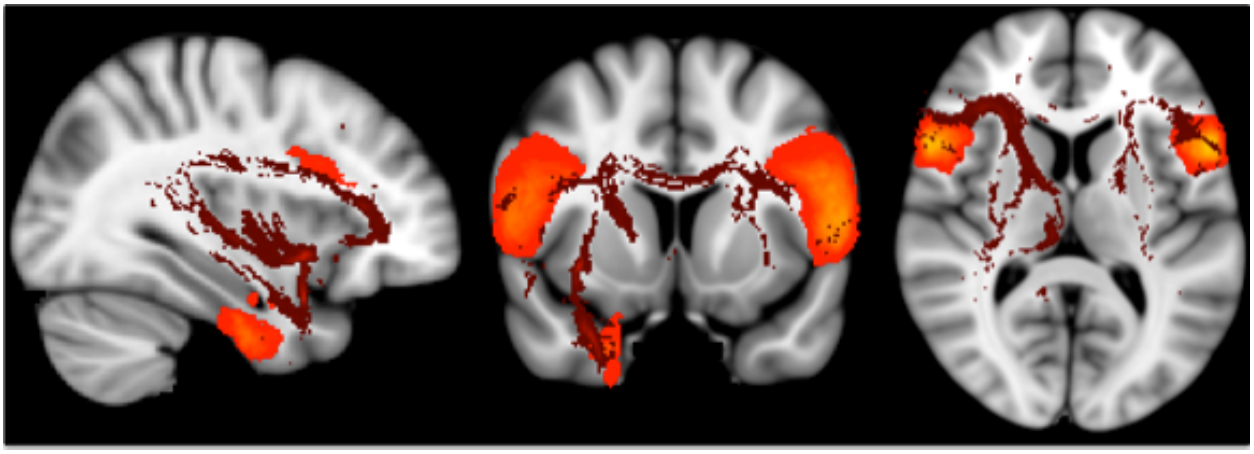

Figure 33. Probabilistic streamlines (brown) are shown from one subject, originating from the right HEC (red and orange areas at the bottom of the sagittal and coronal slices) and terminating at the left and right IFG (red and orange areas at the top of the sagittal, coronal and transverse slices). All three brain slices are presented in radiological convention.

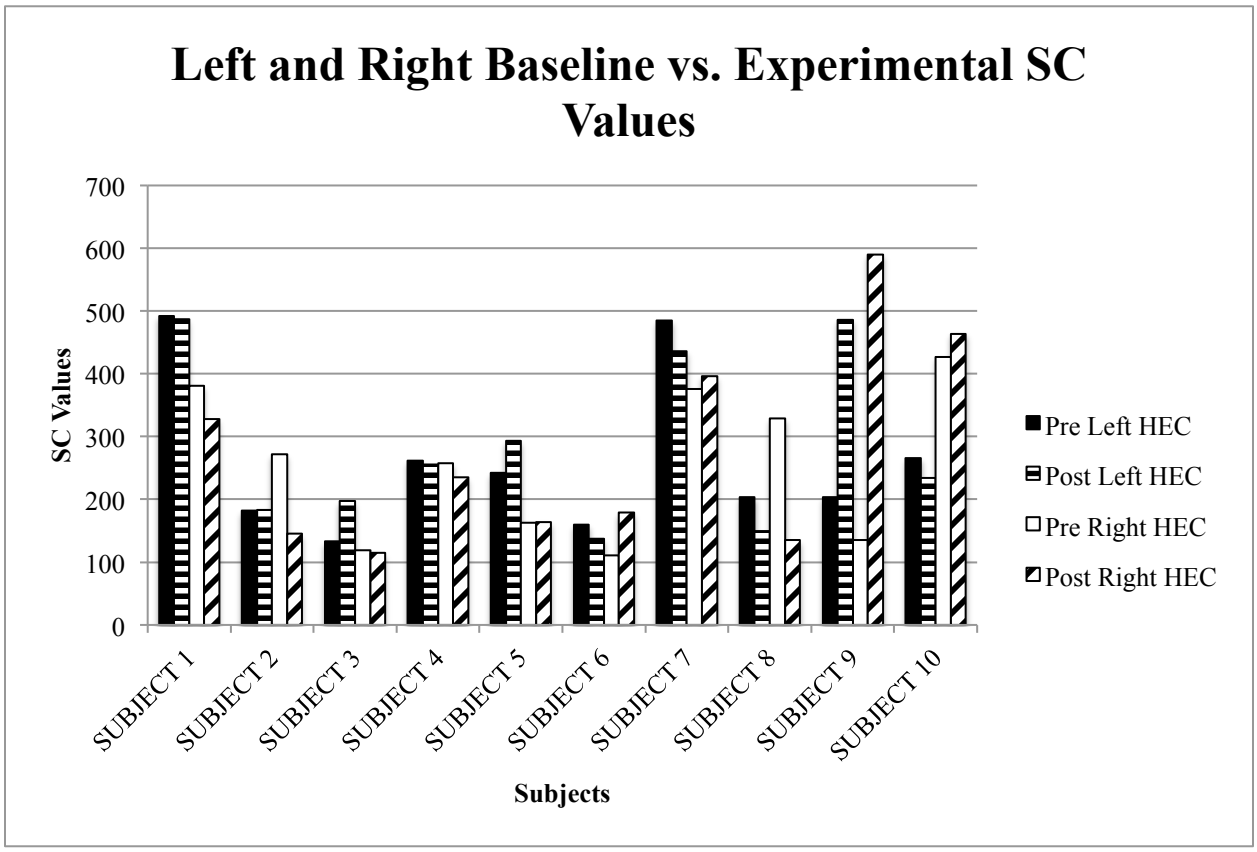

Figure 34. SC values from ten participants' baseline and experimental scans. The black bars represent SC values from the baseline scan with streamlines originating from the left HEC and terminating at the left and right IFG; the horizontal striped bars represent SC values from the experimental scan with streamlines originating from the left HEC and terminating at the left and right IFG; the white bars represent SC values from the baseline scan with streamlines originating from the right HEC and terminating at the left and right IFG; the diagonal striped bars represent SC values from the experimental scan with streamlines originating from the right HEC and terminating at the left and right IFG. No consistent trends in the data were found.

3.3 Correlations

To determine whether there were any relationships between the brain and behavioural measures, correlation analyses were performed. Subtraction values (i.e. experimental value minus baseline value) of the significant results were computed to plot the correlation graphs, and a linear line of best fit was added to data. It was found that congruent face errors significantly correlated with right IFG FA values (Table 13 in Appendix F; Pearson's R Correlation = 0.822, $p < 0.005$; Figure 35), congruent face errors significantly correlated with right IFG MD values

(Table 14 in Appendix F; Pearson's R Correlation = 0.684, $p < 0.05$; Figure 36), and incongruent word errors significantly correlated with left IFG FA values (Table 15 in Appendix F; Pearson's R Correlation = -0.743, $p < 0.01$; Figure 37).

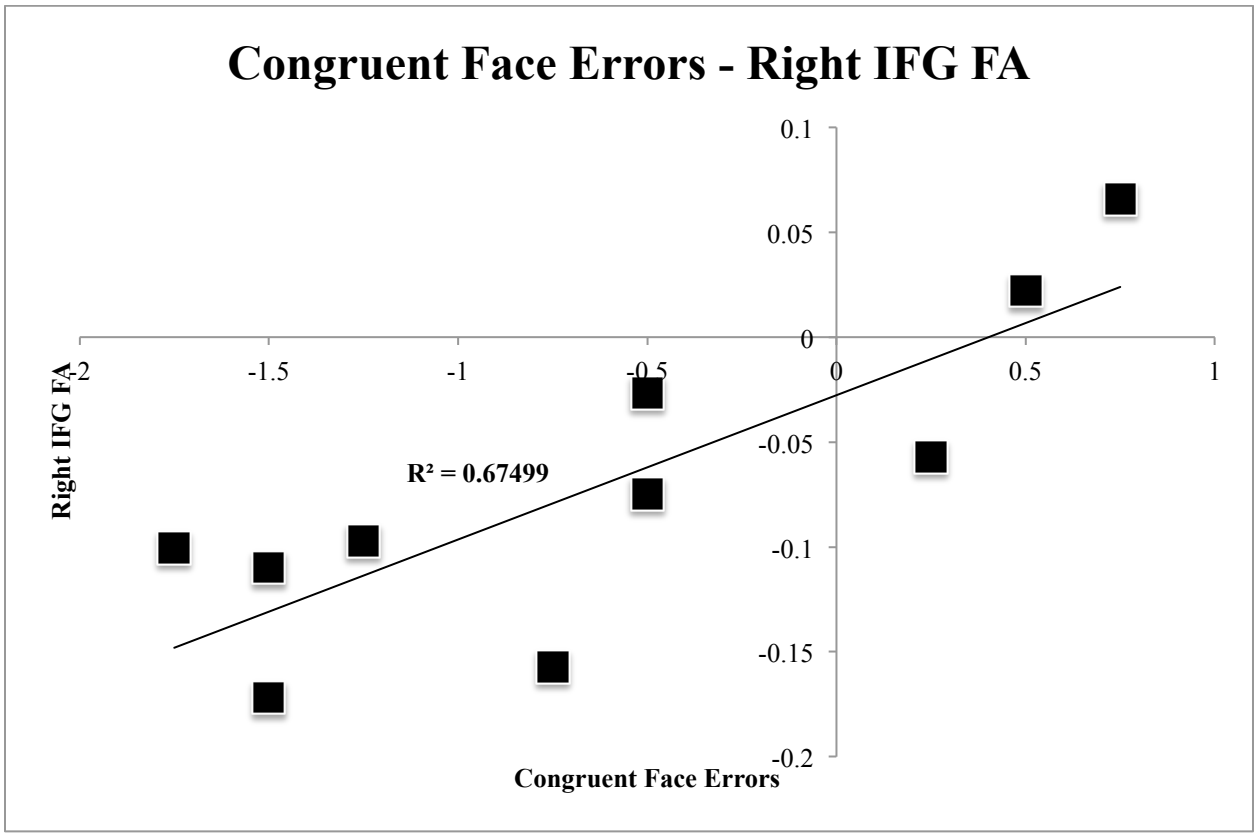

Figure 35. Graph correlating congruent face errors and right IFG FA values. Numbers on the x-axis represent congruent face error subtraction values; numbers on the y-axis represent right IFG FA subtraction values. Each square represents one participant. A significant positive correlation was found ($p < 0.005$), with decreases in congruent face errors correlated with decreases in right IFG FA values.

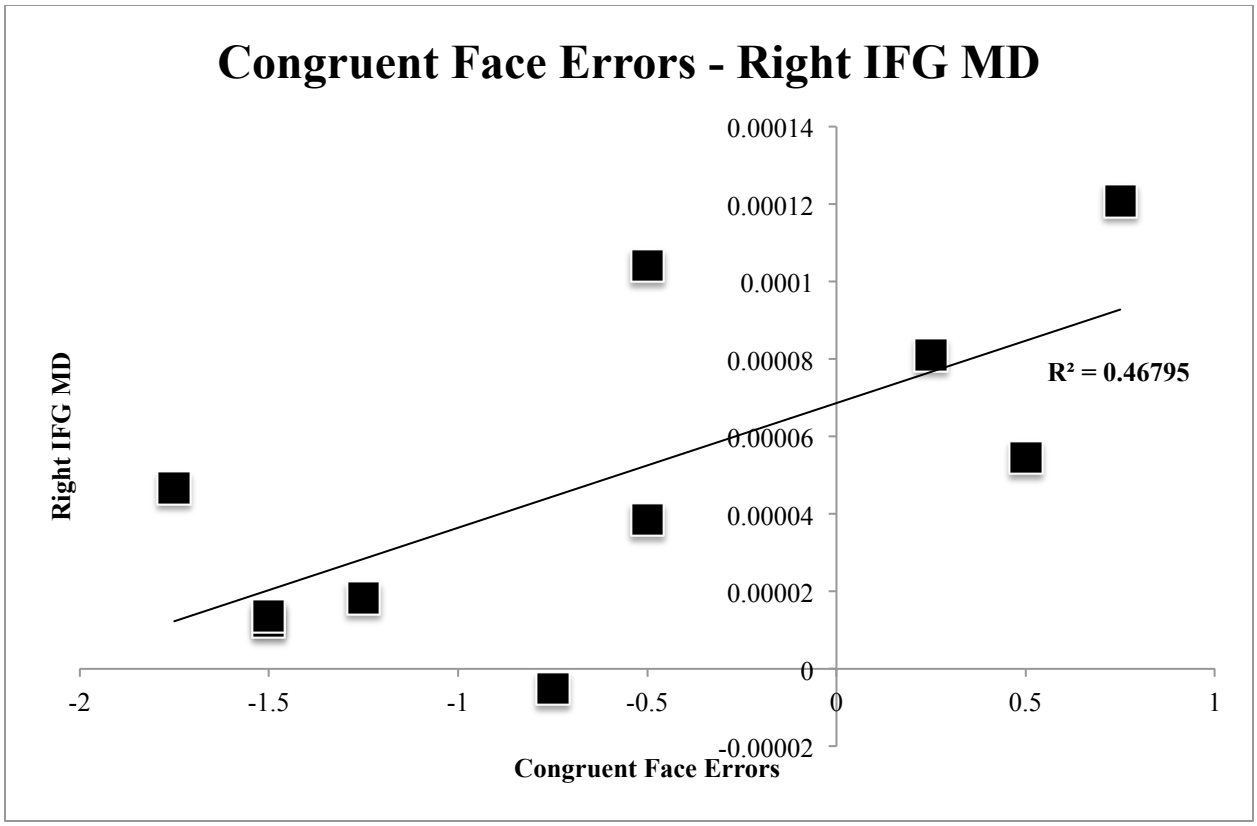

Figure 36. Graph correlating congruent face errors and right IFG MD values. Numbers on the x-axis represent congruent face error subtraction values; numbers on the y-axis represent right IFG MD subtraction values. Each square represents one participant. A significant positive correlation was found ($p < 0.05$), with decreases in congruent face errors correlated with decreases in right IFG MD values.

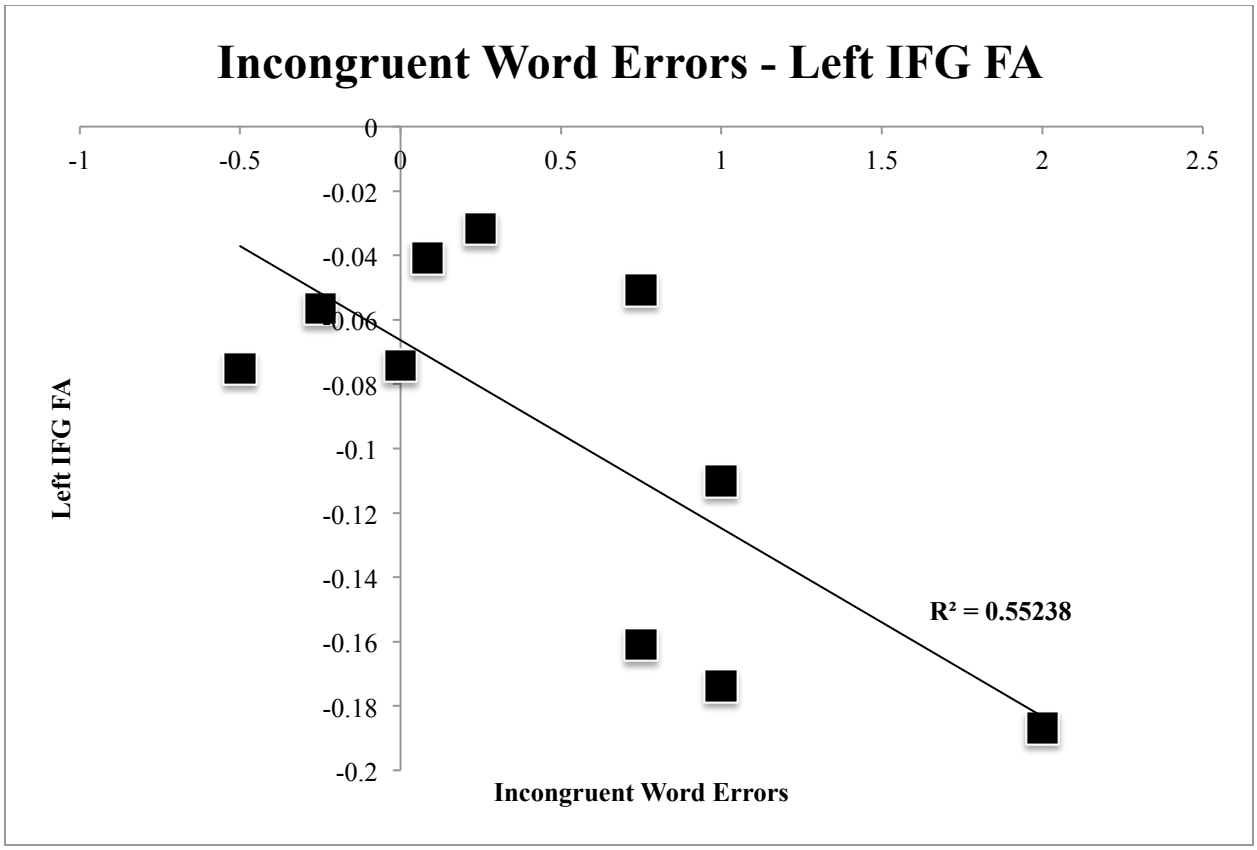

Figure 37. Graph correlating incongruent word errors and left IFG FA values. Numbers on the x-axis represent incongruent word error subtraction values; numbers on the y-axis represent left IFG FA subtraction values. Each square represents one participant. A significant negative correlation was found ($p < 0.01$), with increases in incongruent word errors correlated with decreases in left IFG FA values.

4. Discussion

4.1 Validation of the Emotional Stroop Test as a Cognitive Measure

The present study used an affective face/word emotional Stroop task to measure participants' cognitive performance. As expected, it was found that the incongruent trials produced significantly greater RTs and significantly more errors compared to the congruent trials, regardless of the instruction given. This Stroop effect has been well documented in the literature since the conception of the Stroop task in 1935, and has been demonstrated on numerous occasions by researchers using the Stroop task and the emotional Stroop task alike (Raccuglia and Phaf, 1997; Etkin *et al*., 2006; Preston and Stansfield, 2008). It was also found that participants responded significantly faster and made significantly fewer errors when instructed to respond to the written word compared to the facial emotion. In contrast to this finding, Beall and Herbert (2008) demonstrated larger interference effects for words than faces in their emotional Stroop task, suggesting a more automatic processing for affective faces compared to affective words. However, Beall and Herbert's emotional Stroop paradigm differed from the current paradigm as their affective words were grey in colour and placed in small font over the nose of the face stimuli, hence making the facial expression easier to identify. In comparison, our affective words were red in colour and placed diagonally across the entire face, possibly making the words easier to identify and resulting in shorter RTs and fewer errors for the word instruction set. Additionally, though the same stimuli were used, the current emotional Stroop task was altered slightly from that of Ovaysikia *et al*. (2011) in that the stimulus presentations were organized into a block design as opposed to a pseudo-event-related design. This change was made in hopes that future collection of fMRI data with this task would result in an increased blood oxygen level dependent (BOLD) signal, as a drawback from the pseudo-

event-related design is that the BOLD signal fluctuates too rapidly, making it hard to measure and requiring sophisticated models to predict the BOLD signal for the stimulus. Nonetheless, the results obtained from this study demonstrated similar trends to those reported by Ovaysikia *et al*. (2011), corroborating the paradigm as a valid measure of cognitive performance.

4.2 Daily Activity Logs

4.2.1 Sleep and Wake Times

In an attempt to induce internal desynchronization, exogenous melatonin was administered to participants in the study over an eight day experimental period. It was found that compared to baseline, participants exhibited significant changes to their sleep schedule, with the overall average reported sleep time advancing by approximately one hour. Similarly, participants' wake times were altered compared to baseline, with the overall average reported wake time advancing by approximately half an hour. Further day-by-day examination of participants' experimental sleep data revealed that all participants' sleep times occurred earlier than average after the first melatonin administration, and sleep times on subsequent days followed a pattern of advance or delay when melatonin was administered in the early afternoon or late morning, respectively. These results are in line with previous studies that have found that doses of exogenous melatonin between 0.3mg and 10mg administered during the afternoon and into the early evening decrease the latency of sleep onset after only one day (Dollins *et al*., 1994; Zhdanova *et al*., 1995). Day-by-day examination of participants' experimental wake data revealed a similar pattern of phase advances and delays as a result of the melatonin treatment, though this pattern was not as robust as that found in the sleep data. Additionally, a trend of increasing variability was found for both sleep and wake times during the experimental period as

compared to a trend of decreasing variability during the baseline period. Though the hypnotic effects of melatonin have been widely reported in the literature (for comprehensive reviews of melatonin's hypnotic effects see Zhdanova, 2005 and Srinivasan *et al*., 2009), this property of melatonin cannot fully explain the changes in sleep and wake behaviours demonstrated here. If the results were solely due to melatonin's hypnotic effects, it would be expected that all participants' sleep times consistently advance when given melatonin in the early afternoon and consistently delay when given melatonin in the late morning, with no variability throughout. Rather, our results are more suggestive of melatonin's chronobiotic effects, altering participants' sleep and wake patterns and producing increasing variability as a result of participants' internal clocks shifting out of phase with each other and with the external environment, leading to an eventual state of internal desynchronization. Consistent with our results, Takahashi *et al.* (2002) and Waterhouse *et al*. (2003) found that those undergoing jet lag had earlier times of sleep onset and offset compared to normal. It was proposed that fatigue in the evening as a result of jet lag could account for the earlier sleep times, and the earlier wake times may be due to the poorer ability to sleep (Waterhouse *et al*., 2003). Moreover, night and rotating shift workers have been shown to have varying sleep and wake times and a high rate of sleep deprivation, both of which are consequences of disrupting circadian rhythmic processes (Haus and Smolensky, 2006). Thus it is inferred from previous research together with the current results that our melatonin treatment successfully induced circadian disruption, resulting in symptoms commonly associated with jet lag and shift work.

4.2.2 Sleep Quality Ratings

In addition to logging their sleep and wake times, participants were asked to report their quality of sleep during both baseline and experimental periods. It was found that participants

reported a significantly decreased quality of sleep while on the melatonin treatment compared to baseline. Studies on those undergoing jet lag after crossing 10 time zones and shift workers working out of phase with their chronotype have similarly demonstrated higher levels of sleep disturbance compared to normal (Waterhouse *et al*., 2003; Juda *et al*., 2013), indicating that the current melatonin protocol induced not only sleep/wake disturbances but also deficits in sleep quality commonly observed as consequences of shift work or jet lag.

The use of melatonin as a treatment for temporal disturbances has garnered much attention from chronobiologists, with the prevailing idea that if taken at the right time, melatonin can be effective in helping to re-adapt sleep/wake cycles and improve sleep quality (Arendt *et al*., 1997; Herxheimer and Petrie, 2002; Smith *et al.*, 2005; Zea and Goldstein, 2010). A few studies have also demonstrated melatonin's beneficial effects on those with Alzheimer's disease, with reports of significantly improved sleep quality and decreased number of sleep disturbances when melatonin was taken before sleep (Fainstein *et al*., 1997; Cardinali *et al*., 2011). The present study differs from those aforementioned studies in that melatonin was used in an attempt to induce internal desynchrony, with our results demonstrating the first evidence of worse and less restful sleeps when taking exogenous melatonin at inappropriate times. This finding holds much importance in society today as melatonin is readily marketed and sold as a health product and is often taken as a sleep aid by the general public without proper use instructions. As a result of taking melatonin at the wrong doses and times, many people likely suffer detrimental side effects similar to those observed in the current study. Thus, educating the public on how to correctly administer melatonin may be beneficial not only to those undergoing shift work and jet lag, but also to those who regularly use melatonin for its soporific effects.

4.3 Emotional Stroop Test and Melatonin

The emotional Stroop task was administered to participants on four days during the experimental period to assess changes in cognitive performance as a result of the melatonin treatment. It was found that the Stroop effect was eliminated only for RTs in the word instruction set, and remained present for RTs in the face instruction set and for errors in both the face and word instruction sets. It was further discovered that the congruent face and incongruent word conditions demonstrated significant changes between the baseline and experimental periods while the incongruent face and congruent word conditions did not. Surprisingly, the only condition in which performance significantly decreased during the experimental period was for errors in the incongruent word condition; all other conditions demonstrated either no significant changes or improved performance on this task. These results are inconsistent with our hypothesis and previous research that has demonstrated increased RTs and error rates (Dijk *et al*., 1992; Horowitz *et al.*, 2001; Santhi *et al*., 2007 and 2008) and falls in alertness and motivation (Waterhouse *et al*., 2005) in shift workers and people experiencing jet lag, as well as changes in cognitive throughput performance (Darwent *et al*., 2010) and slower and more variable RTs in the psychomotor vigilance task in people subjected to a forced desynchrony protocol (Zhou *et al*., 2011). In contrast to the simple reactionary tasks used in these studies, however, the emotional Stroop task is much more complex, involving the use of higher order cognitive functions. To date, the emotional Stroop task has not been employed as a measure of cognitive performance in studies on shift work and jet lag, though studies on circadian rhythms and conflict processing using the colour/word Stroop task have shown circadian variations in components of executive functions including cognitive inhibition and flexibility (i.e. how well one adapts to a shift in task criteria) (Marek *et al.*, 2010; Schmidt *et al*., 2012; Ramirez *et al*.,

2012; Garcia *et al*., 2012). Of particular interest is a study by Bratzke *et al*. (2012), in which it was reported that there were no changes in inhibitory control in the Stroop task over a 40 hour constant routine protocol. This finding challenges the predominant view that executive functions are particularly vulnerable to sleep loss and changes in circadian rhythms, and may help explain why most conditions in our task did not produce significant performance deficits.

It is well established in the literature that visual word processing is lateralized to the left hemisphere and that face processing is lateralized to the right hemisphere (Maurer *et al*., 2008; Dundas *et al*., 2013; Li *et al.*, 2013). It has also been postulated by Raccuglia *et al*. (1997) that word and face processing occurs through the dual-pathway hypothesis, an affective computation model first described by Joseph LeDoux in 1989. In short, this model purports that affective words are addressed through the thalamo-amygdala pathway (also referred to as the "short pathway") and appraised directly, while affective faces are addressed through cortical pathways that feed back to the amygdala (also referred to as the "long pathway") and appraised indirectly (Raccuglia *et al*., 1997). Moreover, word processing has been shown to occur faster and more automatically than face processing, as evidenced by the fact that face lateralization occurs at a later stage in development than word lateralization (Dundas *et al*., 2013). Thus in relation to the current study, the observed decrease in performance for the word instruction set may have been due to the melatonin treatment affecting the subcortical thalamo-amygdala pathway and resulting in the less automatic processing of words, as MT_1 receptors have been characterized in both these areas of the brain. On the other hand, the face processing pathway may have been affected to a lesser extent as the cortical pathways may have been able to compensate for this change in the amygdala. Facial stimuli processing would therefore be minimally affected, as the cortical pathways that result in the conscious impression of these stimuli would still be able to encode the

faces presented. It is also thought that participants performed significantly better in the congruent face condition during the experimental period as a result of practice – that is, not only were participants able to encode the faces without trouble, they were also able to recognize them faster due to the fact that they had already performed the emotional Stroop task several times prior. This ultimately resulted in faster RTs and less errors compared to baseline. Conversely, disruption of the thalamo-amygdala pathway for word processing by the melatonin treatment may have caused a trade-off between RTs and error rates, resulting in significantly faster RTs but significantly more errors for the incongruent word condition. The incongruent face and congruent word conditions demonstrated no significant changes in RTs and error rates between the baseline and experimental periods, and it is hypothesized that this occurred because they were the hardest and easiest conditions, respectively. It has been shown that incongruent face trials for the emotional Stroop task elicit more negative N170 event related potentials than congruent face trials (Zhu *et al*., 2010), potentially because face processing must be enhanced in order for a person to overlook the more salient word and give a correct response, a difficult task to master. The congruent word trials, on the other hand, were simply too easy – participants reached ceiling relatively quickly, thus allowing no room for significant improvements to be made. In general, the difficulty levels of these two tasks made them less sensitive to changes in performance, with the result being no significant findings when comparing the two testing periods.

4.4 Diffusion Tensor Imaging

4.4.1 Tract-Based Spatial Statistics and Voxelwise Statistics

To determine whether the melatonin treatment affected areas in the brain associated with

the emotional Stroop task, TBSS and voxelwise statistics were performed on the DTI data. It was found that whole brain, left IFG, and right IFG FA values decreased significantly during the experimental period while whole brain, left IFG, and right IFG MD values increased significantly compared to baseline. Whole brain FA and MD values have been shown to increase in the morning and decrease in the evening, perhaps as an adaptation of neural activities to the environmental light/dark cycle (Jiang *et al*., 2014). Indeed, neural activities are performed more regularly during the daytime relative to the evening, and the subsequent increase in FA and MD values in the morning may indicate improved functional performance (Jiang *et al*., 2014). Comparatively, our results show a decrease in FA values and an increase in MD values between the baseline and experimental scans, though the time of scanning was kept consistent for all time points and participants. Circadian variations in these DTI metrics can be thus ruled out, and the observed changes may instead be due to the melatonin treatment and its effects on the pathways underlying performance on the emotional Stroop task.

Although no studies to date have used DTI as a tool for understanding the neural networks associated with the emotional Stroop task, other studies using memory and inhibition tasks have demonstrated correlations between DTI metrics and task performance in some common brain areas. For example, a study by Sasson *et al*. (2010) in which participants performed a non-verbal memory task found a large accuracy- and RT-MD correlation in the IFG. It was shown that shorter RTs and less errors were correlated with increased FA and decreased MD values, potentially because dendritic density and synaptic spines were reduced and the higher organization and integrity of white matter allowed for faster transmission of information in the associated brain networks (Sasson *et al*., 2010). Moreover, Madsen *et al*. (2010) found that faster response inhibition in the go/no go task was significantly associated with higher FA and

lower MD values in the IFG, possibly reflecting the faster speed of neural conduction as a result of better myelinated or more densely packed fibre tracts. In the present study, it was demonstrated that overall, participants had shorter RTs and less errors during the experimental period but decreased FA and increased MD values in the IFG. In general, higher MD and lower FA values indicate impaired fibre integrity due to an increased rate of diffusion and loss of coherence on the principle diffusion axis (Soares *et al*., 2013). It is therefore hypothesized that though participants may be performing better on the task due to task repetition, underlying pathways are being disrupted as evidenced by the changes in DTI metrics observed.

It may be argued that eight days is a relatively short period of time for changes in the brain to occur. However, a study by Sagi *et al*. (2012) demonstrated structural changes in the brain within two hours of learning a new video game. They also performed a concomitant study on rats learning a Morris water maze and found that spatial learning was associated with a decrease in MD values within the hippocampus detected the following day (Sagi *et al*., 2012). Because DTI is used to determine tissue microstructure, increases or decreases in tissue density and enhancement or deterioration of tissue organization will lead to changes in water diffusion properties (Assaf and Pasternak, 2008). It is thus postulated that the decrease in MD values may be a result of rapid activity-dependent astrocyte swelling, reflecting a shift in the ratio of extracellular to intracellular space (Sagi *et al*., 2012). In the current study, it was hypothesized that changes in DTI metrics would be found in the left and right HEC, though analysis of the results identified no significant changes in FA and MD values. In comparison to the video game task used by Sagi *et al.* (2012), the emotional Stroop task employed in our study does not require spatial navigation and may thus need to recruit fewer resources from the hippocampus. As a result, it is proposed that the eight day melatonin treatment combined with the eight time points

of emotional Stroop task administration may indeed be too short of a time frame for changes in the hippocampus to be observed. Extending the experimental period for a longer amount of time or altering the task to involve aspects of spatial learning may produce the significant changes in DTI metrics initially expected within the hippocampus.

4.4.2 Tractography

Changes in white matter microstructure were also assessed in this study via the use of probabilistic tractography. No significant changes were found in the number of valid tracts between the left HEC and the left and right IFG nor between the right HEC and the left and right IFG when comparing baseline and experimental scans. Several factors are thought to have contributed to these non-significant findings. Firstly, as tractography is influenced by many anatomy- and algorithm-based factors (Jones *et al*., 2012), our small sample size of 10 participants may have affected the results. Furthermore, as tractography is sensitive to ROI size and placement (Jones *et al*., 2012), the masks of the ROIs generated from the standard atlases provided by FSL may have lacked specificity and consistency across participants. Future studies will extract ROIs from individual participant's functional data and apply it directly to the DTI data to ensure a more accurate comparison between these regions and their streamline counts. Though studies on response inhibition have characterized a network of fibre tracts between the IFG, presupplementary motor area, and the basal ganglia, specifically the subthalamic nuclei (Aron *et al.*, 2007; Leh *et al.*, 2007; King *et al.*, 2012; Swann *et al*., 2012) and studies on learning and memory encoding have found fibre tracts connecting the prefrontal cortex, hippocampus and basal ganglia (Bennett *et al*., 2011; Schott *et al*., 2011), no studies to date have looked at the direct connections between the hippocampus and the IFG. Thus it is not known whether the lack of change in SC values found is a result of the paradigm used, or whether these

fibres are particularly resistant to change. Future work will look to clarify these results by incorporating additional ROIs (such as the presupplementary motor area, basal ganglia, and retinal pathways to the SCN, and amygdala and hippocampus pathways to the IFG) into the current tractography analysis and specifically targeting the hippocampus and IFG by modifying the cognitive task to include aspects of both inhibition and memory encoding.

4.5 Correlations

Correlation analyses were performed on the sleep, wake, sleep quality, emotional Stroop, and DTI data to determine whether there were any associations between the behavioural, attentional, and neural components of the study. It was found that increases in incongruent word errors in the emotional Stroop task were significantly correlated with decreases in left hemisphere IFG FA values. As mentioned in section 4.3, word processing is known to be lateralized to the left hemisphere (Dundas *et al*., 2013; Li *et al.*, 2013). Thus the decrease in left hemisphere IFG FA values may explain why increases in incongruent word errors were found, as FA values closer to zero indicate poorer alignment of fibres and therefore less streamlined connections (Jones *et al*., 2012). Additionally, it was found that decreases in congruent face errors in the emotional Stroop task were significantly correlated with decreases in both right hemisphere IFG FA and MD values. This was an interesting finding, as FA and MD values often have an inverse relationship – that is, an increase in one metric is regularly accompanied by a decrease in the other, and vice versa (Soares *et al*., 2013). It was thus expected that FA values would increase while MD values decreased in the right IFG, as this indicates more efficient fibre organization and more streamlined connections. That this was not the case may again be explained by the fact that, as mentioned in section 4.3, face processing occurs through several

cortical pathways which feedback into the amygdala (Raccuglia *et al*., 1997). Therefore although there were poorer organization of fibres in the right IFG as inferred by the decrease in FA found, other brain regions involved in the face processing pathway may have overcompensated to allow for more accurate face encoding, resulting in fewer errors in the congruent face condition.

4.6 Limitations and Future Work

Several limitations are present in this study. Firstly, we were not able to recruit enough participants to have a completely separate control population; thus the control group consisted only of within-subject controls. Future work will incorporate a sample of independent, healthy controls who will be given placebos to parse out what effects are due to learning and what effects are due to the melatonin treatment alone. Furthermore, only two scans were conducted for each participant – one at the end of the baseline period and one at the end of the experimental period. Incorporating a third scan prior to exposure to the emotional Stroop task could have perhaps provided insight into the structural make-up prior to learning, allowing for a clearer determination of learning versus desynchrony effects on the brain. Moreover, external factors that may have affected the results could not be controlled for in this study as participants were not secluded in a laboratory setting for the duration of the experiment. Additionally, we did not include shift workers or people undergoing jet lag to test how the current desynchrony model compares to internal desynchronization caused by temporal disruption. Future studies will incorporate a subset of these populations to determine how accurate and effective melatonin is at causing circadian disruption and the associated deficits in cognitive performance. As mentioned previously, the emotional Stroop task used in this study may not have been challenging enough to discriminate between minor differences in baseline and experimental performance. Future

studies using this paradigm can alter the pictures to make them greyscale so that neither the face nor the word stimuli are more salient than the other, or shorten the stimulus presentation times to create a more sensitive titer to examine cognitive performance. Also, though the eight days of melatonin-induced desynchrony produced observable results, a longer period of desynchronization may lend more insight into how circadian disruption affects cognitive processes and the associated structural networks in the brain. Methodologically, tractography analysis using DTI data does not take into consideration crossing, diverging, or kissing fibres. Thus regions of the brain containing voxels that have two or more fibre bundles oriented in different directions may lead to incorrect estimation of fibre directions and may even result in the abrupt termination of fibre tracts (Soares *et al*., 2013). Alternatives to DTI tractography include more sophisticated approaches such as diffusion spectrum imaging and Q-ball imaging, which use probability density functions instead of single tensors to identify diffusion in different directions at each voxel (Soares *et al*., 2013). Lastly, though the ELISAs were not performed on the full set of collected data due to financial constraints, melatonin measurements via saliva sample collections were restricted to waking hours only. Analysis of these samples will therefore need to model the data for nighttime hours, when melatonin levels are generally at their highest point.

4.7 Applications: Alzheimer's and Parkinson's Disease

As demonstrated in the present study, melatonin taken at inappropriate times during the day can elicit behavioural changes similar to those exhibited by people undergoing temporal disruption. However, proper administration of melatonin can have many positive effects. For example, melatonin's antioxidant properties have been shown to prevent oxidative damage in

cultured neuronal cells (Mayo *et al*., 1998) as well as in the brains of animals treated with neurotoxic agents (Jin *et al*., 1998), lending favour towards its use as a potential therapeutic drug for neurodegenerative diseases such as Alzheimer's disease (AD) and Parkinson's disease (PD). Indeed, studies on AD and PD patients have found that melatonin supplements not only aid in reducing sleep/wake disturbances (for a comprehensive review on sleep disturbances in AD and PD patients see Rothman and Mattson, 2012), but may also play a role in slowing down the progression of these diseases (for a comprehensive review on the therapeutic uses of melatonin see Pandi-Perumal *et al*., 2013). In addition, Adi *et al*. (2010) found that MT_1 and MT_2 receptors are down-regulated in the amygdala and substantia nigra of PD patients, providing further evidence of the possible involvement of melatonin in the development of PD. Thus it is of extreme importance to understand the role of melatonin not only in the circadian system, but also in the development and treatment of AD and PD.

The use of DTI may also be a good tool to uncover changes in white matter microstructure in AD and PD patients. Hasan *et al*. (2012) found that in people with AD, fibre paths from the hippocampus towards the amygdala, thalamus, and caudate and from these regions back to the hippocampus were more scattered and had less neurotransmitters than that of controls. Moreover, Baggio *et al*. (2012) found significant positive correlations between performance in identifying sad facial expressions and FA levels in the right frontal lobe, inferior fronto-occipital fasciculus, and inferior longitudinal fasciculus of PD patients. Tractography studies on healthy controls have found fibres that connect the hippocampus and the amygdala and that extend to the fornix, dorsal hippocampal commissure, stria terminalis, uncinate fasciculus and the orbitofrontal cortex (Colnat-Coulbois *et al*., 2010), some of which are regions of the brain that are known to be affected by AD and PD. Therefore, administration of properly

timed melatonin treatment along with the emotional Stroop task to people with AD and PD in combination with DTI and tractography analyses may provide insight into the structural changes underlying the cognitive impairment associated with these diseases.

5. Conclusion

The present study demonstrates the first evidence of the effects of inappropriately timed melatonin on cognitive performance and structural changes in the brain. While we did not find increases in RTs and error rates on all conditions of the emotional Stroop task as we had hypothesized, we did find decreases in FA and increases in MD values in the IFG, consistent with signs of impaired fibre integrity. Thus the current work demonstrates that though short-term desynchronization may not always produce observable deficits in performance on cognitive tasks, brain networks underlying executive functions show disruption after only eight days of melatonin treatment. Long-term internal desynchronization as a result of shift work or constant jet lag may therefore lead to negative white matter microstructure adaptations that can further impair cognitive performance. In addition, this study is also the first to demonstrate that melatonin can effectively induce circadian desynchronization as evidenced by the changes in sleep/wake behaviours reported by our participants. Unexpectedly, participants also reported significant decreases in sleep quality during the melatonin treatment period. It is thus beneficial to educate the general public on the proper use of melatonin as a sleep aid, as taking melatonin at inappropriate times may in fact be doing more harm than good. Further studies need to be conducted using populations of shift workers and frequent sufferers of jet lag to assess whether similar structural changes in the brain occur in those undergoing internal desynchronization as a result of temporal disruption.

6. References

Abe, M., Herzog, E.D., Yamazaki, S., Straume, M., Tei, H., Sakaki, Y., Menaker, M., and Block, G.D. 2002. Circadian rhythms in isolated brain regions. *J. Neurosci.* **22**, 350-356.

Adi, N., Mash, D.C., Ali, Y., Singer, C., Shehadeh, L., and Papapetropoulos, S. 2010. Melatonin MT1 and MT2 receptor expression in Parkinson's disease. *Med. Sci. Monit.* **16**, BR61-67.

Agez, L., Laurent, V., Pevet, P., Masson-Pevet, M., and Gauer, F. 2007. Melatonin affects nuclear orphean receptors mRNA in the rat suprachiasmatic nuclei. *Neurosci*. **144**, 522-530.

Allada, R. and Chung, B.Y. 2010. Circadian organization of behaviour and physiology in *Drosophila*. *Annu. Rev. Physiol.* **72**, 605-624.

Al-Naimi, S., Hampton, S.M., Richard, P., Tzung, C., and Morgan, L.M. 2004. Postprandial metabolic profiles following meals and snacks eaten during simulated night and day shift work. *Chronobiol. Int.* **21**, 937-947.

Alonso-Vale, M.I., Andreotti, S., Mukai, P.Y., Borges-Silva, C.N., Peres, S.B., Cipolla-Neto, J., and Lima, F.B. 2008. Melatonin and the circadian entrainment of metabolic and hormonal activities in primary isolated adipocytes. *J. Pineal Res.* **45**, 422-429.

Amir, S., Lamont, E.W., Robinson, B., and Stewart, J. 2004. A circadian rhythm in the expression of PERIOD2 protein reveals a novel SCN-controlled oscillator in the oval nucleus of the bed nucleus of the stria terminalis. *J. Neurosci.* **24**, 779-781.

Anisimov, V.N., Baturin, D.A., Popovich, I.G., Zabezhinski, M.A., Manton, K.G., Semenchenko, A.V., and Yashin, A.I. 2004. Effect of exposure to light-at-night on life span and spontaneous carcinogenesis in female CBA mice. *Int. J. Cancer*. **111**, 475-479.

Arendt, J., Skene, D.J., Middleton, B., Lockley, S.W., and Deacon, S. 1997. Efficacy of melatonin treatment in jet lag, shift work, and blindness. *J. Biol. Rhythms*. **12**, 604-617.

Arendt, J. 2006. Melatonin and human rhythms. *Chronobiol. Int*. **23**(1&2): 21-37.

Arendt, J. 2010. Shift work: coping with the biological clock. *Occup. Med-c.* **60**, 10-20.

Aron, A.R., Behrens, T.E., Smith, S., Frank, M.J., and Poldrack, R.A. 2007. Triangulating a cognitive control network using diffusion-weighted magnetic resonance imaging (MRI) and functional MRI. *J. Neurosci.* **27**, 3743-3652.

Assaf, Y. and Pasternak, O. 2008. Diffusion tensor imaging (DTI)-based white matter mapping in brain research: A review. *J. Mol. Neurosci.* **34**, 51-61.

Baggio, H.C., Segura, B., Ibarretxe-Bilbao, N., Valldeoriola, F., Marti, M.J., Compta, Y., Tolosa, E., and Junqué, C. 2012. Structural correlates of facial emotion recognition in deficits in Parkinson's disease patients. *Neuropsychologia.* **50**, 2121-2128.

Bao, S., Rihel, J., Bjes, E., Fan, J.Y., and Price, J.L. 2001. The *Drosophila double-time*^{S} mutation delays the nuclear accumulation of *period* protein and affects the feedback regulation of *period* mRNA. *J. Neurosci.* **21**, 7117-7126.

Beall, P.M. and Herbert, A.M. 2008. The face wins: Stronger automatic processing of affect in facial expressions than words in a modified Stroop task. *Cogn. Emot.* **22**, 1613-1642.

Bedrosian, T.A., Herring, K.L., Walton, J.C., Fonken, L.K., Weil, Z.M., and Nelson, R.J. 2013. Evidence for feedback control of pineal melatonin secretion. *Neurosci Lett.* **542**, 123-125.

Behrens, T.E.J., Woolrich, M.W., Walton, M.E., and Rushworth, M.F.S. 2007. Learning the value of information in an uncertain world. *Nat. Neurosci*. **10**, 1214-1221.

Bennett, I.J., Madden, D.J., Chandan, J.V., Howard, J.H., Jr., and Howard, D.V. 2011. White matter integrity correlates of implicit sequence learning in healthy aging. *Neurobiol. Aging.* **32**, 2317.e1-2317.e12.

Bonnefort-Rousselot, D. and Collin, F. 2010. Melatonin: Action as antioxidant and potential applications in human disease and aging. *Toxicol.* **278**, 55-67.

Bradshaw, W.E. and Holzapfel, C.M. 2007. Evolution of Animal Photoperiodism. *Annu. Rev. Ecol. Evol. S.* **38**, 1-25.

Bratzke, D., Steinborn, M.B., Rolke, B., and Ulrich, R. 2012. Effects of sleep loss and circadian rhythm on executive inhibitory control in the Stroop and Simon tasks. *Chronobiol. Int.* **29**, 56-61.

Breslow, E.R., Phillips, A.J.K., Huang, J.M., St. Hilaire, M.A., and Klerman, E.B. 2013. A mathematical model of the circadian phase-shifting effects of exogenous melatonin. *J. Biol Rhythms.* **28**, 79-89.

Brodsky, V.Y. and Zvezdina, N.D. 2010. Melatonin as the most effective organizer of the rhythm of protein synthesis in hepatocytes *in vitro* and *in vivo*. *Cell Biol. Int.* **34**, 1199-1204.

Buijs, R.M., Hou, Y.X., Shinn, S., and Renauld, L.P. 1994. Ultrastructural evidence for intra- and extranuclear projections of GABAergic neurons of the suprachiasmatic nucleus. *J. Comp. Neurol.* **340**, 381-391.

Bullough, J.D., Rea, M.S., and Figueiro, M.G. 2006. Of mice and women: light as a circadian stimulus in breast cancer research. *Cancer Causes Control*. **17**, 375-383.

Burgess, H.J., Revell, V.L., and Eastman, C.I. 2008. A three pulse phase response curve to three milligrams of melatonin in humans. *J. Physiol.* **586**, 639-647.

Burgess, H.J., Revell, V.L., Thomas, A.M., and Eastman, C.I. 2010. Human phase response curves to three days of daily melatonin: 0.5mg *versus* 3.0mg. *J. Clin. Endocrinol. Metab.* **95**, 3325-3331.

Burgess, H.J., Sharkey, K.M., and Eastman, C.I. 2002. Bright light, dark and melatonin can promote circadian adaptation in night shift workers. *Sleep Med. Rev*. **6**, 407-420.

Cardinali, D.P., Furio, A.M., and Brusco, L.I. 2011. The use of chronobiotics in the resynchronization of the sleep/wake cycle: Therapeutical application in the early phases of Alzheimer's disease. *Recent Pat. Endocr. Metab. Immune Drug Discov.* **5**, 80-90.

Chakravarty, S. and Rizvi, S.I. 2011. Circadian modulation of sodium-potassium ATPase and sodium-proton exchanger in human erythrocytes: *In vitro* effect of melatonin. *Cell Mol. Biol.* **57**, 80-86.

Challet, E., Caldelas, I., Graff, C., and Pevet, P. 2003. Synchronization of the molecular clockwork by light- and food-related cues in mammals. *Biol. Chem.* **384**, 711-719.

Cho, K. 2001. Chronic 'jet lag' produces temporal lobe atrophy and spatial cognitive deficits. *Nat. Neurosci.* **4**, 567-568.

Cho, K., Ennaceur, A., Cole, J.C., and Suh, C.K. 2000. Chronic jet lag produces cognitive deficits. *J. Neurosci.* **20** (6), RC66.

Chustecka, Z. Denmark pays compensation for breast cancer after night-shift work. Medscape. 2009 March 23; Medical News.

Cisek, P., Puskas, G.A., and El Murr, S. 2009. Decisions in changing conditions: The urgency-gating model. *J. Neurosci.* **29**, 11560-11571.

Clark, R.E., Broadbent, N.J., and Squire, L.R. 2004. Hippocampus and remote spatial memory in rats. *Hippocampus*. **15**, 260-272.

Colnat-Coulbois, S., Mok, K., Klein, D., Penicaud, S., Tanriverdi, T., and Olivier, A. 2010. Tractography of the amygdala and hippocampus: Anatomical study and application to selective amygdalohippocampectomy. *J. Neurosurg.* **113**, 1135-1143.

Darwent, D., Ferguson, S.A., Sargent, C., Paech, G.M., Williams, L., Zhou, X., Matthews, R.W., Dawson, D., Kennaway, D.J., and Roach, G.D. 2010. Contribution of core body temperature, prior wake time, and sleep stages to cognitive throughput performance during forced desynchrony. *Chronobiol. Int.* **27**, 898-910.

Davis, S., Mirick, D.K., Chen, C., and Stanczyk, FZ. 2012. Night shift work and hormone levels in women. *Cancer. Epidemio. Biomarkers. Prev.* **21**, 609-618.

de Mairan, J.J.O. 1729. Observation Botanique. *Histoire de l'Academie Royale des Sciences*, Paris. 35-36.

DeSouza, J.F.X., Menon, R.S., and Everling, S. 2003. Preparatory set associated with pro-saccades and anti-saccades in humans investigated with event-related fMRI. *J. Neurophysiol.* **89**, 1016-1023.

Devan, B.D., Goad, E.H., Petri, H.L., Antoniadis, E.A., Hong, N.S., Ko, C.H., Leblanc, L., Lebovic, S.S., Lo, Q., Ralph, M.R., and McDonald, R.J. 2001. Circadian phase-shifted rats show normal acquisition but impaired long-term retention of place information in the water task. *Neurobiol. Learn. Mem.* **75**, 51-62.

Dijk, D.J., Duffy, J.F., and Czeisler, C.A. 1992. Circadian and sleep/wake dependent aspects of subjective alertness and cognitive performance. *J. Sleep Res.* **1**, 112-117.

Dollins, A.B., Zhdanova, I.V., Wurtman, R.J., Lynch, H.J., and Deng, M.H. 1994. Effect of inducing nocturnal serum melatonin concentrations in day on sleep, mood, body temperature, and performance. *Proc. Natl. Acad. Sci. USA*. **91**, 11824-1828.

Dubocovich, M.L. and Markowska, M. 2005. Functional MT1 and MT2 melatonin receptors in mammals. *Endocrine*. **27**, 101-110.

Dundas, E.M., Plaut, D.C., and Behrmann, M. 2013. The joint development of hemispheric lateralization for words and faces. *J. Exp. Psychol.* **142**, 348-358.

Egner, T., Etkin, A., Gale, S., and Hirsch, J. 2008. Dissociable neural systems resolve conflict from emotional versus nonemotional distracters. *Cereb. Cortex.* **18**, 1475-1484.

Eichenbaum, H., Yonelina, A.P., and Ranganath, C. 2007. The medial temporal lobe and recognition memory. *Annu. Rev. Neurosci.* **30**, 123-152.

Etkin, A., Egner, T., Peraza, D.M., Kandel, E.R., and Hirsch, J. 2006. Resolving emotional conflict: A role for the rostral anterior cingulate cortex in modulating activity in the amygdala. *Neuron.* **51**, 871-882.

Fainstein, I., Bonetto, A.J., Brusco, L.I., and Cardinali, D.P. 1997. Effects of melatonin in elderly patients with sleep disturbances: A pilot study. *Curr. Ther. Res. Clin. E.* **58**, 990-1000.

Ferguson, S.A., Kennaway, D.J., Baker, A., Lamond, N., and Dawson, D. 2011. Sleep and circadian rhythms in mining operators: Limited evidence of adapation to night shifts. *Appl. Ergon.* **43**, 695-701.

Folkard, S., Ardent, J., and Clark, M. 1993. Can melatonin improve shift workers' tolerance of the night shift? Some preliminary findings. *Chronobiol. Int*. **10**, 315-320.

Gachon, F., Nagoshi, E., Brown, S.A., Ripperger, J., and Schibler, U. 2004. The mammalian circadian timing system: From gene expression to physiology. *Chromosoma.* **113**, 103-112.

Garcia, A., Ramirez, C., Martinez, B., and Valdez, P. 2012. Circadian rhythms in two components of executive functions: Cognitive inhibition and flexibility. *Biol. Rhythm Res.* **43**, 49-63.

Gaston, K.J., Bennie, J., Davies, T.W., and Hopkins, J. 2013. The ecological impacts of nighttime light pollution: A mechanistic appraisal. *Biol. Rev.* **88**, 912-927.

Gekakis, N., Staknis, D., Nguyen, H.B., Davis, F.C., Wilsbacher, L.D., King, D.P., Takahasi, J.S., and Weitz, C.J. 1998. Role of the CLOCK protein in the mammalian circadian mechanism. *Science*. **280**, 1564-1569.

Giannotti, F., Cortesi, F., Sebastiani, T., and Ottaviano, S. 2002. Circadian preference, sleep and daytime behaviour in adolescence. *J. Sleep Res.* **11**, 191-199.

Gibson, E.M., Wang, C., Tjho, S., Khattar, N., and Kriegsfeld, L.J. 2010. Experimental 'jet lag' inhibits adult neurogenesis and produces long-term cognitive deficits in female hamsters. *PLoS One.* **5**, e15267.

Gillette, M.U. and McArthur, A.J. 1996. Circadian actions of melatonin at the suprachiasmatic nucleus. *Behav. Brain Res.* **73**, 135-139.

Golombek, D.A., Casiraghi, L.P., Agostino, P.V., Paladino, N., Duhart, J.M., Plano, S.A., and Chiesa, J.J. 2013. The times they're a-changing: Effects of circadian desynchronization on physiology and disease. *J. Physiol. Paris.* **107**, 310-322.

Groos, G.A., and Meijer, J.H. 1985. Effects of illumination on suprachiasmatic nucleus electrical discharge. *Ann. NY Acad. Sci.* **453**, 134-146.

Hagenauer, M.H., Ku, J.H., and Lee, T.M. 2011. Chronotype changes during puberty depend on gonadal hormones in the slow-developing rodent, *Octodon degus*. *Horm. Behav.* **60**, 37-45.

Hagmann, P., Jonasson, L., Maeder, P., Thiran, J-P., Wedeen, V.J., and Meuli, R. 2006. Understanding diffusion MR imaging techniques: From scalar diffusion-weighted imaging to diffusion tensor imaging and beyond. *Radiographics*. **26**, S205-S223.

Hardeland, R., Cardinali, D.P., Srinivasan, V., Spence, D.W., Brown, G.M., and Pandi-Perunal, S.R. 2011. Melatonin – A pleiotropic, orchestrating regulator molecule. *Prog. Neurobiol.* **93**, 350-384.

Hardin, P.E. 2011. Molecular genetic analysis of circadian timekeeping in Drosophila. *Adv. Genet.* **74**, 141-173.

Hardin, P.E., Hall, J.C., and Rosbash, M. 1990. Feedback of the *Drosophila period* gene product on circadian cycling of its messenger RNA levels. *Nature*. **343**, 536-540.

Harma, M. 2006. Workhours in relation to work stress, recovery and health. *Scand. J. Work Environ. Health*. **32**, 502-514.

Harms, E., Kivimae, S., Young, M.W., and Saez, L. 2004. Posttranscriptional and posttranslational regulation of clock genes. *J. Biol. Rhythms*. **19**, 361-373.

Hasan, M.K. Lee, W., Park, B., and Han, K. 2012. Connectivity analysis of hippocampus in Alzheimer's brain using probabilistic tractography. *BIC-TA*. **7**, 521-528.

Hattar, S., Liao, H.W., Takao, M., Berson, D.M., and Yau, K.W. 2002. Melanopsin-containing retinal ganglion cells: Architecture, projections, and intrinsic photosensitivity. *Science*. **295**, 1065-1070.

Haus, E. and Smolensky, M. 2006. Biological clocks and shift work: circadian dysregulation and potential long-term effects. *Cancer Causes Control*. **17**, 489-500.

Hazlerigg, D. 2012. The evolutionary physiology of photoperiodism in vertebrates. *Prog. Brain Res.* **199**, 413-422.

Herxheimer, A. and Petrie, K.J. 2002. Melatonin for the prevention and treatment of jet lag. *Cochrane Database Syst. Rev*. **2**, 1-23.

Horowitz, T.S., Cade, B.E., Wolfe, J.M., and Czeisler, C.A. 2001. Efficacy of bright light and sleep/darkness scheduling in alleviating circadian maladaptation to night work. *Am. J. Physiol. Endocrinol. Metab.* **281**, E384-391.

Jarrard, L.E. 1993. On the role of the hippocampus in learning and memory in the rat. *Behav. Neural. Biol.* **60**, 9-26.

Jiang, C., Zhang, L., Zou, C., Long, X., Liu, X., Zheng, H., Liao, W., and Diao, Y. 2014. Diurnal microstructural variations in healthy adult brain revealed by diffusion tensor imaging. *PLoS One.* **9**, e84822.

Jin, B.K., Shin, D.Y. Jeong, M.Y., Gwag, M.R., Baik, H.W., Yoon, K.S., Cho, Y.H., Joo, W.S., Kim, Y.S., and Baik, H.H. 1998. Melatonin protects nigral dopaminergic neurons from 1-methyl-4-phenylpyridinium (MPP+) neurotoxicity in rats. *Neurosci. Lett.* **245**, 61-64.

Johnson, R.F., Moore, R.Y., and Morin, L.P. 1988. Loss of entrainment and anatomical plasticity after lesions of the hamster retinohypothalamic tract. *Brain Res.* **460**, 297-313.

Jones, D.K., Knösche, T.R., and Turner, R. 2012. White matter integrity, fiber count, and other fallacies: The do's and don'ts of diffusion MRI. *Neuroimage*. **73**, 239-254.

Juda, M., Vetter, C., and Roenneberg, T. 2013. Chronotype modulates sleep duration, sleep quality, and social jet lag in shift workers. *J. Biol. Rhythms.* **28**, 141-151.

Kalsbeek, A., and Buijs, R.M. 2002. Output pathways of the mammalian suprachiasmatic nucleus: Coding circadian time by transmitter selection and specific targeting. *Cell Tissue Res.* **309**, 109-118.

Kalsbeek, A., Garidou, M.L., Palm, I., van der Vliet, J., Simonneaux, V., Pevet, P., and Buijs, R.M. 2000. Melatonin sees the light: blocking GABA-ergic transmission in the paraventricular nucleus induces daytime secretion of melatonin. *Eur. J. Neurosci.* **12**, 3146-3154.

Karlsson, B.H., Knutsson, A.K., and Lindahl, B.O. 2001. Is there an association between shift work and having a metabolic syndrome? Results from a population based study of 27,485 people. *Occup. Environ. Med.* **58**, 747-752.

Karlsson, B.H., Knutsson, A.K., Lindahl, B.O., and Alfredsson, L.S. 2003. Metabolic disturbances in male workers with rotating three-shift work. Results of the WOLF study. *Int. Arch. Occup. Environ. Health*. **76**, 424-430.

Katzenberg, D., Young, T., Finn, L., Lin, L., King, D.P., Takahashi, J.S., and Mignot, E. 1998. A CLOCK polymorphism associated with human diurnal preference. *Sleep*. **21**, 569-576.

Kerkhof, G.A. and Van Dongen, H.P. 1996. Morning-type and evening-type individuals differ in the phase position of their endogenous circadian oscillator. *Neurosci*. *Lett.* **218**, 153-156.

Kiessling, S., Eichele, G., and Oster, H. 2010. Adrenal glucocorticoids have a key role in circadian resynchronization in a mouse model of jet lag. *J. Clin. Invest.* **120**, 2600-2609.

King, A.V., Linke, J., Gass, A., Hennerici, M.G., Tost, H., Poupon, C., and Wessa, M. 2012. Microstructure of a three-way anatomical network predicts individual differences in response inhibition: A tractography study. *NeuroImage*. **59**, 1949-1959.

King, D.P., Zhao, Y., Sangoram, A.M., Wilsbacher, L.D., Tanaka, M., Antoch, M.P., Steeves, T.D., Vitaterna, M.H., Kornhauser, J.M., Lowrey, P.L., Turek, F.W., and Takahashi, J.S. 1997. Positional cloning of the mouse circadian clock gene. *Cell*. **89**, 641–653.

Korkmax, A. and Reiter, R.J. 2008. Epigenetic regulation: A new research area for melatonin? *J. Pineal Res.* **44**, 41-44.

Knutsson, A.K., Akerstedt, T., Jonsson, B.G., and Orth-Gomer, K. 1986. Increased risk of ischaemic heart disease in shift workers. *Lancet*. **2**, 89-92.

Lakin-Thomas, P.L. 2000. Circadian rhythms: New functions for old clock genes? *Trends Genet.* **16**, 135-142.

Larsen, P.J., Enquist, L.W., and Card, J.P. 1998. Characterization of the multisynaptic neuronal control of the rat pineal gland using viral transneuronal tracing. *Eur. J. Neurosci.* **10**, 128-145.

Le Bihan, D., Mangin, J.F., Poupon, C., Clark, C.A., Pappata, S., Molko, N., and Chabriat, H. 2001. Diffusion tensor imaging: Concepts and applications. *J. Magn. Reson. Im.* **13**, 534-546.

Lee, C., Etchegaray, J.P., Cagampang, F.R., Loudon, A.S., and Reppert, S.M. 2001. Posttranslational mechanisms regulate the mammalian circadian clock. *Cell*. **107**, 855-867.

Leh, S.E., Ptito, A., Chakravarty, M.M., and Strafella, AP. 2007. Fronto-striatal connections in the human brain: A probabilistic diffusion tractography study. *Neurosci. Lett.* **419**, 113-118.

Lerchl, A and Partsch, C-J. 1994. Reliable analysis of individual human melatonin profiles by complex cosinor analysis. *J. Pineal Res.* **16**, 85-90.

Lerner, A.B., Case, J.D., and Takahashi, Y. 1960. Isolation of melatonin and 5-methoxyindole-3-acetic acid from bovine pineal glands. *J. Biol. Chem.* **235**,1992-1997.

Levandovski, R., Dantas, G., Fernandes, L.C., Caumo, W., Torres, I., Roenneberg, T., Hidalgo, M.P., and Allebrandt, K.V. 2011. Depression scores associate with chronotype and social jetlag in a rural population. *Chronobiol. Int.* **28**, 771-778.

Lewy, A.J., Bauer, V.K., Ahmed, S., Thomas, K.H., Cutler, N.L., Singer, C.M., Moffit, M.T., and Sack, R.L. 1998. The human phase response curve (PRC) to melatonin is about 12 hours out of phase with the PRC to light. *Chronobiol. Int.* **15**, 71-83.

Li, S., Lee, K., Zhao, J., Yang, Z., He, S., and Weng, X. 2013. Neural competition as a development process: Early hemispheric specialization for word processing delays specialization for face processing. *Neuropsychologia.* **51**, 950-959.

Lin, J.M., Kilman, V.L., Keegan, K., Paddock, B., Emery-Le, M., Rosbash, M., and Allada, R. 2002. A role for casein kinase 2alpha in the *Drosophila* circadian clock. *Nature*. **420**, 816-820.

Livrea, M.A., Tesoriere, L., D'Arpa, D., and Morreale, M. 1997. Reaction of melatonin with lipoperoxyl radicals in phospholipid bilayers. *Free Radic. Biol. Med.* **23**, 706-711.

Loh, D.H., Navarro, J., Hagopian, A., Wang, L.M., Deboer, T., and Colwell, C.S. 2010. Rapid changes in the light/dark cycle disrupt memory of conditioned fear in mice. *PLoS One*. **5**, e12546.

Madsen, K.S., Baaré, W.F.C., Vestergaard, M., Skimminge, A., Ejersbo, L.R., Ramsøy, T.Z., Gerlach, C., Âkeson, P., Paulson, O.B., and Jerniga, T.L. 2010. Response inhibition is associated with white matter microstructure in children. *Neuropsychologia.* **48**, 854-862.

Maguire, E.A., Burgess, N., Donnett, J.G., Frackowiak, R.S.J., Frith, C.D., and O'Keefe, J. 1998. Knowing where and getting there: A human navigation network. *Science*. **280**, 921-924.

Maguire, E.A., Gadian, D.G., Johnsrude, I.S., Good, C.D., Ashburner, J., Frackowiak, R.S.J., and Frith, C.D. 2000. Navigation-related structural change in the hippocampi of taxi drivers. *Proc. Natl. Acad. Sci. USA*. **97**, 4398-4403.

Marek, T., Fafrowicz, M., Golonka, K., Mojsa-Kaja, J., Oginska, H., Tucholska, K., Ubranik, A., Beldzik, E., and Domagalik, A. 2010. Diurnal patterns of activity of the orienting and executive attention neuronal networks in subjects performing a Stroop-like task: A functional magnetic resonance imaging study. *Chronobiol. Int.* **27**, 945-958.

Martin, S.K. and Eastman, C.I. 2002. Sleep logs of young adults with self-selected sleep times predict the dim light melatonin onset. *Chronobiol. Int.* **19**, 695-707.

Martinek, S., Inonog, S., Manoukian, A.S., and Young, M.W. 2001. A role for the segment polarity gene *shaggy*/GSK-3 in the *Drosophila* circadian clock. *Cell*. 105:769-779.

Masson-Pevet, M., George, D., KAlsbeek, A., Saboureau, M., Ladkhar-Ghazal, N., and Pevet, P. 1994. An attempt to correlate brain areas containing melatonin binding sites with rhythmic functions: A study in five hibernator species. *Cell Tiss. Res.* **278**, 97-106.

Matuszak, Z., Reszka, K.J., and Chignell, C.F. 1997. Reaction of melatonin and related indoles with hydroxyl radicals: EPR and spin trapping investigations. *Free Radic. Biol. Med.* **23**, 367-372.

Maurer, U., Rossion, B., and McCandliss, B.D. 2008. Category specificity in early perception: Face and word N170 responses differ in both lateralization and habituation properties. *Front. Hum. Neurosci.* **2**, 1-7.

Mayo, J.C., Sainz, R.M., Uria, H., Antolin, I., Esteban, M.M., and Rodríguez, C. 1998. Melatonin prevents apoptosis induced by 6-hydroxydopamine in neuronal cells: Implications for Parkinson's disease. *J. Pineal Res.* **24**, 179-192.

Mendoza, J., Pevet, P., Felder-Schmittbuhl, M.P., Bailly, Y., and Challet, E. 2010. The cerebellum harbors a circadian oscillator involved in food anticipation. *J. Neurosci.* **30**, 1894-1904.

Miller, E.K. 2000. The prefrontal cortex and cognitive control. *Nat. Rev. Neurosci.* **1**, 59-65.

Miller, E.K. and Cohen, J.D. 2001. An integrative theory of prefrontal cortex function. *Annu. Rev. Neurosci.* **24**, 167-202.

Moller, M. and Baeres, F.M.M. 2002. The anatomy and innervation of the mammalian pineal gland. *Cell Tiss. Res.* **309**, 139-150.

Moore, R.Y. 1996a. Entrainment pathways and the functional organization of the circadian system. *Prog. Brain Res.* **111**, 103-119.

Moore, R.Y. 1996b. Neural control of the pineal gland. *Behav. Brain Res.* **73**, 125-130.

Moore, R.Y. and Eichler, V.B. 1972. Loss of a circadian adrenal corticosterone rhythm following suprachiasmatic lesions in the rat. *Brain Res.* **42**, 201-206.

Moore, R.Y. and Klein, D.C. 1974. Visual pathways and the central neural control of a circadian rhythm in pineal serotonin *N*-acetyltransferase activity. *Brain Res.* **71**, 17-33.

Moore, R.Y. and Lenn, N.J. 1972. A retinohypothalamic projection in the rat. *J. Comp. Neurol.* **146**, 1-14.

Moore, R.Y. and Speh, J.C. 1993. GABA is the principal neurotransmitter of the circadian system. *Neurosci. Lett*. **150**, 112-116.

Morgan, P.J., Barrett, P., Howell, H.E., and Helliwell, R. 1994. Melatonin receptors: localization, molecular pharmacology and physiological significance. *Neurochem. Int.* **24**, 101-146

Morris, R.G.M., Garrud, P., Rawlins, J.N.P., and O'Keefe, J. 1982. Place navigation impaired in rats with hippocampal lesions. *Nature*. **297**, 681-683.

Navara, K.J. and Nelson, R.J. 2007. The dark side of light at night: Physiological, epidemiological and ecological consequences. *J. Pineal Res.* **43**, 215-224.

Nilsson, M., van Westen, D., Stahlberg, F., Sundgren, P.C., and Latt, J. 2013. The role of tissue microstructure and water exchange in biophysical modeling of diffusion in white matter. *Magn. Reson. Mater. Phy.* **26**, 345-370.

Okamura, H., Berod, A., Julien, J.F., Geffard, M., Kitahama, K., Mallet, J., and Bobillier, P. 1989. Demonstrations of GABAergic cell bodies in the suprachiasmatic nucleus: *In situ* hybridization of glutamic acid decarboxylase (GAD) mRNA and immunocytochemistry of GAD and GABA. *Neurosci. Lett.* **102**, 131-136.

Ovaysikia, S., Tahir, K.A., Chan, J.L., and DeSouza, J.F.X. 2011. Word wins over face: emotional Stroop effect activates the frontal cortical network. *Front. Hum. Neurosci.* **4**, 234-242.

Pandi-Perumal, S.R., BaHammam, A.S., Brown, G.M., Spence, D.W., Bharti, V.K., Kaur, C., Hardeland, R., and Cardinali, D.P. 2013. Melatonin antioxidant defense: Therapeutical implications for aging and neurodegenerative processes. *Neuroto*. *Res*. **23**, 267-300.

Pandi-Perumal, S.R., Srinivasan, V., Maestroni, G.J.M., Cardinali, D.P., Poeggeler, B., and Hardeland, R. 2006. Melatonin: Nature's most versatile biological signal? *FEBS J.* **273**, 2813-2838.

Partch, C.L., Green, C.B., and Takahashi, J.S. 2014. Molecular architecture of the mammalian circadian clock. *Trends Cell Biol.* **24**, 90-99.

Perreau-Lenz, S., Kalsbeek, A., Garidou, M.L., Wortel, J., van der Vliet, J., van Heijningen, C., Simonneaux, V., Pevet, P., and Buijs, R.M. 2003. Suprachiasmatic control of melatonin synthesis in rats: inhibitory and stimulatory mechanisms. *Eur. J. Neurosci.* **17**, 221-228.

Perreau-Lenz, S., Kalsbeek, A., Pevet, P., and Buijs, R.M. 2004. *In vivo* evidence for a glutamatergic clock output involved in the stimulation of melatonin synthesis. *Eur. J. Neurosci.* **19**, 318-324.

Perreau-Lenz, S., Kalsbeek, A., van der Vliet, J., Pevet, P., and Buijs, R.M. 2005. *In vivo* evidence for a controlled offset of melatonin synthesis at dawn by the suprachiasmatic nucleus in the rat. *Neurosci.* **130**, 797-803.

Peter, R., Alfredsson, L., Knutsson, A., Siegrist, J., and Westerholm, P. 1999. Does a stressful psychosocial work environment mediate the effects of shift work on cardiovascular risk factors? *Scand. J. Work Environ. Health.* **25**, 376-381.

Pevet, P., Agez, L., Bothorel, B., Saboureau, M., Gauer, F., Laurent, V., and Masson-Pevet, M. 2006. Melatonin in the multi-oscillatory mammalian circadian world. *Chronobiol. Int.* **23**, 39-51.

Pevet, P. and Challet, E. 2011. Melatonin: Both master clock output and internal time-giver in the circadian clocks network. *J. Physiol. Paris.* **105**, 170-182.

Pieri, C., Marra, M., Moroni, F., Recchioni, R., and Marcheselli, F. 1994. Melatonin: A peroxyl radical scavenger more effective than vitamin E. *Life Sci.* **55**, PL271-PL276.

Pitrosky, B., Kirsch, R., Malan, A., Mocaer, E., and Pevet, P. 1999. Organization of rat circadian rhythms during daily infusion of melatonin or S20098, a melatonin agonist. *Am. J. Physiol.* **277**, R8126-R8128.

Poeggeler, B., Thuermann, S., Dose, A., Schoenke, M., Burkhardt, S., and Haderland, R. 2002. Melatonin's unique radical scavenging properties-roles of its functional substituents as revealed by a comparison with its structural analogs. *J. Pineal Res.* **33**, 22-30.

Poirel, V.J., Boggio, V., Dardente, H., Pevet, P., Masson-Pevet, M., and Gauer, F. 2003. Clock gene mRNA expressions are differentially regulated in the rat suprachiasmatic by acute melatonin injection. *Neurosci.* **120**, 745-755.

Preston, S.D. and Stansfield, R.B. 2008. I know how you feel: Task-irrelevant facial expressions are spontaneously processed at a semantic level. *Cog. Affect Behav. Ne.* **8**, 54-64.

Raccuglia, R.A. and Phaf, R.H. 1997. Asymmetric affective evaluation of words and faces. *Brit. J. Psychol.* **88**, 93-116.

Ralph, C.L., Mull, D., Lunch, H.J., and Hedlund, L. 1971. A melatonin rhythm persists in rat pineals in darkness. *Endocrinol.* **89**, 1361-1366.

Ralph, M.R., Ko, C.H., Antoniadis, E.A., Seco, P., Irani, F., Presta, C., and McDonald, R.J. 2002. The significance of circadian phase for performance on a reward-based learning task in hamsters. *Behav. Brain Res.* **136**, 179-184.

Ramirez, C., Garcia, A., and Valdez, P. 2012. Identification of circadian rhythms in cognitive inhibition and flexibility using a Stroop task. *Sleep Biol. Rhythms.* **10**, 136-144.

Redman, J.R., Armstrong, S., and Ng, K.T. 1983. Free-running activity rhythms in the rat: Entrainment by melatonin. *Science.* **219**, 1089-1091.

Reiter, R.J., Tan, D.X., Sainz, R.M., Mayo, J.D., and Lopez-Burillo, S. 2002. Melatonin: reducing the toxicity and increasing the efficacy of drugs. *J. Pharm. Pharmacol.* **54**, 1299-1321.

Reiter, R.J., Tan, D.X., Gitto, E., Sainz, R.M., Mayo, J.C., Leon, J., Manchester, L.C., Vijayalaxmi, Kilic, E., and Kilic, U. 2004. Pharmacological utility of melatonin in reducing oxidative cellular and molecular damage. *Pol. J. Pharmacol.* **56**, 159-170.

Reiter, R.J., Tan, D.X., Sanchez-Barcelo, E., Mediavilla, M.D., Gitto, E., and Korkmaz, A. 2011. Circadian mechanisms in the regulation of melatonin synthesis: Disruption with light at night and the pathophysiological consequences. *J. Exp. Integr. Med.* **1**, 13-22.

River-Bermudez, M.A., Masana, M.I., Brown, G.M., Earnest, D.J., and Dubocovich, M.L. 2004. Immortalized cells from the rat suprachiasmatic nucleus express functional melatonin receptors. *Brain Res*. **1002**, 21-27.

Roberts, J.E., Hu, D.H., and Wishart, J.F. 1998. Pulse radiolysis studies of melatonin and chloromelatonin. *J. Photochem. Photobiol*. **42**, 125-132.

Roenneberg, T., Wirz-Justice, A., and Merrow, M. 2003. Life between clocks: Daily temporal patterns of human chronotypes. *J. Biol. Rhythms*. **18**, 80-90.

Rosenberg, J., Maximov, I.I., Reske, M., Grinberg, F., and Shah, N.J. 2013. "Early to bed, early to rise": Diffusion tensor imaging identifies chronotype-specificity. *NeuroImage*. **84**, 428-434.

Rothman, S.M. and Mattson, M.P. 2012. Sleep disturbances in Alzheimer's and Parkinson's diseases. *Neuromol. Med.* **14**, 194-204.

Rouch, I., Wild, P., Ansiau, D., and Marquie, J.C. 2005. Shift work experience, age and cognitive performance. *Ergonomics*. **48**, 1282-1293.

Sagi, Y., Tavor, I., Hofstetter, S., Tzur-Moryosef, S., Blumenfeld-Katzir, T., and Assaf, Y. 2012. Learning in the fast lane: New insights into neuroplasticity. *Neuron*. **73**, 1195-1203.

Sanchez-Barcelo, E.J., Mediavilla, M.D., Alonso-Gonzalez, C., and Rueda, N. 2012. Breast cancer therapy based on melatonin. *Recent Pat. Endocr. Metab. Immune Drug Discov.* **6**, 108-118.

Santhi, N., Horowitz, T.S., Duffy, J.F., and Czeisler, C.A. 2007. Acute sleep deprivation and circadian misalignment associated with transition onto the first night of work impairs visual selective attention. *PLoS One*. **2**, e1233.

Santhi, N., Aeschbach, D., Horowitz, T.S., and Czeisler, C.A. 2008. The impact of sleep timing and bright light exposure on attentional impairment during night work. *J. Biol. Rhythms.* **23**, 341-352.

Sasson, E., Doniger, G.M., Pasternak, O., and Assaf, Y. 2010. Structural correlates of memory performance with diffusion tensor imaging. *NeuroImage*. **50**, 1231-1242.

Sato, T.K., Yamada, R.G., Ukai, H., Baggs, J.E., Miraglia, L.J., Kobayashi, T.J., Welsh, D.K., Kay, S.A., Ueda, H.R. and Hogenesch, J.B. 2006. Feedback repression is required for mammalian circadian clock function. *Nat. Genet.* **38**, 312–319.

Schernhammer, E.S., Laden, F., Speizer, F.E., Willett, W.C., Hunter, D.J., Kawachi, I., and Colditz, G.A. 2001. Rotating night shifts and risk of breast cancer in women participating in the nurses' health study. *J. Natl. Cancer Inst*. **93**, 1563-1568.

Schibler, U., Ripperger, J., and Brown, S.A. 2003. Peripheral circadian oscillators in mammals: time and food. *J. Biol. Rhythms.* **18**, 250-260.

Schmidt, C., Peigneux, P., Leclercq, Y., Sterpenich, V., Vandewalle, G., Phillips, C., Berthomier, P., Berthormier, C., Tinguely, G., Gais, S., Schabus, M., Desseilles, M., Thanh, D.V., Salmon, E., Degueldre, C., Balteau, E., Luxen, A., Cajochen, C., Maquet, P., and Collette, F. 2012. Circadian preference modulates the neural substrate of conflict processing across the day. *PLoS One*. **7**, e29658.

Schomerus, C and Korf, H-W. 2005. Mechanisms regulating melatonin synthesis in the mammalian pineal organ. *Ann. N. Y. Acad. Sci.* **1057**, 372-383.

Schott, B.H., Niklas, C., Kaufmann, J., Bodammer, N.C., Machts, J., Schütze, H., and Düzel, E. 2011. Fiber density between rhinal cortex and activated ventrolateral prefrontal regions predicts episodic memory performance in humans. *Proc. Natl. Acad. Sci. USA.* **108**, 5408-5413.

Schulmeister, K., Weber, M., and Bogner, W. 2004. Application of melatonin action spectra on practical lighting issues. In: Final Report. The Fifth International LRO Lighting Research Symposium, Light and Human Health, November 3-5, 2002. Report No. 1009370. Palo Alto, CA: The Electric Power Research Institute. 103–114.

Shearman, L.P., Sriram, S., Weaver, D.R., Maywood, E.S., Chaves, I., Zheng, B., Kume, K., Lee, C.C., van der Horst, G.T., Hastings, M.H., and Reppert, S.M. 2000. Interacting molecular loops in the mammalian circadian clock. *Science*. **288**, 1013–1019.

Shrager, Y., Bayley, P.J., Bontempi, B., Hopkins, R.O., and Squire, L.R. 2007. Spatial memory and the human hippocampus. *PNAS.* **104**, 2961-2966.

Skene, D.J. and Arendt, J. 2006. Human circadian rhythms: Physiological and therapeutic relevance of light and melatonin. *Ann. Clin. Biochem.* **43**, 344-353.

Skene, D.J. and Arendt, J. 2007. Circadian rhythm sleep disorders in the blind and their treatment with melatonin. *Sleep Med.* **8**, 651-655.

Slotten, H.A., Pitrosky, B., and Pevet, P. 1999. Entrainment of rat circadian rhythms by daily administration of melatonin: Influence of the role of administration. *J. Biol. Rhythms.* **14**, 347-353.

Slotten, H.A., Pitrosky, B., Krekling, S., and Pevet, P. 2002. Entrainment of circadian activity rhythms in rats to melatonin administered at T cycles different from 24 hours. *Neurosignals.* **11**, 73-80.

Smith, M.R., Lee, C., Crowley, S.J., Fogg, L.F., and Eastman, C.I. 2005. Morning melatonin has limited benefit as a soporific for daytime sleep after night work. *Chronobiol. Int.* **22**, 873-888.

Soares, J.M., Marques, P., Alves, V., and Sousa, N. 2013. A hitchhiker's guide to diffusion tensor imaging. *Front. Neurosci.* **7**, 1-14.

Squire, L.R. 1992. Memory and the hippocampus: A synthesis from findings with rats, monkeys and humans. *Psychol. Rev.* **99**, 195-231.

Srinivasan, V., Pandi-Perumal, S.R., Trahkt, I., Spence, D.W., Poeggeler, B., Hardeland, R., and Cardinali, D.P. 2009. Melatonin and melatonergic drugs on sleep: Possible mechanisms of action. *Int. J. Neurosci.* **119**, 821-846.

Statistics Canada. *Table 102-0561 – Leading causes of death, total population, by age group and sex, Canada, annual.* CANSIM (database). [Accessed on: March 22, 2014].

Stephan, F.K. and Zucker, I. 1972a. Circadian rhythms in drinking and locomotor activity of rats are eliminated by hypothalamic lesions. *Proc. Natl. Acad. Sci. USA*. **69**, 1583-1586.

Stephan, F.K. and Zucker, I. 1972b. Rat drinking rhythms: Central visual pathways and endocrine factors mediating responsiveness to environmental illumination. *Phyiol. Behav.* **8**, 315-326.

Stevens, R.G. 2009. Light-at-night, circadian disruption and breast cancer: assessment of existing evidence. *Int. J. Epidimiol.* **38**, 963-970.

Stroop, J.R. 1935. Studies of interference in serial verbal reactions. *J. Exp. Psychol.* **18**, 643-662.

Sutherland, R.J., Kolb, B., and Whishaw, I.Q. 1982. Spatial mapping: Definitive disruption by hippocampal or medial frontal cortical damage in the rat. *Neurosci. Lett.* **31**, 271-276.

Sutherland, R.J., Weisend, M.P., Mumby, D., Astur, R.S., Thomas, M.J., Wu, Y., Moses, S.N., Cole, C., Hamilton, D.A., and Hoesing, J. 2001. Retrograde amnesia after hippocampal damage: Recent vs. remote memories in two tasks. *Hippocampus.* **11**, 27-42.

Swann, N.C., Cai, W., Conner, C.R., Pieters, T.A., Claffey, M.P., George, J.S., Aron, A.R., and Tandon, N. 2012. Roles for the pre-supplementary motor area and the right inferior frontal gyrus in stopping action: Electrophysiological responses and functional and structural connectivity. *NeuroImage*. **59**, 2860-2870.

Takahasi, M., Nakata, A., and Arito, H. 2002. Disturbed sleep-wake patterns during and after short-term international travel among academics attending conferences. *Int Arch. Occup. Environ. Health.* **75**, 435-440.

Tapp, W.N. and Holloway, F.A. 1981. Phase shifting circadian rhythms produces retrograde amnesia. *Science*. **291**, 1056-1058.

Teclemariam-Mesbah, R., Ter Horst, G.J., Postema, F., Wortel, J., and Buijs, R.M. 1999. Anatomical demonstration of the suprachiasmatic nucleus-pineal pathway. *J. Comp. Neurol.* **406**, 171-182.

Torres-Farfan, C., Mendez, N., Abarzua-Catalan, L., Vilches, N., Valenzuela, G.J., and Seron-Ferre, M. 2011. A circadian clock entrained by melatonin is ticking in the rat fetal adrenal. *Endocrinol.* **152**, 1891-1900.

Uz, T., Arslan, A.D., Kurtuncu, M., Imbesi, M., Akhisaroglu, M., Dwivedi, Y., Pandey, G.N., and Manev, H. 2005. The regional and cellular expression profile of the melatonin receptor MT1 in the central dopaminergic system. *Mol. Brain. Res.* **136**, 45-53.

Verwey, M. and Amir, S. 2009. Food-entrainable circadian oscillators in the brain. *Eur. J. Neurosci.* **30**, 1650-1657.

Vijayalaxmi, Reiter, R.J., Meltz, M.L., and Herman, T.S. 1998. Melatonin: possible mechanisms involved in its 'radioprotective' effect. *Mutat. Res*. **40**, 187-189.

Waterhouse, J., Nevill, A., Edwards, B., Godfrey, R., and Reillly, T. 2003. The relationship between assessments of jet lag and some of its symptoms. *Chronobiol. Int.* **20**, 1061-1073.

Waterhouse, J., Nevill, A., Finnegan, J., Williams, P., Edwards, B., Kao, S.Y., and Reilly, T. 2005. Further assessments of the relationship between jet lag and some of its symptoms. *Chronobiol. Int.* **22**, 121-136.

Wood, J., Birmaher, B., Axelson, D., Ehmann, M., Kalas, C., Monk, K., Turkin, S., Kupfer, D.J., Brent, D., Monk, T.H., and Nimgainkar, V.L. 2009. Replicable differences in preferred circadian phase between bipolar disorder patients and control individuals. *Psychiatry Res.* **166**, 201-209.

Winiarska, K., Fraczyk, T., Malinska, D., Drosaz, J., and Bryla, J. 2006. Melatonin attenuates diabetes-induced oxidative stress in rabbits. *J. Pineal Res.* **40**, 168-176.

Wittmann, M., Dinich, J., Merrow, M., and Roenneberg, T. 2006. Social jet lag: Misalignment of biological and social time. *Chronobiol. Int.* **23**, 497-509.

Ye, R., Selby, C.P., Ozturk, N., Annayev, Y., and Sancar, A. 2011. Biochemical analysis of the canonical model for the mammalian circadian clock. *J. Biol. Chem.* **286**, 25891-25902.

Zee, P.C. and Goldstein, C.A. 2010 Treatment of shift work disorder and jet lag. *Curr. Treat. Options Neurol.* **12**, 396-411.

Zhao, I. and Turner, C. 2008. The impact of shift work on people's daily health habits and adverse health outcomes. *Austr. J. Adv. Nursing.* **25**, 8-22.

Zhdanova, I.V., Wurtman, R.J., Lynch, H.J., Ives, J.R., Dollins, A.B., Morabito, C., Matheson, J.K., and Schomer, D.L. 1995. Sleep-inducing effects of low-doses of melatonin ingested in the evening. *Clin. Pharmacol. Ther.* **57**, 552-558.

Zhdanova, I.V. 2005. Melatonin as a hypnotic: Pro. *Sleep Med. Rev.* **9**, 51-65.

Zhou, X., Ferguson, S.A., Matthews, R.W., Sargent, C., Darwent, D., Kennaway, D.J., and Roach, G.D. 2011. Sleep, wake and phase dependent changes in neurobehavioural function under forced desynchrony. *Sleep.* **34**, 931-941.

Zhu, X-R., Zhang, H-J., Wu, T-T., Luo, W-B., and Luo, Y-J. 2010. Emotional conflict occurs at an early stage: Evidence from the emotional face-word Stroop task. *Neurosci. Lett.* **478**, 1-4.

Appendix A – Timeline of Data Collection

Baseline period data collection:

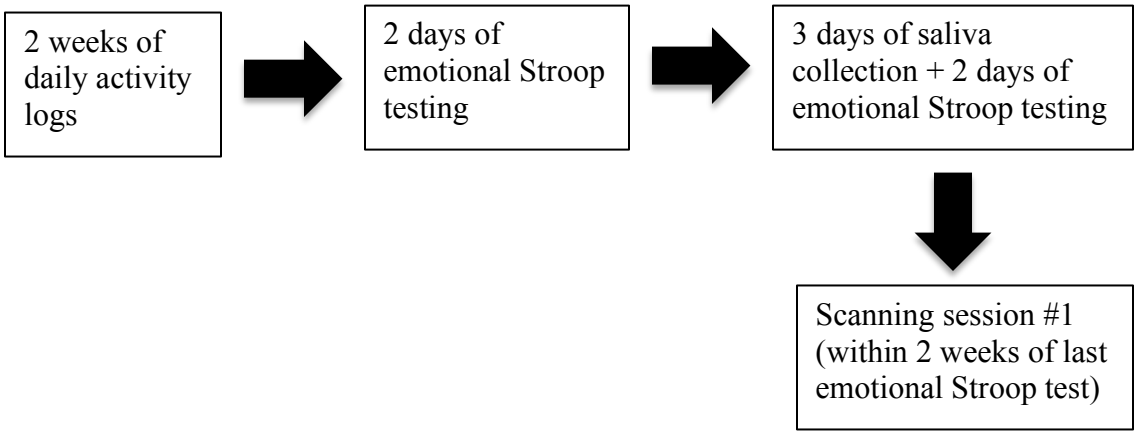

Experimental period data collection:

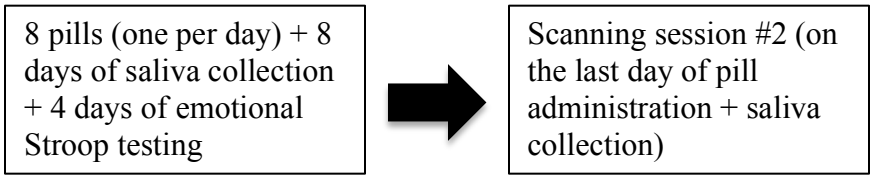

Appendix B – MCTQ Results

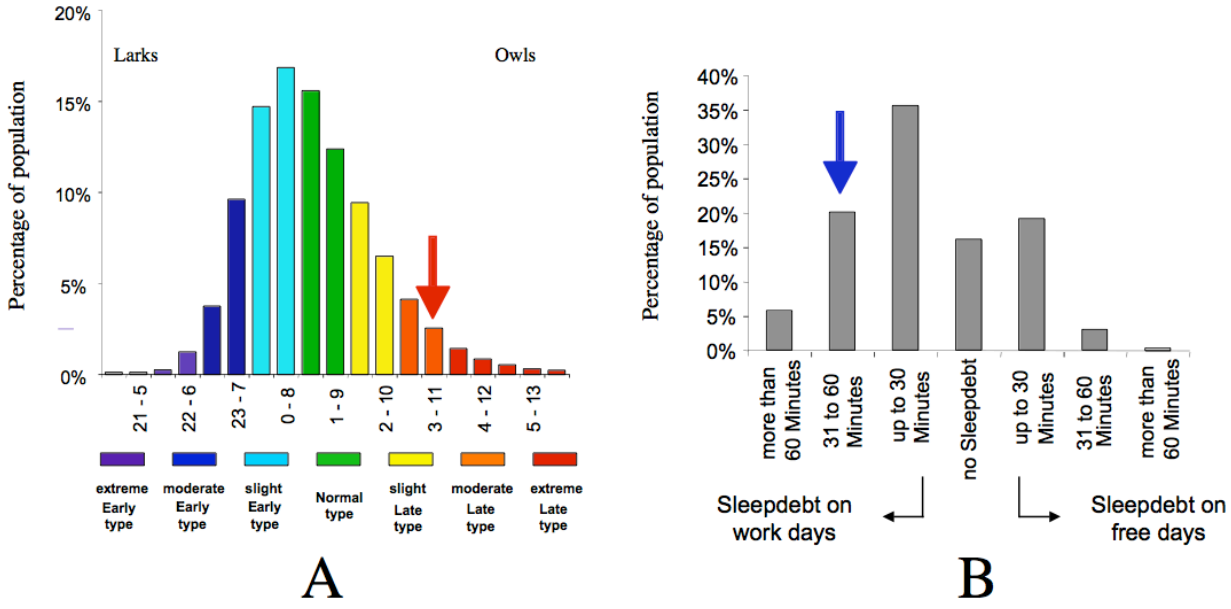

You are a moderate late type. These chronotypes often get too little sleep during the work week, because their biological clock usually lets them fall asleep well after midnight. By the time your alarm clock rings, you have slept much too little and you probably sleep long into the day on free days to catch up. (Figure A)

According to the sleep times that you have given, on work days you sleep between 31 minutes and an hour less than your average sleep need. (Figure B)

When you feel that your biological clock "puts you to bed" too early and you would like to be able to fall asleep later (for example to enjoy more of the evening), you can experiment with the effects of brighter light: try to avoid bright light in the morning but seek outside light in the afternoon and evening (even relatively bright artificial lighting is far lower in intensity than sunlight outside). Even without sports or activity, especially evening light can nudge your biological clock to a later time, so that you can stay up longer.

Appendix C – Protocol for Pill Administration

Please read the following instructions carefully before administering the pills. You are expected to follow the timeline exactly as outlined below.

1. Eight (8) pills have been provided for you to take over the course of eight (8) days (one pill a day).

2. To take these pills, please place the entire pill under your tongue and wait for it to dissolve completely. The pill should take approximately five (5) minutes to dissolve.

3. Within 5 minutes of taking the pill, please provide a saliva sample and mark it on your saliva protocol sheet with an asterisk (*****). This will allow the researcher to identify the saliva sample given directly after administration of the pill.

Thank you!

Day of Pill Administration	Time of Pill Administration
1	6:30pm
2	5:00pm
3	8:30am
4	10:00am
5	6:30pm
6	5:00pm
7	8:30am
8	10:00am

Appendix D – Instructions for Saliva Collection

Please read the following instructions carefully before starting the saliva collection process. The more carefully you follow the instructions, the more reliable the results obtained from your samples will be.

1. Before starting collection, ensure that the number on your collection container matches the one in the attached protocol.

2. 5 minutes before each saliva collection, rinse your mouth thoroughly with cold water. Nothing should be eaten during the collection time. The last drink and meal should be taken at least 15 minutes prior to starting the collection. Chewing gum and brushing teeth should also be avoided in the 15 minutes prior to collection. Refrain from drinks containing artificial colorants, caffeine or alcohol on the days of collection. If possible, no aspirin and medicines that contain ibuprofen should be taken on collection days.

3. When it is time for your saliva to be collected, deposit your saliva into the container. You must provide a **minimum of 1mL per collection**. There are markings on the side of the collection container to use as reference points.

4. When finished, close the top of the tube and place in the box provided. Store the box containing the samples in the freezer at -20˚C. Repeat steps 1 – 4 for each collection. Refer back to the protocol provided for dates and times of each collection.

5. Please bring your collected samples to the researcher on day three of collection. If possible, try to minimize the time the collected samples remain above the -20˚C range.

Thank you!

Appendix E – Timeline for Saliva Collection

Please follow the protocol outlined below for saliva sample collection. The schedule for saliva collection, along with the sample number that you will need to match to your collection container, is as follows:

Day 1 – Sunday, November 17th, 2013

Collection Time	Sample #
8:30 am	1
9:00 am	2
9:30 am	3
10:00 am	4
1:30 pm	5
5:00 pm	6
6:00 pm	7
7:00 pm	8
8:00 pm	9
8:30 pm	10
9:00 pm	11
9:30 pm	12
10:00 pm	13
10:30 pm	14
11:00 pm	15
11:30 pm	16
12:00 am	17
12:30 am	18
*1:00 am	*19
*1:30 am	*20

* The starred sample times indicate times at which you do not need to provide samples if you are not awake. If you do happen to either wake up before the indicated collection time or sleep after the last collection time for the day, please feel free to provide more samples at your convenience. If you do choose to provide extra samples, please adjust the sample numbers accordingly. Thank you!

Day 2 – Monday, November 18th, 2013

Collection Time	Sample #
8:30 am	21
9:00 am	22
9:30 am	23
10:00 am	24
1:30 pm	25
5:00 pm	26
6:00 pm	27
7:00 pm	28
8:00 pm	29
8:30 pm	30
9:00 pm	31
9:30 pm	32
10:00 pm	33
10:30 pm	34
11:00 pm	35
11:30 pm	36
12:00 am	37
12:30 am	38
*1:00 am	*39
*1:30 am	*40

* The starred sample times indicate times at which you do not need to provide samples if you are not awake. If you do happen to either wake up before the indicated collection time or sleep after the last collection time for the day, please feel free to provide more samples at your convenience. If you do choose to provide extra samples, please adjust the sample numbers accordingly. Thank you!

Day 3 – Tuesday, November 19th, 2013

Collection Time	Sample #
8:30 am	41
9:00 am	42
9:30 am	43
10:00 am	44
1:30 pm	45
5:00 pm	46
6:00 pm	47
7:00 pm	48
8:00 pm	49
8:30 pm	50
9:00 pm	51
9:30 pm	52
10:00 pm	53
10:30 pm	54
11:00 pm	55
11:30 pm	56
12:00 am	57
12:30 am	58
*1:00 am	*59
*1:30 am	*60

* The starred sample times indicate times at which you do not need to provide samples if you are not awake. If you do happen to either wake up before the indicated collection time or sleep after the last collection time for the day, please feel free to provide more samples at your convenience. If you do choose to provide extra samples, please adjust the sample numbers accordingly. Thank you!

Appendix F – Statistical Tables

Table 1. Paired samples *t*-test for the RTs and errors of the face and word instruction sets. Pre = baseline; F = face instruction; W = word instruction; RT = reaction times; Err = errors.

		Paired Differences					t	df	Sig. 2-tailed
		Mean	Std. Deviation	Std. Error Mean	95% Confidence Interval of the Difference				
					Lower	Upper			
Pair 1	Pre_F_RT - Pre_W_RT	143.060017	43.1164075	13.6346052	112.2163980	173.9036378	10.492	9	**.000**
Pair 2	Pre_F_Err - Pre_W_Err	2.4166667	1.6347641	.5169578	1.2472269	3.5861065	4.675	9	**.001**

Table 2. Paired samples *t*-test for the RTs and errors of the face and word instruction sets during the baseline period, with each instruction broken down into its component congruent and incongruent trials. Con = congruent condition; Incon = incongruent condition; F = face instruction; W = word instruction; RT = reaction times; Err = errors.

		Paired Differences					t	df	Sig. 2-tailed
		Mean	Std. Deviation	Std. Error Mean	95% Confidence Interval of the Difference				
					Lower	Upper			
Pair 1	Con_F_RT - Incon_F_RT	-77.423220	51.191052	16.188032	-114.043092	-40.803347	-4.783	9	**.001**
Pair 2	Con_W_RT - Incon_W_RT	-11.951567	16.033003	5.0700809	-23.4208873	-.4822477	-2.357	9	**.043**
Pair 3	Con_F_Err - Incon_F_Err	-5.1750000	3.0732945	.9718610	-7.3735024	-2.9764976	-5.325	9	**.000**
Pair 4	Con_W_Err - Incon_W_Err	-1.2750000	.7945124	.2512469	-1.8433600	-.7066400	-5.075	9	**.001**

Table 3. Paired samples *t*-test for sleep times in the baseline and experimental periods. Baseline_Sleep = baseline sleep times; Experimental_Sleep = experimental sleep times.

		Paired Differences					t	df	Sig. 2-tailed
		Mean	Std. Deviation	Std. Error Mean	95% Confidence Interval of the Difference				
					Lower	Upper			
Pair 1	Baseline_Sleep - Experimental_Sleep	.787500	.8454586	.2673575	.18269531	1.3923046	2.945	9	**.016**

Table 4. Paired samples *t*-test for wake times in the baseline and experimental periods. Baseline_Wake = baseline wake times; Experimental_Wake = experimental wake times.

		Paired Differences					t	df	Sig. 2-tailed
		Mean	Std. Deviation	Std. Error Mean	95% Confidence Interval of the Difference				
					Lower	Upper			
Pair 1	Baseline_Wake - Experimental_Wake	.37000000	.65420515	.20687783	-.097990	.83799017	1.788	9	.107

Table 5. Linear mixed models test for sleep quality ratings in the baseline and experimental periods.

Parameter	Estimate	Std. Error	df	t	Sig.	95% Confidence Interval	
						Lower Bound	Upper Bound
Intercept	3.232143	.137174	118	23.562	.000	2.960500	3.503786
[Condition=1]	.564732	.187834	118	3.007	**.003**	.192770	.936694
[Condition=2]	0[a]	0	.	.	.	.	.

Dependent Variable: Sleep Rating.

a. This parameter is set to zero because it is redundant.

Table 6. Paired samples *t*-test for the RTs and errors of the face and word instruction sets during the experimental period, with each instruction broken down into its component congruent and incongruent trials. Con = congruent condition; Incon = incongruent condition; F = face instruction; W = word instruction; RT = reaction times; Err = errors.

		Paired Differences					t	df	Sig. 2-tailed
		Mean	Std. Deviation	Std. Error Mean	95% Confidence Interval of the Difference				
					Lower	Upper			
Pair 1	Con_F_RT - Incon_F_RT	-101.55392	64.5789349	20.421652	-147.750913	-55.356939	-4.973	9	**.001**
Pair 2	Con_W_RT - Incon_W_RT	-4.2507308	15.2696532	4.8286883	-15.1739827	6.6725211	-.880	9	.402
Pair 3	Con_F_Err - Incon_F_Err	-4.9166666	3.06337384	.96872386	-7.10807230	-2.7252610	-5.075	9	**.001**
Pair 4	Con_W_Err - Incon_W_Err	-1.8000000	.69522179	.21984843	-2.29733171	-1.3026682	-8.187	9	**.000**

Table 7. Paired samples *t*-test for the RTs and errors of the face and word instruction sets comparing baseline and experimental periods, with each instruction broken down into its component congruent and incongruent trials. Pre = baseline; Post = experimental; Con = congruent; Incon = incongruent; F = face; W = word; RT = reaction times; Err = errors.

		Paired Differences					t	df	Sig. 2-tailed
		Mean	Std. Deviation	Std. Error Mean	95% Confidence Interval of the Difference				
					Lower	Upper			
Pair 1	Pre_Con_F_RT - Post_Con_F_RT	39.213064	51.16025	16.178293	2.61522074	75.810907	2.424	9	**.038**
Pair 2	Pre_Incon_F_RT - Post_Incon_F_RT	15.082357	23.309351	7.3710641	-1.5921480	31.756863	2.046	9	.071
Pair 3	Pre_Con_W_RT - Post_Con_W_RT	23.633802	34.091169	10.780574	-.75355114	48.021156	2.192	9	.056
Pair 4	Pre_Incon_W_RT - Post_Incon_W_RT	31.334639	31.633564	10.003411	8.70535043	53.963927	3.132	9	**.012**
Pair 5	Pre_Con_F_Err - Post_Con_F_Err	.62500000	.89170561	.28198207	-.01288776	1.2628877	2.216	9	**.054**
Pair 6	Pre_Incon_F_Err - Post_Incon_F_Err	.88333333	2.4611800	.77829348	-.87728884	2.6439555	1.135	9	.286
Pair 7	Pre_Con_W_Err - Post_Con_W_Err	.01666667	.37018514	.11706282	-.24814783	.28148116	.142	9	.890
Pair 8	Pre_Incon_W_Err - Post_Incon_W_Err	-.5083333	.73958822	.23387833	-1.0374028	.02073621	-2.173	9	**.054**

Table 8. Repeated measures ANOVA for the RTs outcome. Three within-subject factors of period, congruency, and instruction were used, with two levels in each factor (baseline and experimental, congruent and incongruent, and face and word, respectively). Interactions between the different factors are also shown.

Source		Type III Sum of Squares	df	Mean Square	F	Sig.	Partial Eta Squared
Period	Sphericity Assumed	14923.240	1	14923.240	7.406	**.024**	.451
	Greenhouse-Geisser	14923.240	1.000	14923.240	7.406	**.024**	.451
	Huynh-Feldt	14923.240	1.000	14923.240	7.406	**.024**	.451
	Lower-bound	14923.240	1.000	14923.240	7.406	**.024**	.451
Error (Period)	Sphericity Assumed	18135.020	9	2015.002			
	Greenhouse-Geisser	18135.020	9.000	2015.002			
	Huynh-Feldt	18135.020	9.000	2015.002			
	Lower-bound	18135.020	9.000	2015.002			
Congruency	Sphericity Assumed	47618.770	1	47618.770	31.835	**.000**	.780
	Greenhouse-Geisser	47618.770	1.000	47618.770	31.835	**.000**	.780
	Huynh-Feldt	47618.770	1.000	47618.770	31.835	**.000**	.780
	Lower-bound	47618.770	1.000	47618.770	31.835	**.000**	.780
Error (Congruency)	Sphericity Assumed	13462.404	9	1495.823			
	Greenhouse-Geisser	13462.404	9.000	1495.823			
	Huynh-Feldt	13462.404	9.000	1495.823			
	Lower-bound	13462.404	9.000	1495.823			
Instruction	Sphericity Assumed	415655.180	1	415655.180	121.543	**.000**	.931
	Greenhouse-Geisser	415655.180	1.000	415655.180	121.543	**.000**	.931
	Huynh-Feldt	415655.180	1.000	415655.180	121.543	**.000**	.931
	Lower-bound	415655.180	1.000	415655.180	121.543	**.000**	.931
Error (Instruction)	Sphericity Assumed	30778.411	9	3419.823			
	Greenhouse-Geisser	30778.411	9.000	3419.823			
	Huynh-Feldt	30778.411	9.000	3419.823			
	Lower-bound	30778.411	9.000	3419.823			
Period * Congruency	Sphericity Assumed	337.426	1	337.426	1.206	.301	.118
	Greenhouse-Geisser	337.426	1.000	337.426	1.206	.301	.118
	Huynh-Feldt	337.426	1.000	337.426	1.206	.301	.118
	Lower-bound	337.426	1.000	337.426	1.206	.301	.118
Error (Period * Congruency)	Sphericity Assumed	2517.637	9	279.737			
	Greenhouse-Geisser	2517.637	9.000	279.737			
	Huynh-Feldt	2517.637	9.000	279.737			
	Lower-bound	2517.637	9.000	279.737			
Period *	Sphericity Assumed	.566	1	.566	.005	.946	.001

Instruction	Greenhouse-Geisser	.566	1.000	.566	.005	.946	.001
	Huynh-Feldt	.566	1.000	.566	.005	.946	.001
	Lower-bound	.566	1.000	.566	.005	.946	.001
	Sphericity Assumed	1052.121	9	116.902			
Error (Period *	Greenhouse-Geisser	1052.121	9.000	116.902			
Instruction)	Huynh-Feldt	1052.121	9.000	116.902			
	Lower-bound	1052.121	9.000	116.902			
	Sphericity Assumed	33119.564	1	33119.564	20.509	**.001**	.695
Congruency *	Greenhouse-Geisser	33119.564	1.000	33119.564	20.509	**.001**	.695
Instruction	Huynh-Feldt	33119.564	1.000	33119.564	20.509	**.001**	.695
	Lower-bound	33119.564	1.000	33119.564	20.509	**.001**	.695
	Sphericity Assumed	14533.911	9	1614.879			
Error (Congruency	Greenhouse-Geisser	14533.911	9.000	1614.879			
* Instruction)	Huynh-Feldt	14533.911	9.000	1614.879			
	Lower-bound	14533.911	9.000	1614.879			
Period * Congruency * Instruction	Sphericity Assumed	1266.559	1	1266.559	5.063	**.051**	.360
	Greenhouse-Geisser	1266.559	1.000	1266.559	5.063	**.051**	.360
	Huynh-Feldt	1266.559	1.000	1266.559	5.063	**.051**	.360
	Lower-bound	1266.559	1.000	1266.559	5.063	**.051**	.360
Error (Period * Congruency * Instruction)	Sphericity Assumed	2251.368	9	250.152			
	Greenhouse-Geisser	2251.368	9.000	250.152			
	Huynh-Feldt	2251.368	9.000	250.152			
	Lower-bound	2251.368	9.000	250.152			

Table 9. Repeated measures ANOVA for the errors outcome. Three within-subject factors of period, congruency, and instruction were used, with two levels in each factor (baseline and experimental, congruent and incongruent, and face and word, respectively). Interactions between the different factors are also shown.

Source		Type III Sum of Squares	df	Mean Square	F	Sig.	Partial Eta Squared
Period	Sphericity Assumed	1.292	1	1.292	.999	.344	.100
	Greenhouse-Geisser	1.292	1.000	1.292	.999	.344	.100
	Huynh-Feldt	1.292	1.000	1.292	.999	.344	.100
	Lower-bound	1.292	1.000	1.292	.999	.344	.100
Error (Period)	Sphericity Assumed	11.644	9	1.294			
	Greenhouse-Geisser	11.644	9.000	1.294			
	Huynh-Feldt	11.644	9.000	1.294			
	Lower-bound	11.644	9.000	1.294			
Congruency	Sphericity Assumed	216.701	1	216.701	38.881	**.000**	.812
	Greenhouse-Geisser	216.701	1.000	216.701	38.881	**.000**	.812
	Huynh-Feldt	216.701	1.000	216.701	38.881	**.000**	.812
	Lower-bound	216.701	1.000	216.701	38.881	**.000**	.812
Error (Congruency)	Sphericity Assumed	50.161	9	5.573			
	Greenhouse-Geisser	50.161	9.000	5.573			
	Huynh-Feldt	50.161	9.000	5.573			
	Lower-bound	50.161	9.000	5.573			
Instruction	Sphericity Assumed	108.113	1	108.113	22.613	**.001**	.715
	Greenhouse-Geisser	108.113	1.000	108.113	22.613	**.001**	.715
	Huynh-Feldt	108.113	1.000	108.113	22.613	**.001**	.715
	Lower-bound	108.113	1.000	108.113	22.613	**.001**	.715
Error (Instruction)	Sphericity Assumed	43.028	9	4.781			
	Greenhouse-Geisser	43.028	9.000	4.781			
	Huynh-Feldt	43.028	9.000	4.781			
	Lower-bound	43.028	9.000	4.781			
Period * Congruency	Sphericity Assumed	.089	1	.089	.150	.707	.016
	Greenhouse-Geisser	.089	1.000	.089	.150	.707	.016
	Huynh-Feldt	.089	1.000	.089	.150	.707	.016
	Lower-bound	.089	1.000	.089	.150	.707	.016
Error (Period * Congruency)	Sphericity Assumed	5.316	9	.591			
	Greenhouse-Geisser	5.316	9.000	.591			
	Huynh-Feldt	5.316	9.000	.591			
	Lower-bound	5.316	9.000	.591			
Period *	Sphericity Assumed	5.000	1	5.000	3.929	.079	.304

Instruction	Greenhouse-Geisser	5.000	1.000	5.000	3.929	.079	.304
	Huynh-Feldt	5.000	1.000	5.000	3.929	.079	.304
	Lower-bound	5.000	1.000	5.000	3.929	.079	.304
	Sphericity Assumed	11.453	9	1.273			
Error (Period *	Greenhouse-Geisser	11.453	9.000	1.273			
Instruction)	Huynh-Feldt	11.453	9.000	1.273			
	Lower-bound	11.453	9.000	1.273			
	Sphericity Assumed	61.542	1	61.542	19.253	**.002**	.681
Congruency *	Greenhouse-Geisser	61.542	1.000	61.542	19.253	**.002**	.681
Instruction	Huynh-Feldt	61.542	1.000	61.542	19.253	**.002**	.681
	Lower-bound	61.542	1.000	61.542	19.253	**.002**	.681
	Sphericity Assumed	28.769	9	3.197			
Error (Congruency	Greenhouse-Geisser	28.769	9.000	3.197			
* Instruction)	Huynh-Feldt	28.769	9.000	3.197			
	Lower-bound	28.769	9.000	3.197			
	Sphericity Assumed	.767	1	.767	1.255	.292	.122
Period *	Greenhouse-Geisser	.767	1.000	.767	1.255	.292	.122
Congruency *	Huynh-Feldt	.767	1.000	.767	1.255	.292	.122
Instruction	Lower-bound	.767	1.000	.767	1.255	.292	.122
	Sphericity Assumed	5.502	9	.611			
Error (Period *	Greenhouse-Geisser	5.502	9.000	.611			
Congruency *	Huynh-Feldt	5.502	9.000	.611			
Instruction)	Lower-bound	5.502	9.000	.611			

Table 10. Paired samples *t*-test for the whole brain, left IFG and right IFG comparing baseline and experimental FA values. FA = fractional anisotropy value; Whole = whole brain; LeftIFG = left inferior frontal gyrus; RightIFG = right inferior frontal gyrus; Pre = baseline; Post = experimental.

		Paired Differences					t	df	Sig. 2-tailed
		Mean	Std. Deviation	Std. Error Mean	95% Confidence Interval of the Difference				
					Lower	Upper			
Pair 1	FA_Whole_Pre - FA_Whole_Post	.050125277	.01663611	.00526080	.0382245	.062026	9.528	9	**.000**
Pair 2	FA_LeftIFG_Pre - FA_LeftIFG_Post	.096077154	.05816812	.01839437	.0544661	.137688	5.223	9	**.001**
Pair 3	FA_RightIFG_Pre - FA_RightIFG_Post	.070671049	.07467109	.02361307	.0172545	.124087	2.993	9	**.015**

Table 11. Paired samples *t*-test for the whole brain, left IFG and right IFG comparing baseline and experimental MD values. MD = mean diffusivity value; Whole = whole brain; LeftIFG = left inferior frontal gyrus; RightIFG = right inferior frontal gyrus; Pre = baseline; Post = experimental.

		Paired Differences					t	df	Sig. 2-tailed
		Mean	Std. Deviation	Std. Error Mean	95% Confidence Interval of the Difference				
					Lower	Upper			
Pair 1	MD_Whole_Pre - MD_Whole_Post	-.00005335	.00002087	.0000066	-.000068	-.0000384	-8.082	9	**.000**
Pair 2	MD_LeftIFG_Pre - MD_LeftIFG_Post	-.00002873	.00004032	.0000127	-.000057	.00000010	-2.254	9	**.051**
Pair 3	MD_RightIFG_Pre - MD_RightIFG_Post	-.00004849	.00004196	.0000132	-.000078	-.0000184	-3.655	9	**.005**

Table 12. Paired samples *t*-test for the baseline and experimental periods comparing right and left hemisphere SC values. Pre = baseline; Post = experimental; L = left hemisphere; R = right hemisphere; HEC = hippocampal entorhinal cortex.

		Paired Differences					t	df	Sig. 2-tailed
		Mean	Std. Deviation	Std. Error Mean	95% Confidence Interval of the Difference				
					Lower	Upper			
Pair 1	Pre_L_HEC - Post_L_HEC	-22.9000	98.83145	31.25325	-93.59976	47.79976	-.733	9	.482
Pair 2	Pre_R_HEC - Post_R_HEC	-18.0000	172.33623	54.49750	-141.2819	105.28192	-.330	9	.749

Table 13. Correlation statistics for the congruent face error and right IFG FA pairing. Con = congruent condition; F = face instruction; Err = errors; Right = right hemisphere; IFG = inferior frontal gyrus; FA = fractional anisotropy value.

		Con_F_Err	Right_IFG_FA
Con_F_Err	Pearson Correlation	1	.822**
	Sig. 2-tailed		**.004**
	N	10	10
Right_IFG_FA	Pearson Correlation	.822**	1
	Sig. 2-tailed	**.004**	
	N	10	10

**. Correlation is significant at the 0.01 level (2-tailed).

Table 14. Correlation statistics for the congruent face error and right IFG MD pairing. Con = congruent condition; face = face instruction; Err = errors; Right = right hemisphere; IFG = inferior frontal gyrus; MD = mean diffusivity value.

		Con_F_Err	Right_IFG_MD
Con_F_Err	Pearson Correlation	1	.684*
	Sig. 2-tailed		**.029**
	N	10	10
Right_IFG_MD	Pearson Correlation	.684*	1
	Sig. 2-tailed	**.029**	
	N	10	10

*. Correlation is significant at the 0.05 level (2-tailed).

Table 15. Correlation statistics for the incongruent word error and left IFG FA pairing. Incon = incongruent condition; W = word instruction; Err = errors; Left = left hemisphere; IFG = inferior frontal gyrus; FA = fractional anisotropy value.

		Incon_W_Err	Left_IFG_FA
Incon_W_Err	Pearson Correlation	1	-.743*
	Sig. 2-tailed		**.014**
	N	10	10
Left_IFG_FA	Pearson Correlation	-.743*	1
	Sig. 2-tailed	**.014**	
	N	10	10

*. Correlation is significant at the 0.05 level (2-tailed).

Appendix G – ELISA Proof of Concept

As a biological measure of internal desynchrony, melatonin levels in participants' baseline and experimental saliva samples were to be measured. However, due to unforeseen circumstances regarding issues with funding (see Appendix H breakdown of costs), data were only analyzed from two participants' baseline collections (Figures A-1 and A-2). As such, the results shown below should be regarded only as a proof of concept for the two participants, and future analyses on the remaining participants' samples and discussion of the salivary melatonin data will be excluded from this thesis. The remaining samples will be kept frozen in storage for analysis at a later date. Note that the concentrations of melatonin presented in Figures A-1 and A-2 are higher than what would normally be found in saliva, and thus future experiments will include the performance of serial dilations and the re-analysis of these samples.

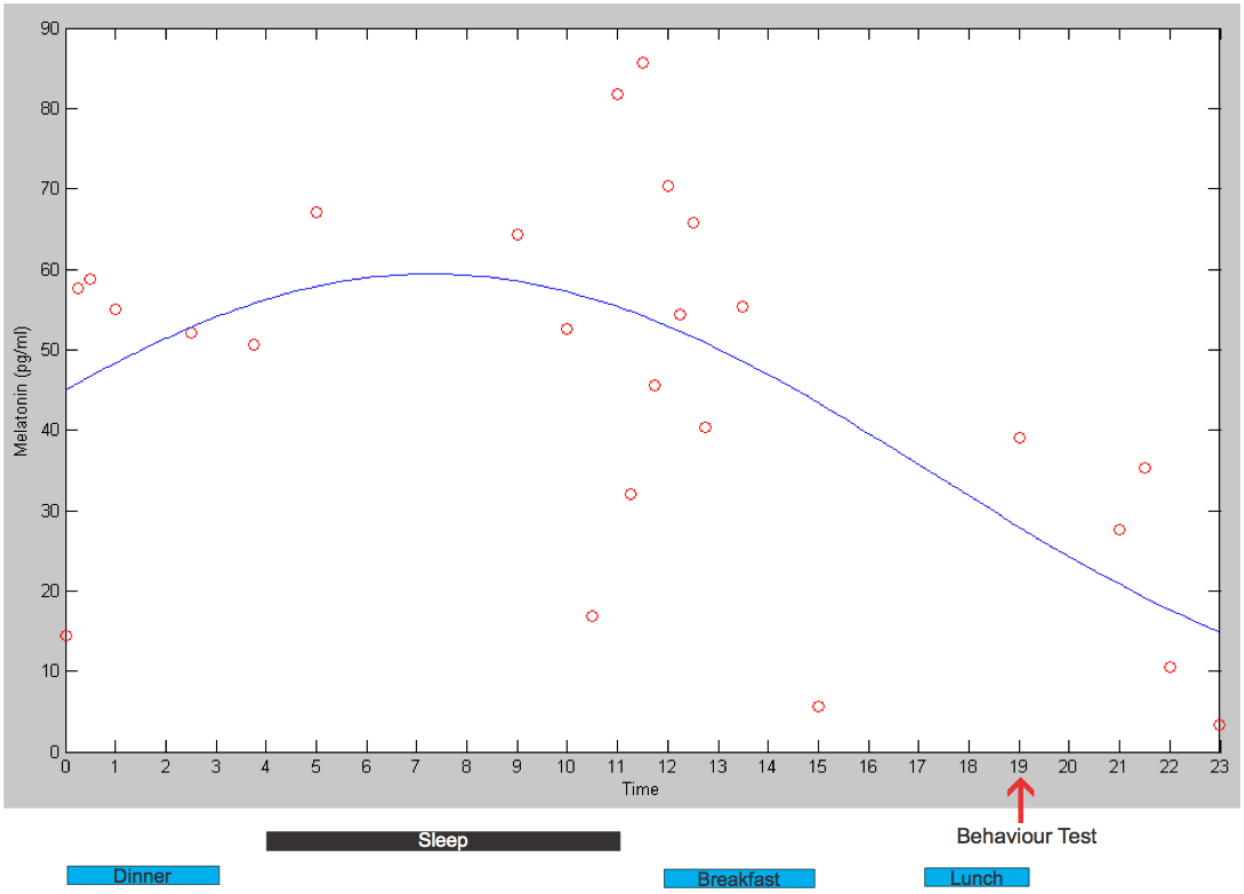

Figure A-1. Compiled baseline data for Subject 1. The graph represents the subject's baseline melatonin profile, generated from three days of saliva samples. The red circles represent the times at which samples were taken relative to DLMO (time 0), as well as the resulting concentration of melatonin in pg/ml (determined using an ELISA). The blue line represents a sinusoidal fit to the data points. The black bar at the bottom represents the subject's average sleep time relative to DLMO. The blue bars represent the average range of times of breakfast, lunch and dinner relative to DLMO. The red arrow indicates the time at which the subject performed the emotional Stroop task on days 2 and 3 of saliva collection (approximately 30 minutes of behavioural testing per day), relative to DLMO.

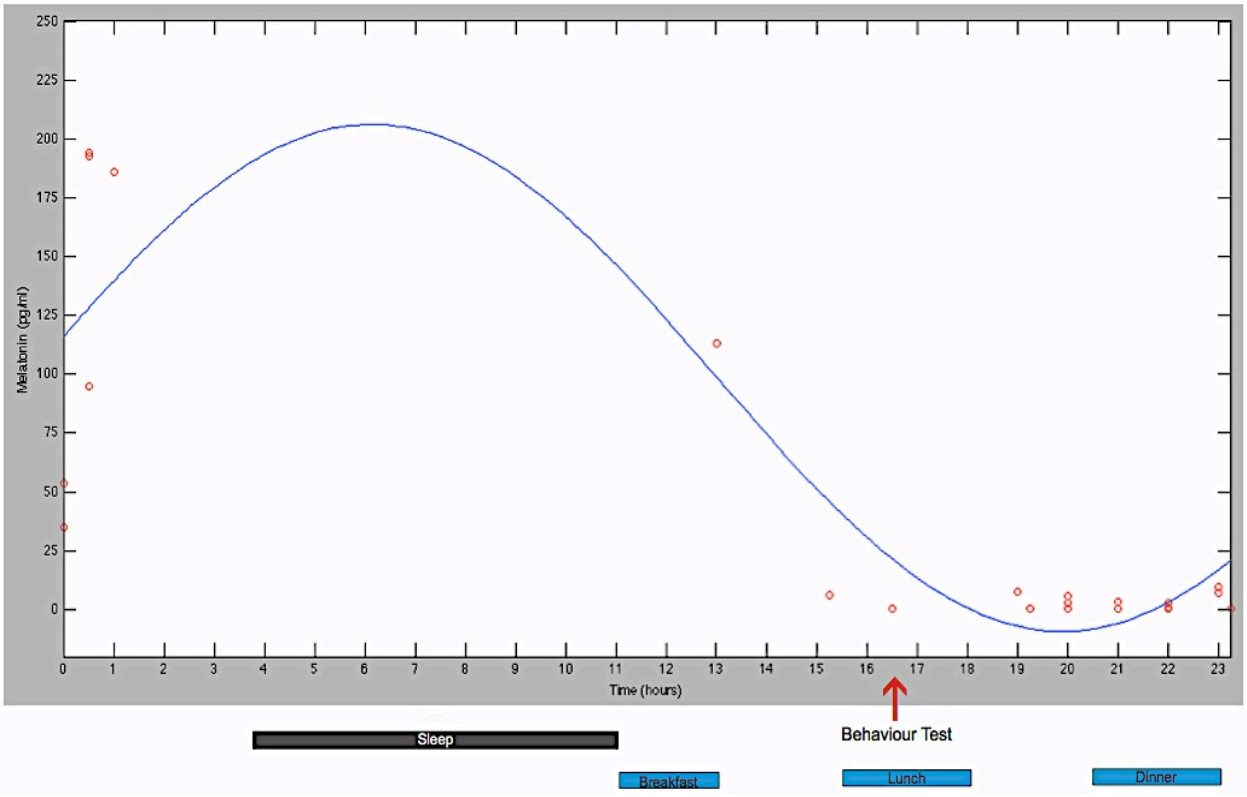

Figure A-2. Compiled baseline data for Subject 2. The graph represents the subject's baseline melatonin profile, generated from three days of saliva samples. Due to circumstances beyond our control, this participant missed several collection time points. The red circles represent the times at which samples were taken relative to DLMO (time 0), as well as the resulting concentration of melatonin in pg/ml (determined using an ELISA). The blue line represents a sinusoidal fit to the data points. The black bar at the bottom represents the subject's average sleep time relative to DLMO. The blue bars represent the average range of times of breakfast, lunch and dinner relative to DLMO. The red arrow indicates the time at which the subject performed the emotional Stroop task on days 2 and 3 of saliva collection (approximately 30 minutes of behavioural testing per day), relative to DLMO.

Appendix H – Cost Breakdown

ELISA Kits:

Price per kit: $649.75

Number of samples collected: 2,480

Kits needed to analyze all samples collected: 57

Kits needed to analyze all samples from experimental period: 44

Total price of 57 kits: **$37,035.75**

Total price of 44 kits: **$28,589**

**5 kits already purchased for $3,248.75 by Dr. Joseph DeSouza's FoH and Start Up Grants*

Microtubes for Saliva Collection:

Prices paid per package (1 package = 500 tubes): $47.54 x 1, $43.00 x 3, $39.54 x 1

Number of packages ordered: 5

Total cost of microtubes: **$216.08**

**Cost of microtubes already paid for in full by Dr. Joseph DeSouza's FoH and Start Up Grants*

MRI Scanning:

Price per hour of scanning: $350

Total participants scanned: 10 participants scanned 2 times each for 0.5 hours per scan

Average hours of scanning used: 10 hours

Total cost of scanning: **$3,500**

**Cost of MRI scanning already paid for in full by Dr. Joseph DeSouza's FoH and Start Up Grants*

Total cost needed to complete all aspects of project: **$40,751.83**